

1988

# Abundance And Magnetic Field Geometries Of The Helium-strong Stars

David Allan Bohlender

Follow this and additional works at: <https://ir.lib.uwo.ca/digitizedtheses>

---

## Recommended Citation

Bohlender, David Allan, "Abundance And Magnetic Field Geometries Of The Helium-strong Stars" (1988). *Digitized Theses*. 1736.  
<https://ir.lib.uwo.ca/digitizedtheses/1736>

This Dissertation is brought to you for free and open access by the Digitized Special Collections at Scholarship@Western. It has been accepted for inclusion in Digitized Theses by an authorized administrator of Scholarship@Western. For more information, please contact [tadam@uwo.ca](mailto:tadam@uwo.ca), [wlsadmin@uwo.ca](mailto:wlsadmin@uwo.ca).



National Library  
of Canada

Bibliothèque nationale  
du Canada

Canadian Theses Service    Service des thèses canadiennes

Ottawa, Canada  
K1A 0N4

## NOTICE

The quality of this microform is heavily dependent upon the quality of the original thesis submitted for microfilming. Every effort has been made to ensure the highest quality of reproduction possible.

If pages are missing, contact the university which granted the degree.

Some pages may have indistinct print especially if the original pages were typed with a poor typewriter ribbon or if the university sent us an inferior photocopy.

Previously copyrighted materials (journal articles, published tests, etc.) are not filmed.

Reproduction in full or in part of this microform is governed by the Canadian Copyright Act, R.S.C. 1970, c. C-30.

## AVIS

La qualité de cette microforme dépend grandement de la qualité de la thèse soumise au microfilmage. Nous avons tout fait pour assurer une qualité supérieure de reproduction.

S'il manque des pages, veuillez communiquer avec l'université qui a conféré le grade.

La qualité d'impression de certaines pages peut laisser à désirer, surtout si les pages originales ont été dactylographiées à l'aide d'un ruban usé ou si l'université nous a fait parvenir une photocopie de qualité inférieure.

Les documents qui font déjà l'objet d'un droit d'auteur (articles de revue, tests publiés, etc.) ne sont pas microfilmés.

La reproduction, même partielle, de cette microforme est soumise à la Loi canadienne sur le droit d'auteur, SRC 1970, c. C-30.

ABUNDANCE AND MAGNETIC FIELD GEOMETRIES  
OF THE HELIUM-STRONG STARS

by

David Allan Bohlender  
Department of Astronomy

Submitted in partial fulfilment  
of the requirements for the degree of  
Doctor of Philosophy

Faculty of Graduate Studies  
The University of Western Ontario  
London, Ontario

June 1988

Permission has been granted to the National Library of Canada to microfilm this thesis and to lend or sell copies of the film.

The author (Copyright owner), has reserved other publication rights, and neither the thesis nor extensive extracts from it may be printed or otherwise reproduced without his/her written permission.

L'autorisation a été accordée à la Bibliothèque nationale du Canada de microfilmer cette thèse et de prêter ou de vendre des exemplaires du film.

L'auteur (titulaire du droit d'auteur) se réserve les autres droits de publication; ni la thèse ni de longs extraits de celle-ci ne doivent être imprimés ou autrement reproduits sans son autorisation écrite.

ISBN 0-315-43310-8

## ABSTRACT

High signal-to-noise coude reticon spectra of five helium-strong stars have been obtained in two spectral regions ( $\lambda\lambda 3980-4160$  and  $\lambda\lambda 4400-4580$ ) at the Canada-France-Hawaii Telescope, Mauna Kea, Hawaii. Phase-resolved sets of spectra have been obtained for the magnetic-variable stars  $\sigma$  Ori E, HD 37776, and HD 64740. Additional observations have also been made of the sharp-lined helium-strong stars HD 58260 and  $\delta$  Ori C. These data, and additional Zeeman analyzer observations, have been used in an attempt to determine the magnetic field geometries and abundance distributions of the program stars. The models have been obtained by use of a line synthesis program that incorporates the effects of an assumed magnetic field and abundance distribution into the calculation of line profiles.

Helium line profile variations of HD 64740 may be modelled with two spots with anomalously high helium abundances near the magnetic poles of the star. Silicon appears to have a large abundance in a high latitude band around the star. The surface magnetic field of HD 64740 is not strong enough to cause magnetic intensification effects in the Si III multiplet 2 line profiles.

The peculiar, broad helium line profiles of  $\delta$  Ori C suggest two possible helium abundance geometries for the

star. A helium-rich spot near the visible magnetic pole of an otherwise extremely helium-poor star, and a vertical helium abundance gradient are both able to reproduce the observed profiles of the star. The second non-variable program star, HD 58260, also shows marginal evidence for such an abundance geometry.

The helium line profiles of  $\sigma$  Ori E are reproduced with two spots of large helium abundance ( $x_{\text{He}} > 0.5$ ) near the intersections of the magnetic and rotation equators of the star. Silicon, magnesium, nitrogen, and oxygen all appear to be overabundant in a high latitude band on the surface of the star. Observations of the variable H $\alpha$  emission of the star are presented.

A theoretical model for the peculiar longitudinal magnetic field variations of HD 37776 is proposed. The model consists of colinear dipole, quadrupole, and octupole field components that result in a magnetic field that varies between 20 and 60 kG over the surface of the star. Helium and silicon abundance geometries consistent with equatorial and polar distributions of the respective elements support the field model, as do the pronounced differential magnetic intensification effects seen in the silicon lines.

Several suggestions for interesting future observational and theoretical work are discussed.

## ACKNOWLEDGEMENTS

This thesis could not have been completed without the support and contributions of a large number of people.

First of all, I would like to thank my thesis supervisor, Dr. J. D. Landstreet, for his endless patience, his tremendous generosity with regards to research and travel support, and for his words of encouragement, support, and advice when they were needed the most.

The Canada-France-Hawaii Telescope Time Allocation Committee is acknowledged for a generous amount of observing time. The CFHT support staff are also thanked for making our observing run both successful, and very enjoyable.

Dr. C. T. Bolton and ~~Dr. A. J. Fullerton~~ Fullerton generously permitted the author the use of data from their earlier CFHT observing run. Dr. Bolton has been a tremendous source of advice and support at all stages of this project.

Much of the data reduction and many of the figures for this work were carried out using modifications of Fortran routines originally written by Dr. P. K. Barker. He is gratefully acknowledged for the use of his programs.

Many thanks are due Mrs. Mira Rasche for her cheerful preparation of several figures for this thesis, and for related work.

I have benefitted from many useful discussions with the entire astronomy department, especially Drs. William Wehlau, John Rice, Romas Mitalas, and Mike Marlborough.

Mr. Henry Leparskas has been a tremendous source of detailed, and thorough, help and information with regards to hardware and software of the department and university computer systems.

Our 'highly skilled technician,' Mr. Mike Debruyne has, over the past four years, made equipment changes on the 1.2 m a chore to look forward to and enjoy. Mike's advice for myself and my 'business associate' (i.e. my wife) has also been cheerfully accepted, and usually rejected.

The likes of such fellow grad students as Jaymie Matthews, Bob Hill, Brian Ventrudo, and Cliff Toner made graduate school an experience. Their friendship will always be valued.

My parents and family have been a constant source of support throughout my university career, and especially during the last four years. Although I may not often tell them to their faces, they are very much appreciated.

Finally, not enough can be said about the contributions made to this thesis, directly and indirectly, by my wife Elaine. Her tireless efforts and moral support, especially in the final months and days (and hours) of preparation of this work, will always be remembered, and hopefully, some day, repaid. I look forward to many more years as happy and full as our first year, together.

# TABLE OF CONTENTS

	Page
CERTIFICATE OF EXAMINATION .....	ii
ABSTRACT .....	iii
ACKNOWLEDGEMENTS .....	v
TABLE OF CONTENTS .....	vii
LIST OF TABLES .....	ix
LIST OF FIGURES .....	x
CHAPTER 1 - INTRODUCTION .....	1
CHAPTER 2 - OBSERVATIONS .....	19
2.1 Spectroscopy .....	19
2.2 Magnetic field observations .....	28
CHAPTER 3 - THE LINE SYNTHESIS PROGRAM .....	34
3.1 Overview .....	34
3.2 Input data .....	36
3.3 Subroutine <i>COMPON</i> .....	45
3.4 Subroutine <i>LTELC</i> .....	47
3.5 Disk Integration .....	50
3.5.1 Subroutine <i>MAGFLD</i> .....	51
3.5.2 Subroutine <i>ABZSP</i> .....	51
3.5.3 Subroutine <i>LINPRO</i> .....	54
3.6 Subroutine <i>SPPROF</i> .....	56
3.7 Additional programming considerations .....	56
CHAPTER 4 - HD 64740 .....	62
4.1 Introduction .....	62
4.2 Observations .....	64
4.3 Modelling .....	73
4.4 Discussion .....	84
CHAPTER 5 - HD 58260 AND $\delta$ ORI C .....	88
5.1 Introduction .....	88
5.1.1 HD 58260 .....	88
5.1.2 $\delta$ Ori C = HD 36485 = HR 1851 .....	89
5.2 Observations .....	90
5.3 Models .....	94
5.4 Discussion .....	115

CHAPTER 6 - $\sigma$ ORI E .....	120
6.1 Introduction .....	120
6.2 Observations .....	129
6.3 Modelling .....	138
6.4 Discussion .....	149
CHAPTER 7 - HD 37776 .....	155
7.1 Introduction .....	155
7.2 Observations .....	159
7.3 Magnetic Model .....	167
7.4 Modelling .....	177
7.5 Discussion .....	193
CHAPTER 8 - CONCLUSION .....	198
8.1 Summary .....	198
8.2 Suggestions for future work .....	204
REFERENCES .....	214
VITA .....	226

## LIST OF TABLES

Table	Description	Page
1.1	The Helium-Strong Stars .....	3
1.2	Progam Star Data .....	15
2.1	Journal of CFHT Observations .....	21
2.2	Summary of Magnetic Field Measurements .....	32
3.1	Derived Coefficients of the Polynomial Approximations of Partition Functions .....	38
3.2	Oscillator Strengths .....	40
3.3	Computed Equivalent Widths ( $\lambda$ ) of Hydrogen and Helium line profiles for various model atmospheres .....	43
3.4	Computed Equivalent Widths ( $m\lambda$ ) of the Si III Multiplet 2 Lines for Various Dipolar Magnetic Field Strengths .....	59
4.1	HD 64740 Abundance Geometries .....	80
5.1	HD 58260 and $\delta$ Ori C Abundance Results .....	103
6.1	$\sigma$ Ori E Abundance Geometries .....	146
7.1	HD 37776 Magnetic Field Fitting Parameters .....	175
7.2	HD 37776 Non-Magnetic Model Abundance Distributions .....	186
7.3	HD 37776 Magnetic Model Abundance Distributions...	192

LIST OF FIGURES.

Figure	Description	Page
1.1	Plot of Stromgren $\beta$ vs. $[u - b]$ for a sample of helium-strong, helium-weak, and Ap stars .....	11
2.1	Representative CFHT coude reticon spectrum of the standard B2 star, gamma Pegasi .....	27
3.1	Relative Zeeman intensities and splittings of the Si III multiplet 2 lines .....	46
3.2	Illustration of the abundance geometry used in the program ZEEMAN .....	53
4.1	Observed and modelled He I $\lambda 4471$ line profiles of HD 64740 .....	65
4.2	Observed and modelled He I $\lambda 4437$ line profiles of HD 64740 .....	66
4.3	Observed and modelled H $\delta$ line profiles of HD 64740 .....	67
4.4	Observed and modelled Si III $\lambda 4567$ line profiles of HD 64740 .....	68
4.5	Observed and modelled N II $\lambda 3995$ line profiles of HD 64740 .....	69
4.6	Observed and modelled O II $\lambda \lambda 4415$ and $4417$ line profiles of HD 64740 .....	70
4.7	Helium line strength index and magnetic curves of HD 64740 .....	72
4.8	Location of HD 64740 in the $\log g$ vs. $\theta_{eff}$ plane .....	77
4.9	Illustration of the helium abundance geometry of HD 64740 .....	81
4.10	Illustration of the silicon abundance geometry of HD 64740 .....	83
5.1	A comparison of the He I $\lambda 4471$ line profiles of 22 Ori, HD 58260, and $\delta$ Ori C .....	91

5.2	A comparison of the H $\delta$ line profiles of 22 Ori, HD 58260, and $\delta$ Ori C .....	92
5.3	Observed and modelled H $\delta$ line profiles of HD 58260 for a uniform hydrogen abundance .....	96
5.4	Observed and modelled He I $\lambda$ 4471 line profiles of HD 58260 for a uniform helium abundance .....	97
5.5	Observed and modelled He I $\lambda$ 4437 line profiles of HD 58260 for a uniform helium abundance .....	98
5.6	Locations of HD 58260 and $\delta$ Ori C in the log $g$ vs. $\theta_{\text{eff}}$ plane .....	99
5.7	Observed and modelled H $\delta$ line profiles of $\delta$ Ori C for a spotted helium abundance geometry .....	107
5.8	Observed and modelled He I $\lambda$ 4471 line profiles of $\delta$ Ori C for a spotted helium abundance geometry .....	108
5.9	Observed and modelled He I $\lambda$ 4437 line profiles of $\delta$ Ori C for a spotted helium abundance geometry .....	109
5.10	Observed and modelled H $\delta$ line profiles of $\delta$ Ori C for a vertically stratified hydrogen abundance geometry .....	111
5.11	Observed and modelled He I $\lambda$ 4471 line profiles of $\delta$ Ori C for a vertically stratified helium abundance geometry .....	112
5.12	Observed and modelled He I $\lambda$ 4437 line profiles of $\delta$ Ori C for a vertically stratified helium abundance geometry .....	113
5.13	Observed and modelled He I $\lambda$ 4471 line profiles of HD 58260 for a spotted helium abundance geometry .....	116
6.1	Helium line strength index, shell line, and photometric and magnetic curves of $\sigma$ Ori E .....	130
6.2	Observed H $\alpha$ line profiles of $\sigma$ Ori E .....	132
6.3	Observed H $\delta$ line profiles of $\sigma$ Ori E .....	133
6.4	Illustration of the radial velocity variations of the helium line profiles of $\sigma$ Ori E .....	135

6.5	Observed and modelled He I $\lambda 4437$ line profiles of $\sigma$ Ori E .....	136.
6.6	Observed and modelled He I $\lambda 4471$ line profiles of $\sigma$ Ori E .....	137
6.7	Observed and modelled Si III $\lambda 4567$ line profiles of $\sigma$ Ori E .....	139
6.8	Location of $\sigma$ Ori E in the $\log g$ vs. $\theta_{\text{eff}}$ plane .....	144
6.9	Observed and modelled H $\delta$ line profiles of $\sigma$ Ori E .....	145
6.10	Illustration of the helium abundance geometry of $\sigma$ Ori E .....	147
6.11	Illustration of the silicon abundance geometry of $\sigma$ Ori E .....	148
7.1	Stromgren $\gamma$ -band light variations, helium line strength index, and magnetic field curves of HD 37776 .....	160
7.2	Observed H $\alpha$ line profiles of HD 37776 .....	161
7.3	Observed H $\delta$ line profiles of HD 37776 .....	162
7.4	Observed He I $\lambda\lambda 4437$ and $4471$ line profiles of HD 37776 .....	163
7.5	Observed Si III $\lambda 4567$ line profiles of HD 37776 .....	164
7.6	Observed and modelled longitudinal magnetic field variations of HD 37776 .....	174
7.7	Observed and modelled He I $\lambda 4437$ line profiles of HD 37776 for the non-magnetic model of the star .....	180
7.8	Observed and modelled H $\delta$ line profiles of HD 37776 .....	181
7.9	Observed and modelled He I $\lambda 4471$ line profiles of HD 37776 .....	182
7.10	Location of HD 37776 in the $\log g$ vs. $\theta_{\text{eff}}$ plane .....	183

7.11	Observed and modelled Si III $\lambda\lambda 4567$ and $4574$ line profiles of HD 37776 for the non-magnetic model of the star .....	185
7.12	Illustration of the helium abundance geometry of HD 37776 .....	187
7.13	Illustration of the silicon abundance geometry of HD 37776 .....	188
7.14	Observed and modelled He I $\lambda 4437$ line profiles of HD 37776 for the magnetic model of the star ...	190
7.15	Observed and modelled Si III $\lambda\lambda 4567$ and $4574$ line profiles of HD 37776 for the magnetic model of the star .....	191
8.1	Helium line strength index, photometric and magnetic curves of HD 37017 .....	203

The author of this thesis has granted The University of Western Ontario a non-exclusive license to reproduce and distribute copies of this thesis to users of Western Libraries. Copyright remains with the author.

Electronic theses and dissertations available in The University of Western Ontario's institutional repository (Scholarship@Western) are solely for the purpose of private study and research. They may not be copied or reproduced, except as permitted by copyright laws, without written authority of the copyright owner. Any commercial use or publication is strictly prohibited.

The original copyright license attesting to these terms and signed by the author of this thesis may be found in the original print version of the thesis, held by Western Libraries.

The thesis approval page signed by the examining committee may also be found in the original print version of the thesis held in Western Libraries.

Please contact Western Libraries for further information:

E-mail: [libadmin@uwo.ca](mailto:libadmin@uwo.ca)

Telephone: (519) 661-2111 Ext. 84796

Web site: <http://www.lib.uwo.ca/>

## CHAPTER 1 INTRODUCTION

More than thirty years ago Berger (1956) reported the discovery of very strong helium lines and helium absorption discontinuity in the star  $\sigma$  Ori E (HD 37479). After examining the radial velocity, proper motion, and interstellar lines of  $\sigma$  Ori E, Greenstein and Wallerstein (1958) suggested that the star is a member of the multiple system  $\sigma$  Ori, which consists of five components, the very close pair AB, and three companions, C, D, and the peculiar star, E. They also demonstrated, from the star's colours and absolute magnitude, that  $\sigma$  Ori E is only half a magnitude from the main sequence, despite its peculiar chemical abundances. Assuming that the helium abundance anomaly of the star reflects an advanced evolutionary state then leads to an interesting problem: the unevolved A component of the system (Greenstein and Wallerstein (1958) classified the AB components as O9.5 V) is more massive than the B2 V E component. To account for the E component's apparently evolved state but low mass, Greenstein and Wallerstein adopted a scenario in which  $\sigma$  Ori E was assumed to have had an unusually large mass originally ( $> 100 M_{\odot}$ , the total mass of the A and B components), and to have evolved very rapidly, losing a large fraction of its original mass in the process.

Some years later, Klinglesmith et al. (1970) performed

2

a fine analysis of  $\sigma$  Ori E. Their best fit model indicated an effective temperature ( $T_{\text{eff}}$ ) of 23500 K,  $\log g = 4.05$ , and hydrogen mass fraction  $X = 0.282$ , compared to a normal value of about 0.70. A derived  $M_{\text{bol}}$  of  $-4.7$ , then led to a mass and radius of  $M = 9.8 M_{\odot}$ , and  $R = 4.6 R_{\odot}$ . They found a  $v \sin i$  of about  $150 \text{ km s}^{-1}$ , but no additional abundance anomalies.

Since then, several spectroscopic surveys have resulted in the discovery of some two dozen objects similar to  $\sigma$  Ori E in many respects (e.g. Hiltner et al. 1969, MacConnell et al. 1970). A list of known members of the helium-strong class is given in table 1.1. The visual magnitude,  $V$ , the galactic longitude and latitude, radial velocity, and cluster or association membership, if known, is given for each object. Several members of the class have been found to demonstrate a rich variety of phenomena. Many of the investigations of these stars were stimulated by Walborn's (1974) discovery of broad, variable H $\alpha$  emission in  $\sigma$  Ori E. Emission has also been observed in HD 37017, HD 37776, HD 64740, and CPD -62° 2124 (Walborn 1974, Pedersen 1979, Drilling 1981). Hunger (1974) reported variability in the equivalent widths of neutral helium lines, as well as Si III in  $\sigma$  Ori E. For the helium-strong stars in general, helium line strengths vary with periods on the order of days, as do those of hydrogen, silicon, and, less conclusively, carbon, nitrogen, and oxygen (Pedersen and Thomsen 1977, Lester 1979, Walborn 1982), with hydrogen and the metals always

Table 1.1 The Helium-Strong Stars

Name	V	l	b	r.v.	Membership
$\delta$ Ori C	6.85	204	-18	+12	Ori OB1
HD 37017	6.54	208	-19	+29	Ori OB1
$\sigma$ Ori E	6.65	207	-17	+29	Ori OB1
HD 37776	6.98	206	-16	+27	Ori OB1
HDE 260858	9.14	200	3		
HDE 264111	9.65	208	1		
CoD-27°3748	9.27	240	-8		
HD 58260	6.73	249	-10	+36	
HD 60344	7.71	239	-2	+30	
HD 64740	4.62	263	-11	+8	
HD 66522	7.21	265	-11	+15	
CoD-46°4639	10.0	266	-2		
HD 26446	6.68	290	0	+7	
CPB-62°2124	11.04	295	-2	-7	IC 2944
HD 133518	6.39	323	5	-2	
HD 144941	10.11	348	18	-53	
HD 149257	8.48	338	1	+6	
CPD-69°2698	9.36	322	-18	-65	
HD 164769	9.25	3	-3		
HD 168785	8.49	3	-8	+5	
HD 184927	7.46	66	5	-16	
HD 186205	8.52	47	-7	-3	
LSII+35°51	11.1	73	1		
LSII+36°37	11.30	74	1		Cyg OB1

varying in antiphase with helium. Extensive photometry of members of the class indicate that low level light variations, ( $< 0.10$  magnitude) are common and are consistent with the periods of the spectroscopic variations (Pedersen and Thomsen 1977, Adelman and Pyper 1985).  $\sigma$  Ori E has a unique eclipse-like light curve (Walborn and Hesser 1976; Hesser, Walborn, and Ugarte P. 1976; Hesser, Moreno, and Ugarte P. 1977) with two unequal minima. A less pronounced low-level light variation, similar to that seen in other helium-strong stars, is superimposed on this eclipsing curve. In addition, a variable shell spectrum has been observed in  $\sigma$  Ori E (Groote and Hunger 1976). At phases very close to the eclipse minima, the number of visible Balmer lines increases from 15 to 21.

In many respects, the nature of the phenomena described above is very similar to the behaviour observed in the peculiar A and B magnetic stars, which in order of increasing temperature include the SrCrEu Ap stars, the Si Bp stars, and the helium-weak stars. The Ap stars show, in some cases, dramatic overabundances of rare earth elements, chromium, and silicon in their atmospheres. The helium-weak stars often also show strong silicon lines but are identified by their anomalously weak neutral helium lines. Most of these stars are also spectrum and photometric variables, each with one well-defined period. Deutsch (1956) pointed out that the periods and  $v \sin i$ 's of many of the peculiar Ap stars satisfy a relation that

suggests that the observed periods represent the rotation periods of the stars. These stars are usually modelled in terms of an *Oblique Rotator Model*.

The *Oblique Rotator Model* (Babcock 1949a, Stibbs 1950) appears to provide a satisfactory conceptual framework for understanding the variations of the peculiar A and B stars. In this model, a magnetic field, usually assumed to be dipolar, is inclined to the rotation axis by an angle  $\beta$ . As the star rotates the longitudinal component of the magnetic field varies as a result of the changing aspect of the field. The strong surface field (typically 5 kG in these stars, but ranging from undetectable to more than 30 kG) stabilizes the atmosphere against turbulent motions, so that diffusion processes may occur (Michaud 1970). The presence of the magnetic field also influences diffusion processes in three ways: 1) by desaturating lines and altering the radiative forces on a given ion; 2) by causing the horizontal migration of various ions high in the photosphere; 3) by suppressing the stellar wind near regions where the magnetic field lines are horizontal. This interaction of diffusion processes and the magnetic field then results in an accumulation of various elements, either in regions where the magnetic field lines are predominantly horizontal, or where the field lines are vertical, and hence spectral variations are also observed as the star rotates. Theoretical calculations illustrating such effects are given by Vauclair, Hardorp, and Peterson (1979), Alecian and

Vauclair (1981), Michaud, Mégessier, and Charland (1981), and Mégessier (1984). These abundance patches presumably alter the atmospheric structure and flux distribution sufficiently over the surface of the star to produce the low amplitude light fluctuations observed as the star rotates (e.g. Stepien 1978; Peterson and Theys 1981; Bolton 1983).

Unfortunately, the prototypical helium-strong star,  $\sigma$  Ori E, is somewhat atypical from the rest of the helium-strong star class, and not as easy to interpret in terms of the usual model for the magnetic Ap stars. The most notable differences between  $\sigma$  Ori E and the Ap stars are its H $\alpha$  emission, the peculiar eclipsing light curve, and the overabundance of helium, which, until recently, was difficult to understand as anything but an evolutionary effect. The complex behaviour of  $\sigma$  Ori E led to many interesting models. Greenstein and Wallerstein (1958) proposed that the star was originally extremely massive ( $> 50 M_{\odot}$ ) but lost a significant fraction of its mass, thus exposing a predominantly helium core. Interpretations in terms of binary mass transfer, fragmentation of a massive star, or stellar capture were discussed by Odell (1974). Hesser et al. (1976) suggested a model involving stable clouds situated at the Lagrangian points of a binary system.

After the previously mentioned spectroscopic surveys, Osmer and Peterson (1974) carried out the first investigation of the helium-strong stars as a group and showed that they form a rather well-defined class with

7

helium number abundance comparable to hydrogen, possible overabundances of oxygen and nitrogen, normal abundances of carbon, silicon, magnesium and aluminum, but temperatures and gravities corresponding to main sequence B2 stars. (One star included in this work, HR 5206, is probably not a helium-strong star [Walborn 1983].) Their most important conclusion was that the helium-strong stars as a class, might represent an extension of the silicon Ap and helium-weak stars to higher temperatures. The eventual discovery of a strong, variable magnetic field in  $\sigma$  Ori E (Landstreet and Borra 1978) and many other helium-strong stars, (Borra and Landstreet 1979; Bohlender et al. 1987) gave strong support to this idea. It now seems firmly established that magnetic peculiar stars occur at all temperatures between 7500 K (the coolest SrCrEu Ap stars) and 25000 K (the hottest helium-strong stars).

Osmer and Peterson (1974) argued that the helium-strong stars must be young, since several are found in the Orion OB1 association, and all are located near the galactic plane with  $|b| < 19$ . Masses, radii, and luminosities can be most easily estimated for the association stars, and their work is consistent with the idea that the helium-strong stars are normal main-sequence stars with masses near  $9 M_{\odot}$ . However Hunger (1975, 1986a,b) points out that the situation may not be as clear cut as this. Spectroscopic fine analyses of various helium-strong stars by several workers have resulted in mass determinations considerably

lower than Osmer and Peterson's. For example, Hunger (1986a,b) suggests that the mass of  $\sigma$  Ori E is closer to  $3 M_{\odot}$ . The differences in the two mass determinations arise from differences in the surface gravities found by modelling the pressure sensitive Balmer and neutral helium lines. Hunger's group suggests a  $\log g$  value for  $\sigma$  Ori E that is about 0.5 dex lower than Osmer and Peterson's value of  $\log g = 4.31$ . The reason for the discrepancy is still uncertain. It may be, however, that the helium-strong stars (also often referred to as helium-rich or intermediate helium stars) are somehow related to the hydrogen deficient or extreme helium stars. These are thought to consist of low mass population II stars in late stages of evolution (e.g. Hunger 1975), that have  $N_{\text{He}}/N_{\text{H}} > 100$ , probably throughout the star, and CNO abundances characteristic of evolved objects. The remainder of this work, however, supports the ideas that the helium anomalies of the helium-strong stars are confined to their atmospheres, and that they do represent high temperature extensions of the peculiar A and B main sequence stars as Osmer and Peterson (1974) have suggested.

It has been believed for some time that the abundance anomalies in the Ap, Am, and helium-weak stars can be understood in terms of competition between gravitational diffusion and radiation pressure on the elements in question (e.g. Michaud 1970). The relative importance of the two processes determines whether an element is pushed into the

region of line formation or sinks below the photosphere. The sole additional requirement is a sufficiently stable atmosphere. Slow rotation, as in the Am stars, or a strong surface magnetic field, as in the Ap and helium-weak stars, satisfies this requirement. In this simple picture, however, helium is expected to sink (because of saturation effects the radiative force can only exceed gravity for very low helium abundances [Michaud et al. 1979]) and only helium-weak B stars should be seen. Osmer and Peterson (1974) first suggested that the helium overabundances observed in the helium-strong stars might be caused by diffusion processes occurring in the presence of a stellar wind. Vauclair (1975) subsequently demonstrated that if a general outflow of material did exist then helium could accumulate in the atmosphere where the downward diffusion velocity of the element was of equal magnitude to the general outward flow velocity, as long as the diffusive mass flux decreases with depth at this point. For suitable mass-loss rates ( $10^{-12} M_{\odot} \text{ yr}^{-1}$ ) and temperatures (about 20000 K) this accumulation would occur in the line-forming region for the helium-strong stars but well below this zone for the helium-weak stars. A small class of stars with high isotopic abundances of  $^3\text{He}$  (Hartoog and Cowley 1979), and temperatures intermediate between those of the helium-strong and helium-weak stars, the so-called helium-3 stars, could also be interpreted using this simple model, since  $^3\text{He}$  would be pushed into the line-forming region at slightly lower

temperatures because of its lower mass.

Michaud et al. (1987) have recently extended this model by allowing for the possible effects of separation of helium in the envelope or wind of a star. They find that in order to explain the helium enrichment by separation in the atmosphere, the mass-loss rate must decrease as the effective temperature rises from 20000 K to 25000 K. At the higher temperature the maximum mass-loss allowing separation is  $3 \times 10^{-13} M_{\odot} \text{ yr}^{-1}$ . A mass-loss rate of less than approximately  $2 \times 10^{-12} M_{\odot} \text{ yr}^{-1}$  allows separation to occur in the wind but this is likely to be less important than separation in the atmosphere. It is also shown that for these mass-loss rates, downward diffusion of helium in the envelope is too slow to reduce the helium abundance in the atmosphere during the main-sequence lifetime of a helium-strong star.

Figure 1.1 shows the positions of a representative sample of the helium-strong stars and other peculiar Bp and Ap stars in a Strömgen  $\beta$  vs.  $[u - b]$  diagram. The  $uvby\beta$  photometric data are from Mermilliod and Hauck (1979) and the plotted reddening free  $[u - b]$  values are determined from the relation given by Lester, Gray, and Kurucz (1986). No allowance has been made for possible time variations of the  $\beta$  index, as might be expected for the variable helium-strong and helium-weak stars. There is considerable overlap in the three classes. The low temperature cutoff of the peculiar stars corresponds to the development of deep

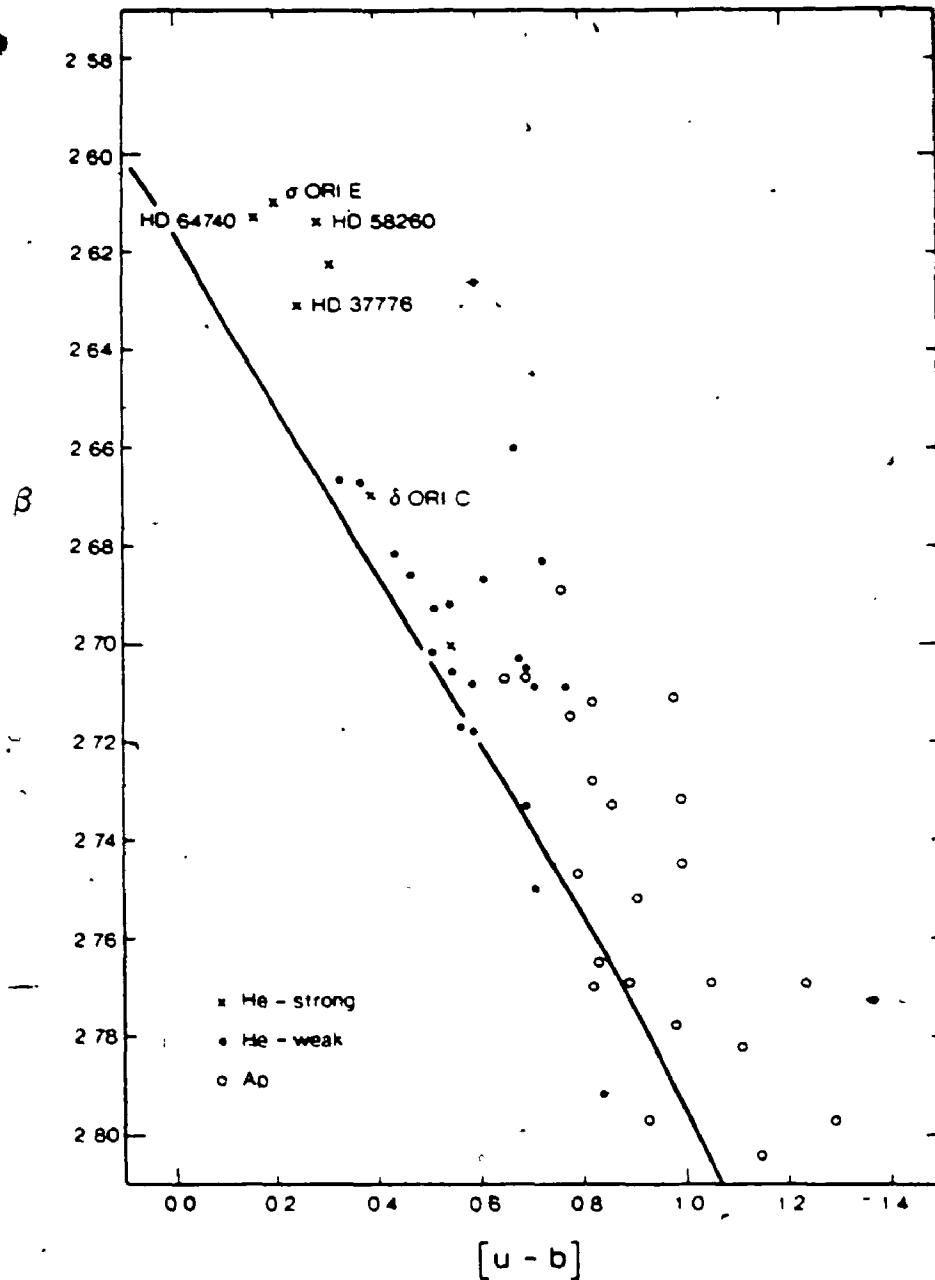


Figure 1.1 A plot of Strömgen  $\beta$  vs.  $[u - b]$  for a sample of helium-strong (crosses), helium-weak (filled circles), and Ap stars (open circles), for which Strömgen photometry are available. The solid line represents the theoretical  $\beta$  vs.  $[u - b]$  relation of Lester, Gray, and Kurucz (1986) for the  $\log g = 4.0$  solar abundance model atmospheres of Kurucz (1979).

surface convection zones (diffusion occurs only beneath these regions, and when they become very extensive the time scale needed for abundance anomalies to manifest themselves at the surface become longer than the main sequence lifetime of the star), while the apparent high temperature cutoff is generally believed to correspond to the onset of strong stellar winds. Stellar winds in the helium-strong stars were first detected from ultraviolet observations of the C IV and Si IV resonance lines using the International Ultraviolet Explorer (IUE) satellite (Shore and Adelman 1981; Barker et al. 1982). For some objects the typical P Cygni profiles indicative of a stellar outflow (e.g. Mihalas 1978, p.471) are variable, again with periods equal to those of the spectroscopic, photometric and magnetic variations. Estimates of the mass-loss rates range from a value of  $5 \times 10^{-12} M_{\odot} \text{ yr}^{-1}$  (Michaud et al. 1987) to a substantially larger value of  $4 \times 10^{-10} M_{\odot} \text{ yr}^{-1}$  (Shore and Adelman 1981). These appear to be somewhat larger than the  $10^{-12} M_{\odot} \text{ yr}^{-1}$  rate required for the helium overabundances in the models of Vauclair (1975) and Michaud et al. (1987). Michaud et al. (1987) suggest that the strong magnetic fields observed in many of the helium-strong and helium-weak stars (e.g. Bohlender et al. 1987; Borra, Landstreet, and Thompson 1983) may suppress the mass flux near the magnetic equator, where the field lines are horizontal, and thus inhibit the flow of ions. The presence of a magnetic field might also alter the diffusion processes themselves, as has been demonstrated to

be the case for silicon (Michaud et al. 1979; Vauclair, Hardorp, and Peterson 1979). Shore (1978; 1987) has developed a qualitative model for such a situation. In his scenario, for the usual case of a dipolar geometry for the magnetic field, the stellar wind is expected to escape only in a small cone, or jet, at each pole of the star and is trapped at the magnetic equator, if the surface field is strong enough. These jets might explain the observed rotational modulation of the UV resonance lines (Shore and Adelman 1981; Barker et al. 1982). Most mass-loss rates estimated from observations assume a spherically symmetric flow, but this is clearly not the case for the helium-strong stars. The values quoted above might then be regarded as upper limits to the mass-loss rates. Shore suggests, that in the hottest helium-strong stars, helium is supported at the magnetic equator but escapes along with the rest of the atmosphere at the poles. In cooler stars the helium is levitated in regions closer to the magnetic poles until, for the coolest helium-strong stars, helium is overabundant at the poles and underabundant near the equator. For still cooler stars the field suppresses motion at the magnetic equator below the region required for upward diffusion of helium, and the wind is too weak to levitate helium at the poles, so that the entire star appears helium-weak.

A number of oblique rotator models have been published for the helium-weak and Ap stars (e.g. Pyper 1969; Wolff and Wolff 1976; Hensler 1979; Landstreet 1988). To date there

have been no quantitative models for the helium-strong stars. The reason for this is simple: for elements other than hydrogen and helium, only recently have solid state detectors given us the required signal-to-noise to effectively record the line profiles of the hot, and rapidly rotating helium-strong stars. Most previous work has been confined to simple measurements of equivalent widths of spectral lines recorded on photographic plates. Often the noise level is higher than any suggested variations.

For these reasons, high signal-to-noise, high resolution spectra of several helium-strong stars throughout their rotation period have been obtained. Using previously published longitudinal magnetic field measurements, it is the aim of this thesis to obtain accurate surface abundance and magnetic field geometries for these stars. The variable stars discussed are  $\sigma$  Ori E (HD 37479), HD 37776, and HD 64740. They were chosen because of their brightness (all are brighter than  $V = 7.0$ ), well determined longitudinal fields and rotation periods, and because all three could be well-observed on one observing run. In addition, observations of two non-variable, helium-strong stars,  $\delta$  Ori C, and HD 58260, have been obtained. The magnitudes, intrinsic  $U - V$  and  $u - b$  colours, and the Geneva photometric index,  $X$  (Cramer and Maeder 1979), of the program stars are given in Table 1.2. The  $(U - V)_0$  values were derived from the observed colours (Egret and Jaschek 1981; Hoffleit and Jaschek 1982), using the  $Q$  method (e.g.

Table 1.2 Program Star Data

Name	V	(U-V) <sub>o</sub>	[u-b]	X
$\delta$ Ori C	6.85	-0.94	0.392	0.4723
$\sigma$ Ori E	6.65	-1.14	0.203	0.2601
HD 37776	6.98	-1.19	0.248	0.3114
HD 58260	6.73	-1.03	0.287	...
HD $\alpha$ 4740	4.63	-1.20	0.164	0.2535

Mihalas and Binney 1981). Again, the Strömgren photometry is from Mermilliod and Hauck (1979), reddening free  $[u - b]$  values were found using the equations in Lester, Gray, and Kurucz (1986), and no allowance has been made for possible variability of the various photometric indices. The Geneva colour index,  $X$ , has been derived for each star (with the exception of HD 58260) from the photometric data of Rufener (1981).

In most cases, modelling efforts for the Ap stars have been restricted to either the magnetic field geometry (e.g. Preston 1969, 1970; Borra and Landstreet 1977, 1978) or the abundance distribution geometry (Mégessier 1975; Van Rensbergen, Hensberge, and Adelman 1984). Only recently have consistent models incorporating the effects of both the magnetic field and abundance geometry appeared (Landstreet 1988). This approach is important because details about the magnetic field geometry or abundance distribution depend, to a great extent, on each other. Many lines used for abundance determinations are sensitive to magnetic fields and are split into a multitude of Zeeman components. If the surface magnetic field is stronger than a few kG then this splitting can desaturate a line and increase its equivalent width substantially (Babcock 1949b). A variable surface field can then lead to considerable spectral variations even when the element is uniformly distributed on the surface of the star (Landstreet 1988). In addition, if the magnetic field is measured using spectral lines of an element that is

not uniformly distributed the field geometry so derived will be distorted from the true geometry (Deutsch 1958; Pyper 1969). Since the helium-strong stars have fields on average about three times larger than those observed on the magnetic Ap stars (Borra and Landstreet 1979; Bohlender *et al.* 1987) the above effects can be considerable, so the magnetic field and abundance geometry models should be found simultaneously.

The modelling approach employed in this study involves the use of a sophisticated line synthesis program developed by J. D. Landstreet (University of Western Ontario) with extensive modifications by the author. The program calculates at a prescribed number of points on the visible surface of a model star the local intensity and polarization profiles of one or more spectral lines. The abundances of the elements in question and the Zeeman splitting for each line at each point are determined from the assumed abundance distributions, magnetic field geometry, and rotational phase and are explicitly accounted for in the calculation of the outward transfer of polarized light. These local profiles are then given a specified Doppler shift, summed over the visible disk, and convolved with an appropriate instrumental profile.

It is hoped that the resulting models of the photospheres of these stars will help to resolve some of the problems, both observational and theoretical, discussed above. Models of the surface magnetic field geometry will

provide constraints for future modelling of the magnetospheres of this representative group of helium-strong stars. Both the surface field and abundance geometries should yield important boundary conditions for the magnetically controlled winds of these stars. This information should then motivate future theoretical work involving consistent treatment of diffusion in the presence of magnetic fields and stellar winds. Finally, estimates of the masses of the above stars should shed some light on the important problems relating to the evolutionary status of the helium-strong stars discussed above.

The remainder of this work will be presented in the following fashion. Chapter 2 will describe the spectral and magnetic observations and the methods of reducing these data to a form suitable for the desired modelling. A detailed discussion of the line synthesis program outlined briefly above will be given in Chapter 3. In Chapters 4 through 7 the resulting models for each program star will be presented along with a summary of previous observations. The two non-variable stars,  $\delta$  Ori C and HD 58260 will be presented together, while separate chapters will be devoted to HD 64740,  $\sigma$  Ori E, and HD 37776. A discussion of the results and suggestions for future work will be contained in the final chapter.

## CHAPTER 2 OBSERVATIONS

### 2.1 Spectroscopy

Spectra for this project were obtained at the Canada-France-Hawaii 3.6 m telescope (CFHT) during a six night observing run in 1986 January. The first night of the run was unusable because of high humidity and the final one-half hour of the last night was lost due to high winds. Four of the five usable nights were of photometric quality, with seeing better than one arc second. The f/7.4 camera was used with the 600 lines per millimeter (lpmm) grating in first order and the 1872 diode Reticon detector (Campbell et al. 1981). The 600 lpmm grating was chosen in preference to the 830 lpmm grating in second order mainly for the greater wavelength coverage it gives, but using it also permitted considerably shorter exposures for the desired signal-to-noise level (approximately 300) than would be required with the 830 lpmm grating. Used in first order, the 600 lpmm grating gives a dispersion  $6.7 \text{ \AA mm}^{-1}$  ( $0.101 \text{ \AA pixel}^{-1}$ ), and therefore a spectrum about 180  $\text{\AA}$  long with 0.3  $\text{\AA}$  resolution. Two spectral windows were observed for each of our program stars and several comparison standards. The region  $\lambda\lambda 4400-4580$  was observed because it contains the Zeeman sensitive second multiplet of Si III ( $\lambda\lambda 4552, 4567,$  and  $4574$ ) as well as a strong and a weak helium line (He I  $\lambda\lambda 4470$  and  $4415$ ). Also observed was a region centered on H $\delta$ , extending from 3980 to 4160  $\text{\AA}$ . This window also

contains a Si II multiplet that (combined with the Si III lines) might be used as a temperature indicator, a N II line ( $\lambda 3995$ ), and several more helium lines including the pair He I  $\lambda\lambda 4009$  and  $4026$ . An additional motivation for observing this spectral region was that C. T. Bolton and A. W. Fullerton (University of Toronto) had previously observed many of these same stars in 1984 December near  $H\alpha$  using the same instrumentation but with the 830  $\mu\text{m}$  grating, giving a wavelength coverage of 130  $\text{\AA}$  and 0.144  $\text{\AA}$  resolution. In a related project, they are attempting to model the wind regions of the helium-strong stars, and observations of  $H\delta$  are useful in estimating the actual strength of the emission at  $H\alpha$ . If it is assumed that  $H\delta$  is free of emission (and, at appropriate phases, the previously mentioned shell absorption) then modelling of this line will permit the removal of the photospheric absorption component of the  $H\alpha$  line, leaving only the circumstellar emission. Bolton and Fullerton have pooled their data with that of the author.

A journal of observations is given in Table 2.1. Included is the star observed, the Julian date of the midpoint of each exposure, the exposure duration in minutes, the wavelength window observed, the observers, and the phases determined from an ephemeris appropriate for each star, which is discussed in the following chapters. As can be seen from the table, phase coverage of  $\sigma$  Ori E and HD 37776 is excellent, while it is only fair for HD 64740. This is a result of the period of the latter star being very

Table 2.1 Journal of CFHT Observations

Star	Julian Date (2446000 +)	Duration (sec)	Wavelength Range (Å)	Obs.	Phase
δ Ori C	452.781	1731	4395-4585	DAB/JDL	...
	453.786	1780	3985-4175	DAB/JDL	...
	455.002	3600	4395-4585	DAB/JDL	...
α Ori E	39.850	4200	6500-6630	CTB/AWF	.498
	39.996	2994	6500-6630	CTB/AWF	.621
	40.119	3729	6500-6630	CTB/AWF	.724
	41.849	1544	6500-6630	CTB/AWF	.177
	41.925	1584	6500-6630	CTB/AWF	.241
	41.990	1512	6500-6630	CTB/AWF	.295
	42.036	1526	6500-6630	CTB/AWF	.334
	42.076	1324	6500-6630	CTB/AWF	.367
	42.158	1088	6500-6630	CTB/AWF	.436
	42.935	3000	6500-6630	CTB/AWF	.089
	42.997	3399	6500-6630	CTB/AWF	.141
	44.859	2037	6500-6630	CTB/AWF	.705
	44.911	1819	6500-6630	CTB/AWF	.748
	44.960	1881	6500-6630	CTB/AWF	.789
	45.010	2038	6500-6630	CTB/AWF	.831
	45.058	1432	6500-6630	CTB/AWF	.872
	45.128	2424	6500-6630	CTB/AWF	.930
	450.775	1656	3985-4175	DAB/JDL	.578
	450.874	1533	4395-4585	DAB/JDL	.662
	450.986	2473	3985-4175	DAB/JDL	.756
	451.722	1000	4395-4585	DAB/JDL	.374
	451.792	1310	3985-4175	DAB/JDL	.432
	451.854	2510	3985-4175	DAB/JDL	.485
	451.928	1499	3985-4175	DAB/JDL	.547
	451.981	1290	4395-4585	DAB/JDL	.591
	452.760	1540	4395-4585	DAB/JDL	.245
	452.845	2300	3985-4175	DAB/JDL	.317
	452.930	1870	3985-4175	DAB/JDL	.388
	453.008	2730	4395-4585	DAB/JDL	.454
	453.736	1942	3985-4175	DAB/JDL	.065
	453.807	1540	3985-4175	DAB/JDL	.125
	453.853	1771	4395-4585	DAB/JDL	.163
	453.911	1510	3985-4175	DAB/JDL	.212
454.726	2628	3985-4175	DAB/JDL	.896	
454.817	3170	4395-4585	DAB/JDL	.973	
454.863	3509	3985-4175	DAB/JDL	.011	
HD 37776	39.903	4584	6500-6630	CTB/AWF	.872
	40.057	5264	6500-6630	CTB/AWF	.972
	41.886	2164	6500-6630	CTB/AWF	.160
	42.056	1674	6500-6630	CTB/AWF	.271
	42.134	1937	6500-6630	CTB/AWF	.322
	42.807	2997	6500-6630	CTB/AWF	.759
	42.852	3009	6500-6630	CTB/AWF	.788

continued...

Table 2.1 (continued)

Star	Julian Date (2446000 +)	Duration (sec)	Wavelength Range (Å)	Obs.	Phase
HD 37776	42.899	3000	6500-6630	CTB/AWF	.819
	43.038	4117	6500-6630	CTB/AWF	.909
	44.798	2684	6500-6630	CTB/AWF	.053
	44.884	2230	6500-6630	CTB/AWF	.109
	45.076	2495	6500-6630	CTB/AWF	.234
	450.801	2594	3985-4175	DAB/JDL	.916
	450.849	2207	4395-4585	DAB/JDL	.947
	450.942	2541	3985-4175	DAB/JDL	.007
	451.023	2700	4395-4585	DAB/JDL	.060
	451.744	1870	4395-4585	DAB/JDL	.529
	451.772	1921	3985-4175	DAB/JDL	.547
	451.825	1471	4395-4585	DAB/JDL	.581
	451.900	3100	3985-4175	DAB/JDL	.630
	451.953	1520	4395-4585	DAB/JDL	.664
	452.012	2671	3985-4175	DAB/JDL	.703
	452.708	2460	3985-4175	DAB/JDL	.155
	452.739	1805	4395-4585	DAB/JDL	.175
	452.817	2421	3985-4175	DAB/JDL	.226
	452.899	2580	4395-4585	DAB/JDL	.279
	452.977	2410	4395-4585	DAB/JDL	.330
	453.707	2039	4395-4585	DAB/JDL	.804
	453.762	2241	3985-4175	DAB/JDL	.840
	453.877	2150	4395-4585	DAB/JDL	.915
	453.933	1990	3985-4175	DAB/JDL	.951
	453.959	1421	4395-4585	DAB/JDL	.968
	453.979	1779	4395-4585	DAB/JDL	.987
	454.008	2949	4395-4585	DAB/JDL	.000
454.770	3600	3985-4175	DAB/JDL	.495	
HD 58260	454.910	3609	3985-4175	DAB/JDL	...
	454.958	3600	4395-4585	DAB/JDL	...
HD 64740	40.035	1499	6500-6630	CTB/AWF	.607
	42.094	633	6500-6630	CTB/AWF	.154
	450.887	451	4395-4585	DAB/JDL	.458
	450.921	666	3985-4175	DAB/JDL	.483
	451.876	700	3985-4175	DAB/JDL	.201
	451.968	497	4395-4585	DAB/JDL	.270
	452.864	623	3985-4175	DAB/JDL	.943
	452.878	570	4395-4585	DAB/JDL	.954
	453.823	919	3985-4175	DAB/JDL	.664
453.894	380	4395-4585	DAB/JDL	.718	

\*CTB/AWF = C. T. Bolton and A. W. Fullerton

DAB/JDL = D. A. Bohlender and J. D. Landstreet

close to  $4/3$  of a day, so that the observed phases of the star repeat almost exactly during the short observing window every four days.

The observations obtained in 1986 January were reduced by the author using a modified version of a reduction package developed for CFHT Reticon spectra by Dr. P. K. Barker (University of Western Ontario). Each spectrum consists of the raw stellar exposure (or comparison lamp or flat field) and eight one-second baseline exposures. The first step in the reduction is the subtraction of the averaged baselines from the raw spectrum. Next, the baseline-subtracted stellar spectrum is divided by a flat-field lamp spectrum to correct for the small pixel-to-pixel variations in sensitivity and amplitude gain. The lamp consists of a 500 W quartz-iodide lamp that is mounted before the last folding mirror of the coude mirror train. An adjustable pupil in the beam produces a flat-field input beam similar to that produced by a star. Four flat field exposures of ten second duration were recorded at the end of each set of observations made at one grating setting. This gives a signal-to-noise value for each flat-field exposure comparable to that of the stellar exposures themselves. The flat-field exposures are then baseline corrected and averaged before dividing the stellar exposures by the averaged flat-field.

The next step is a determination of the wavelength scale of the spectra. An iron-argon comparison lamp was

observed at the beginning and end of each set of exposures at a given grating setting. The usual exposure time was ten seconds. The wavelength-pixel relation is then determined by fitting a third order polynomial to the measured pixel numbers of several well-exposed lines of the comparison lamp spectrum covering the entire wavelength range. The polynomial fit is then used to calculate the wavelength corresponding to each pixel in the observed spectrum. A correction is then applied to this wavelength scale to convert it to a heliocentric frame of reference. The wavelength scales derived from comparisons taken at the start and end of each set of exposures at a particular grating setting differ typically by only 0.02 Å, and at most, 0.1 Å in the blue wavelength region on a few occasions. This indicates that any flexure of the spectrograph is minimal during each three or four hour period.

The final step in the data reduction is the continuum fitting. Normally, this procedure consists of specifying a number of 1 Å sections of the stellar spectrum that are free of lines and distributed at approximately equal intervals (usually 10 Å in this work). The intensities in these wavelength regions are averaged and a polynomial of a specified order is fitted to these average continuum points. The stellar spectrum is then divided by the continuum curve derived from the polynomial fit to produce a flattened spectrum, normalized to a continuum level of 1.0.

This continuum fitting was originally thought to be a rather straightforward procedure for these hot stars, since the total number of lines present is small, and this indeed was the case for the  $\lambda\lambda 4400-4580$  spectral region. Here, a sixth-order polynomial fit to continuum points spread throughout the spectrum produces a sufficiently flat spectrum. This was not the case for the spectral window centered on H $\delta$ . In addition to a gradual continuum slope from blue to red, the continua of spectra taken in this region show significant additional curvature in several localized regions. The overall continuum slope is caused by the fact that the flat field lamp is considerably cooler than the stars observed, hence the divided stellar spectrum is more intense at the blue end. The localized dips in the continuum are not as easy to explain, but are probably caused by defects in the interference coatings of the coude mirrors. One future solution to this problem would be to use the illuminated inside of the telescope dome as the flat field source so that the light from both star and flat field exposures follows the same light path to the detector.

Another method, the one used here, is to change the continuum fitting routine. After much experimenting, the usual polynomial fit to the continuum was discarded. With a manageable number of continuum points tenth-order fits were able to smooth the problem areas in the continuum but only at the expense of other regions that were formerly well-behaved. An attempt was also made to fit the continuum

by splitting the spectrum into several shorter wavelength regions and fitting each separately. This was not very successful. Instead, it was found that almost any continuum can be fit very well by using cubic spline interpolation (Burden, Faires, and Reynolds 1981) to fit the continuum. In this method, piecewise smooth cubic splines are fitted between the averaged continuum points. The stellar spectrum is then divided by the continuum so that the spectrum is normalized to a continuum level of 1.0. An example of a completely reduced spectrum is given in Figure 2.1. The continuum is very flat. Note that the final reduced spectra have not been smoothed in any way.

The CFHT data obtained in 1984 December were reduced by Bolton and Fullerton. Obviously, the details of their observing routine and data processing differ somewhat from the above procedure. The most noteworthy difference is that their final spectra have been smoothed by filtering out high-frequency noise in the frequency domain.

Time constraints permitted repeated observation of only one of the chosen standard stars in the blue spectral range, and none in the red region. However, one helium-strong star with low  $v \sin i$  and constant magnetic field,  $\delta$  Ori C, was observed twice at the red wavelength setting. Since this star is presumably a slow rotator with a period much greater than 6 days, or viewed pole-on, large spectral variations are not expected. The two spectra of  $\delta$  Ori C in the red region are indistinguishable at the noise level of the



observations. However, in the blue region the H $\delta$  profiles display a difference in depth of a few percent. The reason for this is not known. A possible contributing factor could be a shift in the wavelength calibration, although these have already been shown to be small. Overall, it is believed that the coude spectrograph instrumentation and the data reduction techniques are reasonably well-behaved and give reproducible spectra.

## 2.2 Magnetic Field Observations

The magnetic field observations for the program stars have been previously published (Landstreet and Borra 1978; Borra and Landstreet 1979; Thompson and Landstreet 1985; Bohlender et al. 1987). However, for completeness, a short discussion of the available data will be presented here.

The magnetic data were obtained at three sites: the du Pont 2.5 m telescope of Las Campanas Observatory, the 1.5 m telescope of Palomar Observatory, and the University of Western Ontario 1.2 m telescope. In all instances the instrument used was the U.W.O. photoelectric Peckels cell polarimeter, or the virtually identical instrument of Laval University. The instrument and observing techniques are discussed in detail elsewhere (e.g. Landstreet 1980, 1982; Borra and Landstreet 1977). Briefly, the circular polarization in the line wings of H $\beta$  or He I  $\lambda$ 5876, caused by the longitudinal Zeeman effect, is measured by using tilt-tuned interference filters set on the short and long

wavelength wings of the relevant line. The filters used have HPBW's of 5 Å and 2.8 Å for Hβ and He I λ5876, respectively. The polarization is measured several times (usually six to eight observations of about fifteen minutes duration each), alternating between the short and long wavelength wings. This eliminates most possible effects of instrumental polarization.

The combined polarization measurements for a single star are converted to a longitudinal magnetic field, B<sub>l</sub>, using the relation (Bray and Loughhead 1964; Landstreet 1982)

$$(V_r - V_b)/2 = 4.67 \times 10^{-13} z B_l \lambda^2 \{dI(\lambda)/d\lambda\} / I(\lambda) \quad (2.1)$$

where V<sub>r</sub> and V<sub>b</sub> represent the fractional circular polarization in the long and short wavelength wings respectively, z is the Landé factor of the line (Babcock 1962), λ is the wavelength and I(λ) is the profile observed. The line profile is obtained by using the polarimeter as a two-channel photoelectric scanner. One filter is set on the stellar continuum near the line while the other is tilt-tuned to various wavelengths over a total range of about 40Å. Then the procedure is repeated with the roles of the filters reversed. The ratio of photon counts in the two channels as a function of wavelength yields directly the line profile.

For Hβ, which has a central depth of about 0.7 of the continuum through the 5 Å filters, it is accurate enough to draw a freehand curve through the observed points and



measure the value of  $dI/d\lambda$  from the drawing. For the He I  $\lambda 5876$  line, which has a central depth of about 0.9 of the continuum for helium strong stars, the scatter in the observed points makes such a procedure less accurate.

Instead, the profile is rectified using continuum points on both sides of the line, the rectified profile is fitted with a gaussian (this is actually usually quite a good approximation, especially in the line core), and then  $I$  and  $dI/d\lambda$  are evaluated numerically at the points in the profile where observations were made.

Errors  $\sigma_B$  for the magnetic measurements are computed from photon counting statistics and are typically on the order of 300 G. An additional source of error not included in  $\sigma_B$  is a possible overall scale of 10 or 20% in  $B_1$  values due to inaccuracy in  $I(\lambda)$  or in equation (2.1).

• The  $H\beta$  magnetic observations have been supplemented with observations using the He I  $\lambda 5876$  line in an attempt to map the surface distribution of helium by comparing magnetic curves obtained with (assumed) uniformly distributed hydrogen with the curves determined from  $\lambda 5876$ . It has long been known (Deutsch 1958, Pyper 1969) that magnetic field curves are affected, not only by the effective longitudinal field but also by nonuniform distribution of the element used to measure the field. In principle, measurements of  $B_1$  using lines of various elements can provide important constraints for abundance distribution geometries of variable elements (Michaud, Mégessier, and Charland 1981).

However, as will be seen later, in the case of the helium-strong stars, the magnetic observations obtained from H $\beta$  and He I  $\lambda$ 5876 yield nearly identical values. This suggests that although helium is certainly unevenly distributed on the surfaces of these stars, the contrast in line strength between regions of high and low abundance is small.

As has already been noted, many of the helium-strong stars show magnetic field variations with the same period as the photometric or spectrum variations. In most cases it is possible to fit the magnetic observations with the equation

$$B_1 = B_0 + B_1 \sin 2\pi(\phi - \phi_0) \quad (2.2)$$

where the phase,  $\phi$ , is determined from the period and an appropriate reference time for each star. The reduced chi-squared deviation of the fit of the data to the best curve is usually less than two (e.g. Bohlender *et al.* 1987).

Table 2.2 contains a summary of the photoelectric, magnetic field observations of the helium-strong stars considered in this thesis. Included for each star is the period (Thompson and Landstreet 1985; Bohlender *et al.* 1987), the observed magnetic field extrema, and the parameters of the field curve fit defined in equation (2.2). As can be seen from the table, each of the program stars has a significant magnetic field, with maximum field strength magnitudes ranging from  $\sim$ 900 G for HD 64740 to 3400 G for  $\delta$  Ori C. The interesting magnetic field variation of HD 37776 (Thompson and Landstreet 1985) can not be modelled satisfactorily by a curve of the form of equation (2.2).

Table 2.2 Summary of Magnetic Field Measurements

Star	Period $\pm \sigma_p$ (d)	$B_p$ extrema (G)	$B_p$	$B_l$ (G)	$\phi_p$
$\delta$ Ori C	... <	-3400, constant	...	...	...
$\sigma$ Ori E	1.19081 $\pm$ .00001	+2810 to -1490	660	2150	0.474
HD 37776	1.53869 $\pm$ .00007	+2540 to -2180	...	...	...
HD 58260	...	+2300, constant	...	...	...
HD 64740	1.33026 $\pm$ .00006	+490 to -890	-200	690	0.250

The magnetic field of this star will be discussed in some detail in chapter 7.

## Chapter 3 The Line Synthesis Program

### 3.1 Overview

This thesis is based on work carried out using modified versions of a line synthesis program developed by J. D. Landstreet (1988). A short summary of the program, here referred to by the name *ZEEMAN*, will be given first, followed by detailed descriptions of the various input parameters, and subroutines that make up the program. The code is written in Fortran 77, and most calculations were performed on the University of Western Ontario's Control Data Corporation Cyber 835 computer. Some use has also been made of the new UWO ETA10-P supercomputer, as well as the CRAY supercomputer at the Ontario Center for Large-Scale Computation.

Briefly, *ZEEMAN* calculates the integrated intensity and polarization profiles of spectral lines for an assumed model atmosphere, magnetic geometry, and surface abundance distribution, in a spectral region defined by the user. The program first reads in various data needed to perform the above calculations. These include atomic masses, ionization potentials, and ground state multiplicities, as well as expansion coefficients for the calculation of partition functions at temperatures appropriate for the program stars. Previously published stellar atmospheres (Klinglesmith 1971; Kurucz 1979) give the required run of temperature, density,

and electron number density with depth in the atmosphere needed to perform the line profile modelling. A spectral window of from 2 to 50 Å is defined by giving a reference wavelength and the number of wavelength points to calculate. Atomic data for the lines to be modelled in this region are read in by the program. Finally, information concerning the surface abundance and magnetic field geometries is given. These data specify the inclination of the star's rotation axis, the obliquity of the magnetic axis, the polar field strengths of the multipoles representing the magnetic field, the location and local abundances of any abundance patches for the elements to be modelled, and the rotational phases at which model profiles are to be calculated.

The subroutine *COMPON* is next called by the main program to calculate the relative splitting and strengths of the lines being modelled using the *LS* coupling approximation and the input line data. The subroutine *LTELC* then determines the line-to-continuum opacity ratios, and line damping constants at each depth in the model atmosphere, for each line being modelled in the specified wavelength window.

The remainder of *ZEEMAN* acts as an integration routine. The visible hemisphere of the star is divided into 60 areas of approximately equal area. For each area, a call to the routine *MAGFLD* uses the magnetic geometry data to calculate the local value of the surface magnetic field. The local abundance is found using the subroutine *ABZSP*, which, given the specified abundance geometry, determines whether the

current surface element is located within an abundance patch or has the default abundance given for the element in question. This subroutine also uses the local value of the magnetic field to determine the wavelength positions of the various Zeeman components of each line relative to the reference wavelength. The bulk of the computational work is then performed by the subroutine *LINPRO*, which calculates the intensity and polarization profiles of each line in the spectral region being modelled, allowing for the local value of the surface abundance of the elements under investigation and the splitting of the spectral lines caused by the surface magnetic field. The local profiles are then summed over the entire hemisphere of the star after giving each area the required rotational Doppler shift. The final profile is then broadened with an approximate instrumental profile.

Details of the required input data and the individual components of *ZEEMAN* are given in the next five sections of this chapter.

### 3.2. Input Data

Required atomic data for the first 72 elements in the periodic table are stored in a file and read by the program *ZEEMAN*. These include the atomic number and mass, a default abundance for each element, the ionization potentials of the first four ionization states of each element, and the ground state multiplicities of the first five ionization states.

Partition functions needed in determining the populations of each ionization state of an element at each depth in the atmosphere are calculated using the polynomial fit by Bolton (1970, 1971). In this approximation, the temperature dependence of the partition function,  $u$ , is given by a polynomial of the form

$$\ln(u - g_0) = \sum a_i (\ln \theta)^i \quad (3.1)$$

where  $g_0$  is the ground state multiplicity,  $\theta = 5040/T$ , and  $T$  is the temperature. For the helium-strong stars most of the dominant 'metal' lines are produced by ions of Si III, N II, O II, Mg II, and C II at temperatures exceeding 30000 K, for which appropriate polynomial approximations could not be found in the literature. The author has therefore made rough estimates of the relevant partition functions by using equation (3.1) and approximately 20 of the lowest energy levels of each ion. This gives an adequate estimate of  $u$  since the spacing of the lower energy levels for these species is quite large. The derived polynomial coefficients are given in table 3.1. A second data file containing a tabulation of the various  $a_i$ 's, needed for the calculation of the partition functions, is then read in by the main program.

Next, the number of lines for which profiles are to be synthesized is specified, as well as a reference wavelength for the spectral window to be modelled. For each line to be modelled, the atomic number, ionization level, wavelength, quantum numbers  $S$ ,  $L$ , and  $J$  for the lower and upper levels

Table 3.1 Derived Coefficients of the Polynomial  
Approximations of Partition Functions

<u>Ion</u>	<u><math>g_0</math></u>	<u><math>a_0</math></u>	<u><math>a_1</math></u>	<u><math>a_2</math></u>	<u><math>a_3</math></u>	<u><math>a_4</math></u>
N II	1.0	2.05643	-0.07780	0.06081	0.00848	0.00894
O II	4.0	-5.37764	-7.79586	-3.60092	-0.90796	-0.09237
Mg II	2.0	-8.42278	-10.21219	-5.08317	-1.63097	-0.21961
Si III	1.0	-12.96870	-15.26566	-7.41686	-1.98781	-0.21203

of the transition, oscillator strength  $gf$ , and the excitation energy of the lower level must be read in by *ZEEMAN*. The wavelengths and quantum numbers are from Moore (1945), while the excitation energies are from Moore (1949) and Wiese, Smith, and Glennon (1966). Oscillator strengths and their sources for the most important lines examined in this work are given in table 3.2.

In this version of *ZEEMAN* the wavelength window to be modelled is specified by three parameters: the reference wavelength given above, the number of wavelength points to be modelled, and the resolution of the model profile. The adjustable resolution was added by the author to permit more economical modelling of the Stark-broadened  $H\delta$  and He I  $\lambda 4471$  profiles. Because of the large range of  $v \sin i$  for the program stars (from about  $10 \text{ km s}^{-1}$  to  $> 100 \text{ km s}^{-1}$ ) the wavelength region modelled ranges from 2 Å to 6 Å for isolated metal lines, 20 Å for He I  $\lambda 4471$ , and 50 Å for  $H\delta$ . For metals and He I  $\lambda 4437$ , the line profile is modelled at 0.01 Å intervals, while a resolution of 0.1 Å is employed for the hydrogen and helium  $\lambda 4471$  lines. Using the finer wavelength spacing for the latter lines would have been prohibitively expensive in terms of CPU time. The above wavelength spacings provide sufficient resolution of each element's intrinsic profile at temperatures appropriate for the stars examined in this work (18000 K - 25000 K), except perhaps in the cores of  $H\delta$  and He I  $\lambda 4471$  where non-LTE effects are likely to be important anyway.

Table 3.2 Oscillator Strengths

Multiplet	$\lambda$	$\log gf$	Reference*
H $\delta$			
	4101.737	-0.7527	WSG
He I			
	4437.550	-2.034	WSG
	4471.477	0.052	WSG
N II			
12	3994.996	0.28	WSG
O II			
5	4414.909	0.305	WSG
	4416.975	0.044	WSG
Si III			
2	4567.872	-0.07	WM
2	4574.777	-0.41	WM

\*WSM = Wiese, Smith, and Glennon (1966)

WM = Wiese, and Martin (1980)

The reference wavelength for the spectral window to be modelled represents either the blue end of the region to model or the center of the line. Blending is not as serious a problem for these early B stars as it is for the cooler Ap stars, so in cases where an individual, symmetric line is being modelled, the author has modified ZEMAN so that only one half of the local profile at each surface element of the star is synthesized. In this case the reference wavelength is the center of the line, and the computation time is reduced by a factor of almost two. The rest of the profile is obtained by a suitable reflection around the center of the line: i.e. the Stokes parameters, I, Q, and U, are symmetric around the line center, while V is antisymmetric.

A model atmosphere gives the run of temperature, mass-density, and electron number density as a function of the standard optical depth,  $\tau_{5000}$ , for a specified number of depths, usually 30. The continuum opacity at the reference wavelength and the Planck function are then calculated at each level in the atmosphere. Landstreet's original code included only electron scattering, bound-free and free-free absorption from neutral hydrogen, and negative hydrogen ions as continuum opacity sources. Because of the higher temperatures of the helium-strong stars the continuum opacities of neutral, singly and doubly ionized helium have been added by the author.

Kurucz's (1979) solar abundance model atmospheres have been employed in this work. A simple linear interpolation,

first in temperature, and then in  $\log g$  has been used to generate atmospheres on a finer grid suitable for estimating the effective temperatures and surface gravities of the program stars. Of course, the anomalous helium abundance of the helium-strong stars makes the use of Kurucz's solar abundance atmospheres somewhat inaccurate. Some use has therefore been made of the helium-rich (but unblanketed) atmospheres of Klinglesmith (1971) in determining the effects of these inconsistencies in helium abundances in the model atmospheres and in the assumed surface abundances of the helium-strong stars considered in this investigation.

The essential difficulty is that Kurucz's (1979) model atmospheres have  $e_{\text{H}} = 0.90$  ( $e_j \equiv N_j / [\sum_j N_j]$  where  $N_j$  is the number density of the element  $j$ ), but helium line profiles in the helium-strong stars must be modelled using different and non-uniform abundances. To give an idea of the magnitude of the error resulting from this problem the following test has been performed. Using Klinglesmith's (1971) grid of  $\log g = 4.0$ ,  $T_{\text{eff}} = 20000$  K atmospheres for four different mass fractions (0.9836, 0.8570, 0.3333, and 0.0) of helium, profiles for H $\delta$ , He I  $\lambda 4437$ , and He I  $\lambda 4471$  have been calculated. Then, for these four helium abundances, the same lines have been synthesised using Kurucz's  $T_{\text{eff}} = 20000$  K atmospheres with  $\log g = 4.0$  and  $\log g = 4.5$ . The resulting equivalent widths are given in table 3.3. The effect on the profiles of He I  $\lambda 4437$  are fairly small. On the other hand, for H $\delta$  and He I  $\lambda 4471$ ,

Table 3.3 Computed equivalent widths ( $\lambda$ ) of hydrogen and helium line profiles for various model atmospheres.

Line	Atmosphere: c <sub>He</sub>	Klinglesmith		Kurucz	
		log $\kappa = 4.0$	log $\kappa = 4.0$	log $\kappa = 4.5$	log $\kappa = 4.5$
H $\delta$	0.9375	3.518	2.272	2.921	
	0.5997	6.002	4.500	5.642	
	0.1111	5.968	5.817	7.076	
	0.0000	5.744	6.025	7.289	
He $\lambda 4471$	0.9375	5.628	4.037	4.711	
	0.5997	4.316	3.444	4.058	
	0.1111	1.753	1.802	2.173	
He $\lambda 4437$	0.9375	0.553	0.400	0.452	
	0.5997	0.409	0.339	0.382	
	0.1111	0.154	0.162	0.172	

Klinglesmith's  $T_{\text{eff}} = 20000$  K,  $\log g = 4.0$  atmosphere with  $\epsilon_{\text{He}} = 0.60$  gives profiles that have much larger equivalent widths than those calculated using Kurucz's atmosphere with the same  $\log g$  and  $T_{\text{eff}}$ , and the same helium abundance in the line. This effect is easily explained by the differences in opacities between the two grids of atmospheres. Helium-rich atmospheres have a substantially reduced continuous opacity, which results in line profiles being formed deeper in the atmosphere and therefore at higher pressures than in normal atmospheres. Comparison of the two grids of atmospheres shows that  $T(\tau)$  is virtually unchanged. Norris (1971) has discussed this problem in the context of the helium-weak stars. In that case, the use of normal atmospheres, results in an underestimate of the surface gravity. Here, an examination of table 3.3 suggests that the surface gravity is overestimated by roughly 0.5 dex, if the actual helium abundance is approximately  $\epsilon_{\text{He}} = 0.50$  and uniformly distributed. Hunger (1975) has also discussed these modelling difficulties in some detail.

Most previous detailed analyses of helium-strong stars have incorporated helium-rich atmosphere models (Hunger and Kaufmann 1973; Wolf 1973; Higginbotham and Lee 1974; Kaufmann, Schönberner, and Rahe 1974; Osmer and Peterson 1974; Kaufmann and Hunger 1975; Lee and O'Brien 1977; Groote and Hunger 1982), but only Groote and Hunger (1982) modelled variations in helium line strengths (for  $\sigma$  Ori E). They modelled the line variations by fitting a uniform helium

content over the entire visible surface of the star to the observed line strengths at each phase and found that the derived  $\epsilon_{He}$  varied from 0.38 to 0.75.

It would be preferable to model line profiles of the helium-strong stars by incorporating atmospheric models with helium abundances consistent with the local abundances of each area element on the stellar disk. However, since generating a sufficiently fine grid of such atmospheres was not possible at this time, it was decided that Kurucz's atmospheres would be used exclusively in the analysis of the program stars. It is expected that the most significant error that will arise from this inconsistency in the modelling is an overestimate of the surface gravity on the order of a few tenths of a dex or less. An allowance will be made for this error in the surface gravities determined for each star.

### 3.3 Subroutine COMPON

The Zeeman pattern and relative strengths of each line are calculated using the LS coupling approximation, using LS quantum numbers from the Revised Multiplet Table (Moore 1945). The resulting intensities and separations of the various  $\sigma$  and  $\pi$  Zeeman components for the important Si III multiplet 2 lines are shown in figure 3.1. The effective Landé  $g$  values ( $g_{eff}$ ) for these lines are 1.25 ( $\lambda 4552$ ), 1.75 ( $\lambda 4567$ ), and 2.0 ( $\lambda 4574$ ). The ranges in the  $g_{eff}$  values and in the complexity of the Zeeman patterns of these lines make

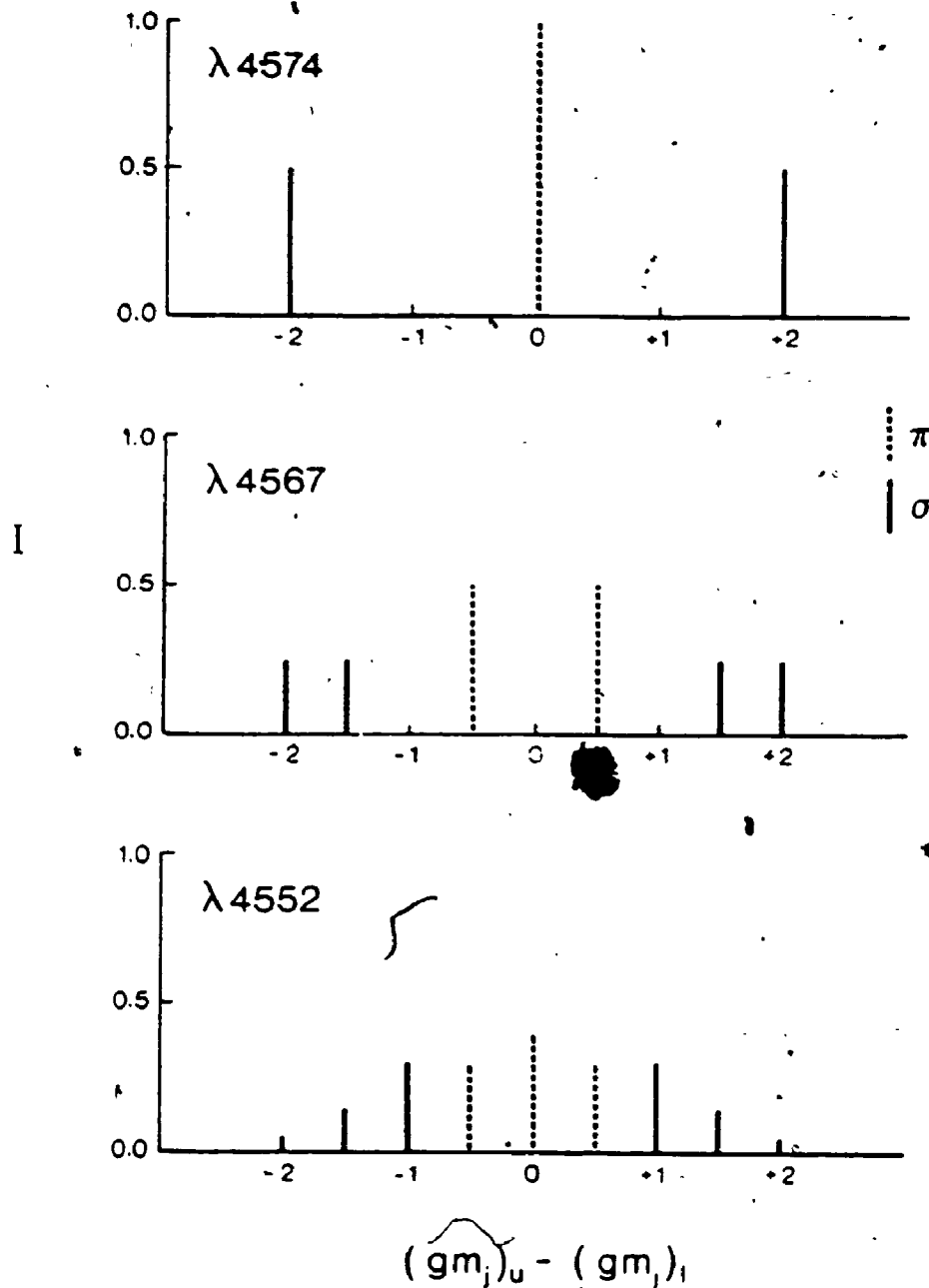


Figure 3.1 Relative Zeeman intensities and splittings of the Si III multiplet 2 lines. The  $\sigma$  and  $\pi$  components are given by the solid and broken lines respectively. The  $(gm_j)_u$  are the multiplicities and magnetic quantum numbers of the upper and lower levels of the transition responsible for each Zeeman component.

them the most sensitive indicators of surface magnetic field strengths in the temperature range of the helium-strong stars. A discussion of the use of these lines in constraining the surface magnetic field geometry is presented later in this chapter.

#### 3.4 Subroutine LTELC

The subroutine *LTELC* determines the line-to-continuum opacity ratios for each line being modelled, as well as the damping parameters at each depth in the model atmosphere. Local thermodynamic equilibrium (LTE) has been assumed in calculating line strengths. At  $T_{\text{eff}} \approx 25000$  K this is a reasonably good assumption for helium and hydrogen (Auer and Mihalas 1973; Heasley and Wolff 1983) except in the line cores. However, non-LTE effects are important for Si III, N II, and O II (Kamp 1973, 1978; Dufton and Hibbert 1981; Brown, Dufton and Lennon 1988) in that non-LTE line profiles result in lower abundances than would be obtained for LTE calculations. Estimates of the abundance errors resulting from ignoring non-LTE effects will be discussed where appropriate.

The relative number of ions in the first five ionization states are determined by the Saha equation for each element in the line list being modelled. If partition function data (see section 3.2) for the element under consideration are available, then equation (3.1) is used to determine the partition function at each depth in the

atmosphere. Otherwise, the ground state multiplicities are used as an approximation of the partition function. The line-to-continuum opacity ratio is then calculated at the center of each line for the default abundance of each element.

In modelling the line profiles, the classical radiation damping constant has been used. It is assumed that the magnetic field suppresses turbulent motions, and so the microturbulence has been set equal to zero. Collisions with neutral hydrogen are treated using the Unsöld approximation for van der Waals broadening (Aller 1963, art. 7-5) or the results of Deridder and van Rensbergen (1976), depending on which theory gives the larger damping constant. For metals, the quadratic Stark effect is calculated using the approximations of Cowley (1971).

As already noted, Landstreet's original code has been modified to permit modelling of hydrogen and helium line profiles. Stark broadening of H $\delta$  is calculated using the unified theory of Vidal, Cooper, and Smith (1973). At each depth in the atmosphere their tabulated Doppler broadened Stark profiles are used to interpolate the local profile using a cubic-spline interpolation scheme. H $\delta$  is treated as a single line. The resulting profiles have been compared with those tabulated by Kurucz (1979). The line shapes and equivalent widths for various  $\log g$  and  $T_{\text{eff}}$  agree within a factor of a few percent, being somewhat deeper for the present models. This can be understood in terms of

differences in the continuum opacities used for the two calculated profiles. Kurucz's (1979) model atmospheres include line blanketing effects of metals, but this additional continuum opacity source has been ignored in this work, with the result that the reduced continuum opacity leads to somewhat stronger line profiles.

The quadratic Stark effect for the isolated helium line  $\lambda 4437$  has been modelled using the simple theory of Griem et al. (1962). This line can be approximated by shifted dispersion profiles for electron densities  $< 10^{18} \text{ cm}^{-3}$  (always the case in the line formation regions of the program stars). The impact half half-widths are then given by

$$h = w(1 + 1.36\alpha^8 / 9\sigma^{-1/3})$$

and the shift,  $s$ , in  $\text{\AA}$  by

$$s = d \pm 2.36w \alpha^8 / 9\sigma^{-1/2}$$

(e.g. Leckrone 1971), where the parameters  $\sigma$ ,  $\alpha$ ,  $d$ , and  $w$  are tabulated by Griem et al. (1962). The diffuse line  $\lambda 4471$  is treated using the broadening theory of Barnard, Cooper, and Smith (1974). Their grid of Stark profiles for hydrogen perturbers is interpolated using the same cubic spline interpolation employed for the H $\delta$  profiles. Fine structure splitting of the 23P level is ignored for electron densities less than  $10^{13} \text{ cm}^{-3}$ . The synthesized  $\lambda 4471$  profiles are in good agreement with theoretical profiles calculated using the same broadening theory and published by Mihalas et al. (1974). The  $\lambda 4437$  line modelling has been

tested by fitting this line in the spectra of several normal, early B stars, including Gamma Peg and  $\tau$  Sco. In all cases, using normal helium abundances ( $\epsilon_{\text{He}} = 0.1$ ) and published temperatures and gravities for the standard stars, the observed and modelled profiles are virtually indistinguishable. Several other helium lines are visible in the spectra of the program stars, but have not been included in this analysis because of blending problems.

### 3.5 Disk Integration

After reading in the necessary model data the program proceeds to function as a surface integration routine. The stellar disk is divided into four concentric rings of equal projected radial width, which are in turn divided into a total of 60 roughly equal projected surface areas. For each surface area element, the program then calculates the local magnitude and direction of the magnetic field, the local abundances, the resulting intensities and wavelength positions of the Zeeman patterns of all lines being investigated in the specified wavelength window, and the local emergent Stokes parameters as a function of wavelength. These individual processes are described below.

Once the above calculations have been performed for each sampled disk point, the program sums all the local components of the Stokes parameters, each weighted according to the fractional area of the total disk which it samples, after giving each component the appropriate Doppler shift

determined from a specified value of  $v \sin i$ . The entire disk integration is then repeated for a number of rotational phases.

### 3.5.1 Subroutine MAGFLD

The magnetic field geometry employed in this work is assumed to be axially symmetric, and can include a combination of colinear dipole, linear or two-dimensional quadrupole, and linear octupole fields, or can consist of a dipole decentered along its axis. A uniform surface field can also be incorporated in the model. The magnetic field is defined by its inclination to the rotational axis,  $\beta$ , the polar field strengths of its constituent components, and, in the case of the decentered dipole, the decentering parameter,  $a$ , of the dipole along its axis as a fraction of the stellar radius.

### 3.5.2 Subroutine ABZSP

Unlike the recent work of Landstreet (1988) for  $\delta$  Cam, the author has not confined the surface abundance geometries of the helium-strong stars to be axisymmetric around the magnetic axis. Early work on the helium-line profiles of the helium-strong stars suggested that the observed line profile variations could not be adequately modelled by such a geometry. Instead, for most of this work, the surface abundances of the various elements are specified by an arbitrary number of circular spots. The position and size

of each spot for each element is specified by the location of its center relative to the magnetic pole visible at  $\phi = 0$ , and its radius; that is, its magnetic colatitude and longitude relative to the pole visible at  $\phi = 0$ . (The magnetic longitude is defined to be  $90^\circ$  on the arc joining this magnetic pole and the nearest rotational pole.) The geometry is illustrated in figure 3.2. Also required by the subroutine are the abundances in each spot. These data for the spots of each element are stored in an array. Then, for each integration area on the stellar surface, and for each element, the subroutine *ABZSP* searches through this array in sequence and determines whether or not the current area is within one of the spots. If it is not, or if the element in question has a uniform surface abundance, the previously defined default abundance of the element is assumed. Such a geometry permits individual spots or bands of enhanced or depleted abundances to be modelled with an appropriate number of distinct or overlapping spots. For example, an equatorial band  $60^\circ$  wide and with a factor of ten overabundance of a given element relative to the rest of the star can be defined by two spots, each centered at the same magnetic pole: the first spot will have a radius of  $120^\circ$  and an abundance ten times greater than the second spot with radius  $60^\circ$  and the default abundance of the element. In order to keep the number of free parameters to a minimum, the line profiles of the program stars have been modelled using the smallest number of spots necessary to give an

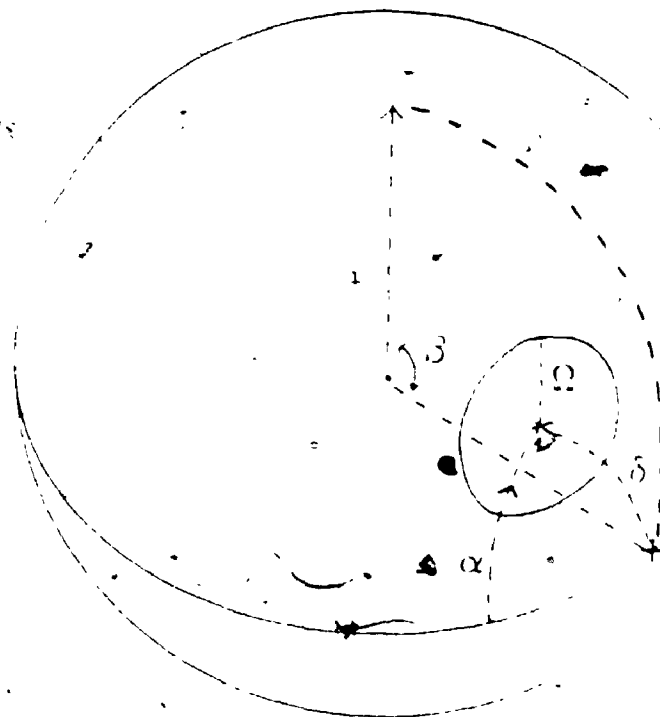


Figure 3.2 Illustration of the abundance and magnetic field geometry used in the program ZEEMAN. In this example, the rotation axis is indicated by the symbol  $\cdot$  and the magnetic pole by the symbol  $+$ . The angles  $i$  and  $\beta$  are the inclination of the rotation axis and the obliquity of the magnetic axis respectively. The magnetic colatitude is defined by the angle  $\delta$  and the magnetic longitude by  $\alpha$ . The longitude is defined as  $90^\circ$  on the arc between the rotation and magnetic poles visible at  $\phi = 0$  (indicated) and is measured in the direction shown. The radius of the spot is given by  $R$ .

5

adequate fit. In most cases two abundances patches (giving two spots or one band) are sufficient.

Using the local value of the magnetic field as determined by the subroutine *MAGFLD*, *ABZSP* then determines the local wavelength positions of the various Zeeman components of each spectral line relative to the reference wavelength of the spectral window. The subroutine then calculates the line-to-continuum opacities at the center of each component using the values previously found in *LTELC* for the default abundances, the intensities of the individual Zeeman components calculated by the subroutine *COMPON*, and the local abundances.

### 3.5.3. Subroutine *LINPRO*

The subroutine *LINPRO* performs the most CPU intensive portion of the line profile calculation, namely the integration of the coupled equations of transfer that describe the transfer of polarized radiation through a stellar atmosphere; at each area element of the stellar surface, and over the specified wavelength window at the required resolution. Many treatments of the radiative transfer of polarized light have appeared in the literature (e.g. Unno 1956; Hardorp, Shore, and Wittmann 1976). It is necessary to calculate the polarized line-to-continuum opacity ratios  $\eta_I$ ,  $\eta_Q$ , and  $\eta_V$ , of the *I*, *Q*, and *V* Stokes components as a function of wavelength and depth in the atmosphere. Anomalous dispersion has been neglected in this

calculation.

Except for hydrogen, the opacity ratios for each line in the spectral window are calculated using the numerical prescription for the Voigt profile calculation given by Baschek and Scholz (1982), and the damping constants determined by the subroutine *LTELC*. The interpolated hydrogen Stark broadening profiles have already been convolved with appropriate Voigt functions (Vidal, Cooper, and Smith 1973). The resulting opacity ratios are summed over all lines and Zeeman components to yield the total ratios  $\eta_I$ ,  $\eta_Q$ , and  $\eta_V$  as functions of wavelength.

To integrate the equations of transfer, *LINPRO* incorporates the efficient numerical technique of Martin and Wickramasinghe (1979), which treats the coupled equations of transfer as having constant coefficients between tabulated depths in the atmosphere. With this approximation the analytical solution of Unno (1956) is used to evaluate the values of the Stokes parameters at a given depth in the atmosphere by using the values determined at the previous depth. The coefficients of the equations are assumed to be the average values between the two depths. The equations of transfer are then integrated outward from the shallowest level in the atmosphere for which  $\tau$  is greater than 10. Unpolarized blackbody radiation is assumed for the lower boundary condition.

### 3.6 Subroutine *SPPROF*

The resulting polarized intensity profiles are convolved with a simple triangular instrumental profile of  $\text{FWHM} = 0.30 \text{ \AA}$  to allow for the finite-resolution of the spectrograph.

Because of the rather coarse surface grid used in modelling the line profiles, and the large  $v \sin i$  values for some of the program stars, there is considerable ripple apparent in the final modelled profiles. This distortion arises because of the large difference in the projected radial velocities of adjacent rings in the surface grid. To remove the effect, the author has modified *SPPROF* so that it carries out a second convolution with a triangular profile with  $\text{FWHM}$  equivalent to one-quarter of the  $v \sin i$  of the star for stars with  $v \sin i$  greater than  $50 \text{ km s}^{-1}$ . This smoothing removes the ripple without affecting the overall shape of the line profile or the equivalent width of the line.

### 3.7 Additional Programming Considerations

For reasons of economy, much of the early modelling of the helium-strong stars was performed with a simplified version of *ZEEMAN* which ignores all effects of the magnetic field, but does allow for non-uniformly distributed surface abundances. In practice, this version of the program has been used to find reasonable first approximations of the surface abundance distributions of the program stars. The

magnetic version is then used to determine the actual surface abundances of the final models. In the case of the hydrogen and helium line profiles the effects of the surface field are ignored entirely because of the large intrinsic widths of these lines, and hence the negligible effect of the magnetic field.

In principle, the Si III multiplet 2 lines can be used to determine the surface magnetic fields of the helium-strong stars, if the field is large enough. A strong surface field has two effects on a line profile: it broadens the line, because of the splitting of the line into its Zeeman components, and, if the line is on the saturated portion of the curve of growth, can cause a strengthening of the line, if the splitting is large enough to desaturate the line profile. Except for the sharp-lined stars  $\delta$  Ori C and HD 58260, the Zeeman broadening of the lines of the program stars will be negligible, because of the high rotation velocities. However, the differential magnetic intensification of the Si III lines may be measurable, if the surface magnetic field is large enough. A discussion of this magnetic intensification can be found in Babcock (1950) and Preston (1970).

Consider a star with a temperature,  $T$ , in the line forming region. The most probable speed of a particle in the star's atmosphere is given by  $v = (2kT/m)^{1/2}$ , where  $m$  is the mass of the atom and  $k$  is Boltzmann's constant. A spectral line will first start to desaturate, and hence

increase in strength, when the separation of the  $\sigma$  and  $\pi$  Zeeman components approaches this Doppler velocity broadening. Now the energy separation of the  $\sigma$  and  $\pi$  components is  $E = 2\mu_B B/c$  where  $\mu_B$  is the Bohr magneton,  $B$  is the magnetic field strength and  $c$  is the speed of light. For silicon, the  $\lambda 4574$  line ( $g_{\text{eff}} = 2.0$ ) will split first, and it is easy to show that this will occur for a field strength of about 3.6 kG at  $T = 18000$  K and at 4.2 kG for  $T = 25000$  K. The separations of the  $\sigma$  and  $\pi$  components of the  $\lambda 4567$  and  $\lambda 4552$  lines are somewhat smaller, so these lines will begin to strengthen at slightly higher magnetic field values.

The  $\lambda 4574$  line will cease to strengthen when the simple triplet pattern of the line is completely resolved. The other two lines will continue to intensify however, because of their more complex Zeeman patterns. They will continue to strengthen until the individual components of the separate  $\sigma$  and  $\pi$  groups desaturate. Following a procedure similar to that outlined above, the separation between the individual Zeeman subcomponents can be shown to approach the Doppler broadening, when the field has a strength of 14 kG at  $T = 18000$  and 17 kG for  $T = 25000$ .

The argument above suggests that differential Zeeman intensification of the silicon lines should be seen in the helium-strong stars, if their surface fields are between about 3 and 20 kG. In table 3:4 equivalent widths of the Si III multiplet 2 lines as calculated by the program ZEMAN

Table 3.4 Computed equivalent widths (mÅ) of the Si III multiplet 2 lines for various dipolar magnetic field strengths, Kurucz (1979)  $T_{\text{eff}} = 22500$ ,  $\log g = 4.0$  model atmosphere, and  $\log \epsilon_{\text{Si}} = -4.5$ .

$B_p$ (kG)	$\lambda 4552$	$\lambda 4567$	$\lambda 4574$
0	86.7	76.3	56.5
3	92.8	84.7	62.9
5	100.7	93.7	68.1
10	123.5	110.8	72.2
20	161.2	132.5	73.0
30	191.8	147.2	73.0

are given for various values of the surface magnetic field, from 0 kG to 30 kG (in this test a dipolar magnetic field is assumed and the magnetic pole is at the subsolar point). The general behaviour expected from the above discussion is illustrated quite nicely by these results. Unfortunately, an application of this effect to the helium-strong stars must be confined to the Si III  $\lambda\lambda 4567$  and  $4574$  lines since the  $\lambda 4552$  line is blended with lines of nitrogen and sulphur at these temperatures.

Finally, some use has been made of Landstreet's latest version of *ZEEMAN*, referred to here as *ZEEABUN*, for the stars  $\sigma$  Ori E, and especially HD 37776. This program is composed of many of the subroutines discussed above, again, modified by the author, but assumes a given magnetic field structure and searches automatically for the best fitting abundance distribution that is axisymmetric about the field axis. The abundance distribution is fixed in the form of six rings, each with a uniform abundance, and each extending over a magnetic latitude of  $30^\circ$ . Observed profiles in one to three specified wavelength windows are read in by the program and compared to the calculated profiles for each wavelength region. The reduced chi-squared of the fit is computed over all phases and wavelength windows is calculated, and an iterative procedure searches the abundance parameter space for the best fit abundance distribution. The iteration is performed using a modified version of the downhill simplex routine *AMOEB*A described by

Press et al. (1987). For each iteration the program determines the current best fit abundance distribution,  $v \sin i$ , and radial velocity. After the final iteration (the number is given by the user) the best fit model and observed profiles are stored in a disk file and plotted. This program is very CPU intensive and its use is practical only on a supercomputer such as the Cray or ETA-10P.

## Chapter 4 HD 64740

### 4.1 Introduction

At  $V = 4.62$ , HD 64740 (HR 3089) is the brightest of the known helium-strong stars (see table 1.1). The helium richness of HD 64740 was discovered during a southern hemisphere MK classification survey (Hiltner et al. 1969). Nissen (1974) confirmed its anomalous helium abundance photometrically and suggested that  $\epsilon_{\text{He}} > 0.20$ . According to Hunger (1975), Kaufmann and Schacht analysed four coude spectrograms and determined  $T_{\text{eff}} = 23500$  K,  $\log g = 3.9$ ,  $v \sin i = 160$  km s $^{-1}$ ,  $N_{\text{He}}/N_{\text{H}} = 0.67$ ,  $r = 200$  pc,  $\log(L/L_{\odot}) = 3.62$ ,  $R/R_{\odot} = 4.0$ , and  $M/M_{\odot} = 4.5$ . Oxygen and silicon show normal abundances, carbon is deficient and nitrogen enhanced. Unfortunately, this work has never been published. The first ultraviolet spectrum of the star was obtained from the TD1 satellite (Swings et al. 1973; Vreux et al. 1973). Because of the low (30Å) resolution, only the strongest lines could be identified, such as Si IV and C IV. Walborn (1974) reported the possible detection of H $\alpha$  emission, similar to that observed in the prototypical helium-strong star  $\sigma$  Ori E. Lester (1976) analysed both ground-based and Copernicus ultraviolet spectra of the star and performed a differential abundance analysis relative to the normal star  $\lambda$  Sco. His adopted model has  $T_{\text{eff}} = 22500$  K,  $\log g = 4.15$ , and  $N_{\text{He}}/N_{\text{H}} = 0.30$ . The helium lines  $\lambda\lambda 4026$ ,

4387, and 4471 yield a  $v \sin i$  of  $160 \pm 20$  km s<sup>-1</sup>. As compared to  $\lambda$  Sco, carbon and silicon abundances are normal, while nitrogen is overabundant by a factor of seven in HD 64740. He also suggested that a magnetic field might be the mechanism responsible for the peculiar atmospheric abundances. Finally, Groote, Kaufmann, and Hunger (1978) have reported the unpublished results of Groote and Kaufmann, based on eight coude spectrograms obtained near helium minimum with the ESO 1.52 m telescope:  $T_{\text{eff}} = 28500$  K,  $\log g = 4.15$ ,  $N_{\text{H}} \gg (N_{\text{H}} + N_{\text{He}}) = 0.76$ , and  $v \sin i = 150$  km s<sup>-1</sup>. Because of the high temperature, they performed a non-LTE analysis of silicon lines in the spectrum and suggested a slightly lower effective temperature of 27000 K. This would still make it one of the hottest known helium-strong stars and the hottest known magnetic star. They also suggested that the star could be a candidate for the X-ray source 4 U 0750-49.

The first indication of variability in the star was reported by Pedersen and Thomsen (1977), who performed narrow-band photometry of the He I  $\lambda 4026$  line and showed that the star's helium line strength appears to vary with a double wave structure on a 1.3295 day period. Their  $uvby\beta$  photometry suggested little or no variation in brightness or colour. Further observations (Pedersen 1979) resulted in an improved period of  $1.33016 \pm 0.00016$  days. Pedersen (1979) also confirmed Walborn's (1974) report of H $\alpha$  emission, observing it near maximum helium line strength.

Borra and Landstreet (1979) discovered a strong magnetic field, which shows a sinusoidal variation on the above period. The amplitude of the effective magnetic field variation is about 700 G. Lester (1979) suggested that ultraviolet lines of C II, N II, Si III, and Si IV are variable on the same period. Some time later Barker et al. (1982) presented further evidence for this UV spectrum variability. However, Walborn (1982) detected no radial velocity variations in the optical spectrum of the star. By combining observations from several epochs Bohlender et al. (1987) have again refined the period of HD 64740 to  $1.33026 \pm 0.00006$  days.

#### 4.2 Observations

A journal of the CFHT observations for HD 64740 has been given in Table 2.1. The phases for this star were calculated from the ephemeris given by Bohlender et al. (1987),

$$JD(B_{e-}) = 2444611.859 + 1.33026 E.$$

The notation  $JD(B_{e-})$  represents the time of the negative extremum of the magnetic field. The uncertainty in the above period is estimated at 0.00006 days, giving a negligible phase uncertainty of 0.033 in the CFHT data, relative to the epoch of the most recent magnetic field data.

Samples of spectra for HD 64740 are given by the dashed lines in figures 4.1 through 4.6. Helium (figure 4.1 and

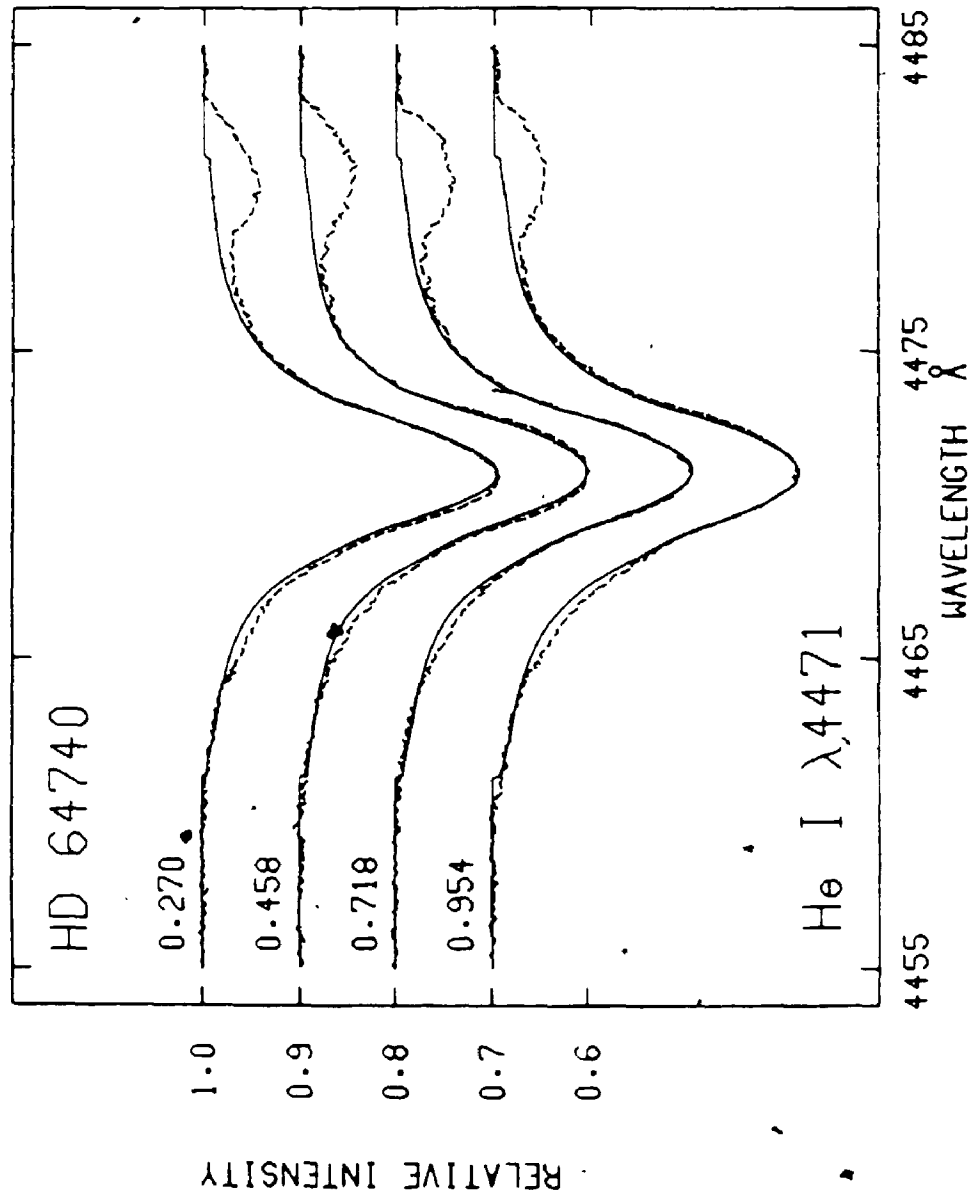


Figure 4.1 Observed (broken line) and modelled (solid line) He I  $\lambda$ 4471 line profiles of HD 64740. Rotational phases are given above each line profile and are calculated from the ephemeris given in the text. The helium abundance geometry is described in the text.

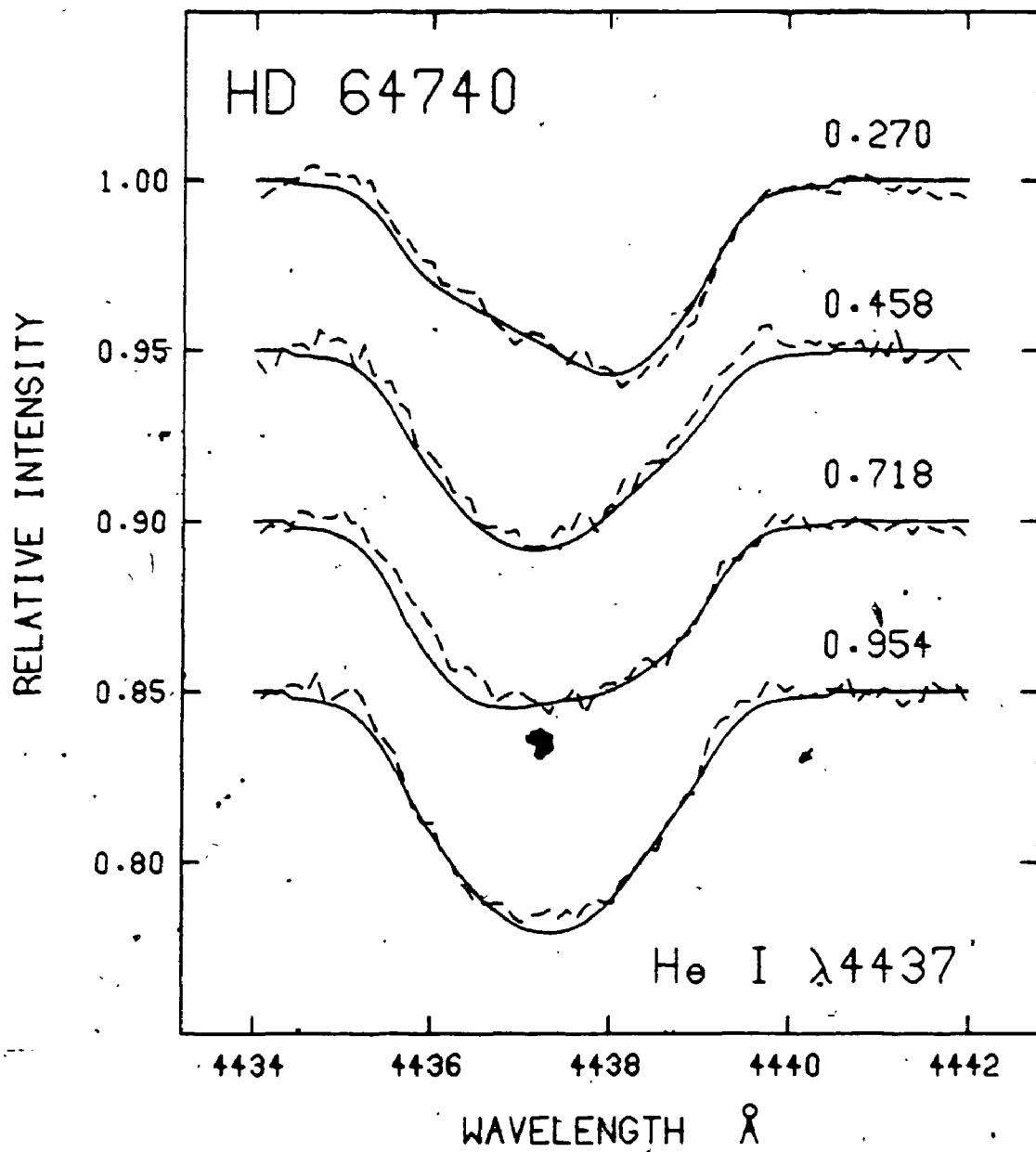


Figure 4.2 Observed (broken line) and modelled (solid line) He I  $\lambda 4437$  line profiles of HD 64740. The helium abundance geometry is described in the text.

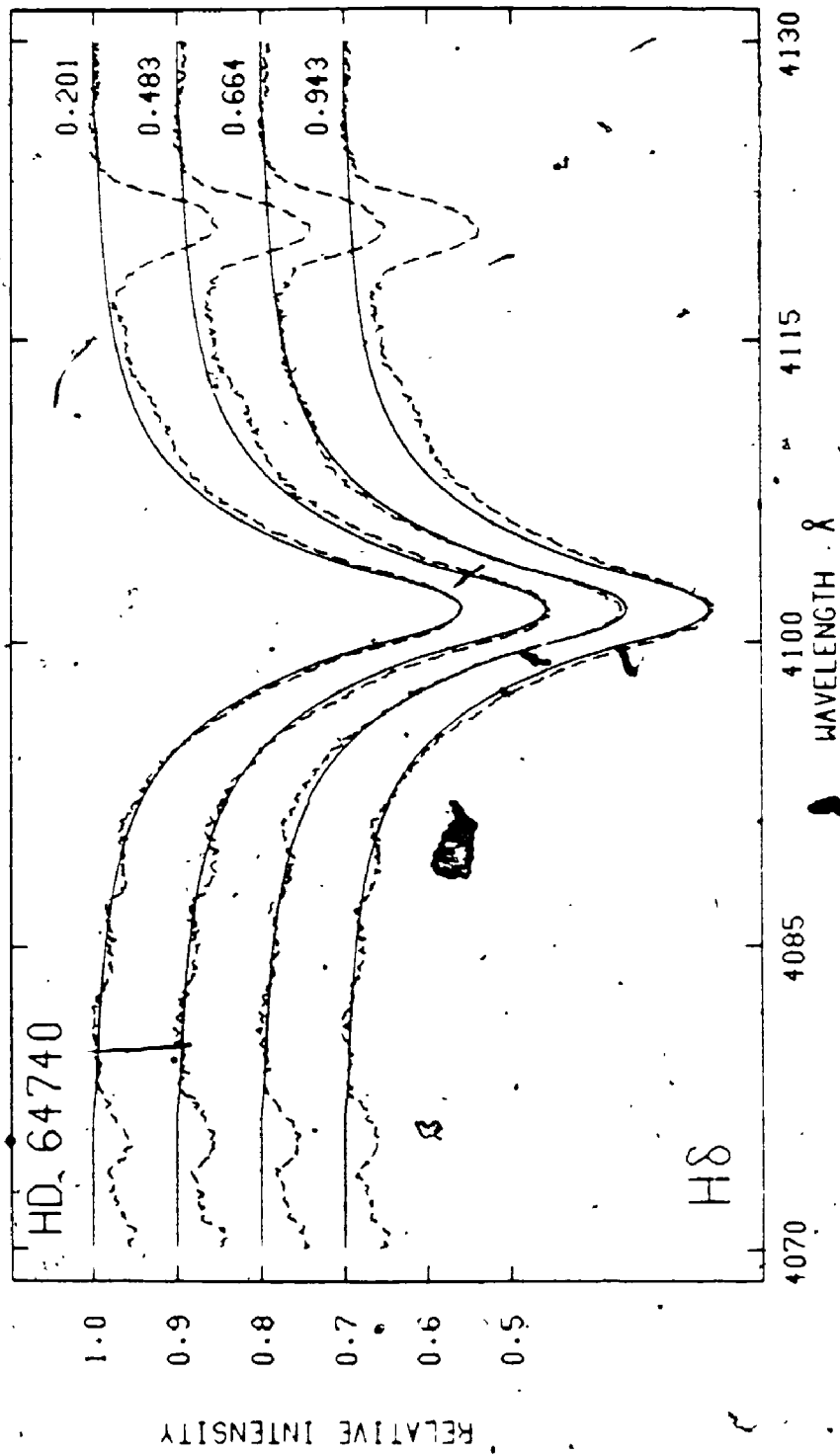


Figure 4.3 Observed (broken line) and modelled (solid line) H $\delta$  line profiles of HD 64740. The hydrogen abundance geometry is described in the text.

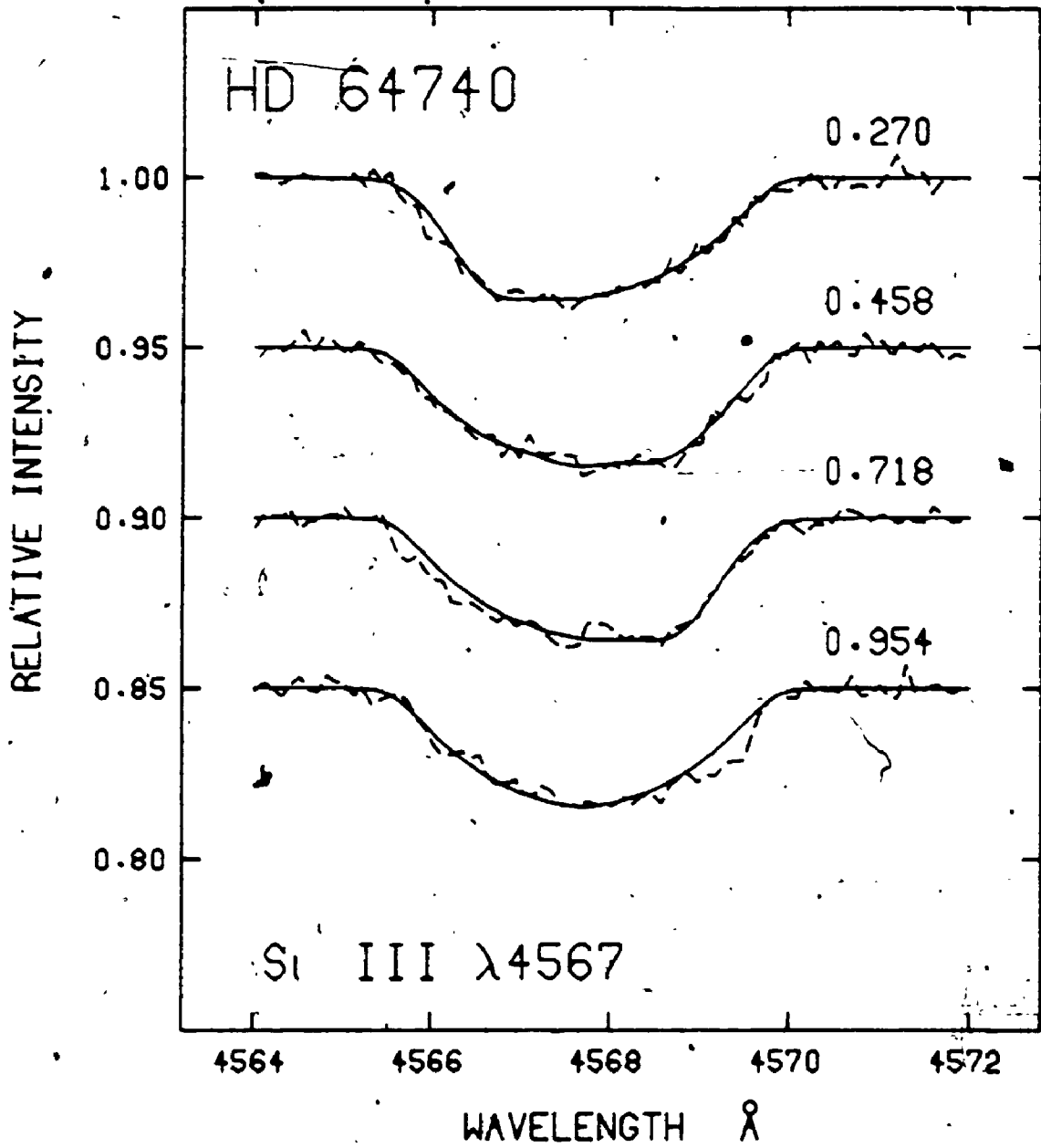


Figure 4.4 Observed (broken line) and modelled (solid line) Si III  $\lambda$ 4567 line profiles of HD 64740. The silicon abundance geometry is described in the text.

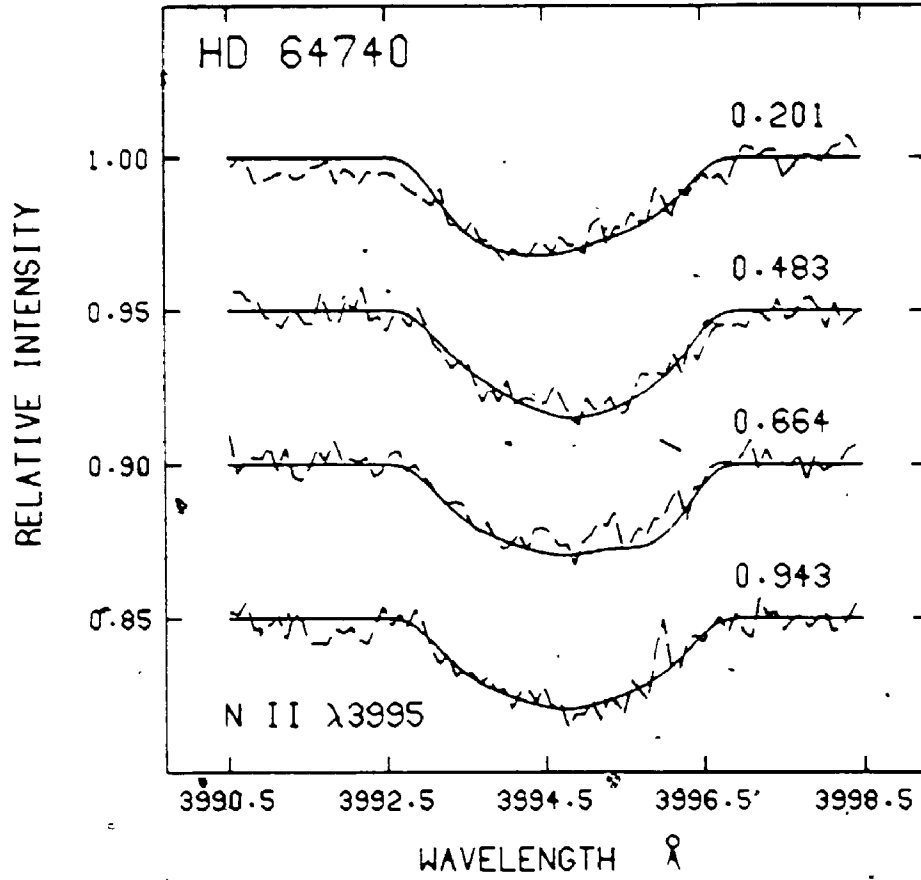


Figure 4.5 Observed (broken line) and modelled (solid line) N II  $\lambda 3995$  line profiles of HD 64740. The nitrogen abundance geometry is described in the text.

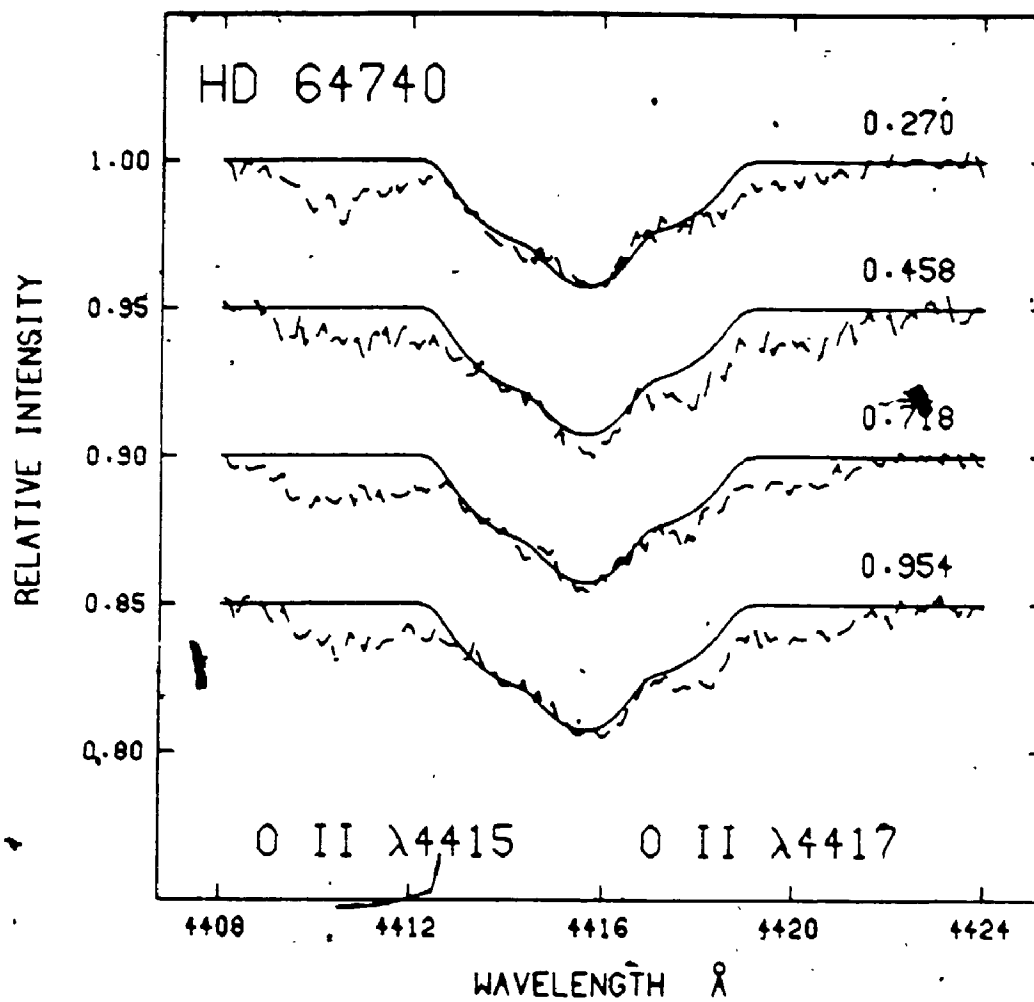


Figure 4.6 Observed (broken line) and modelled (solid line), O II  $\lambda$ 4415 and 4417 line profiles of HD 64740. A uniform oxygen abundance of  $\epsilon_0 = -3.5$  is assumed.

4.2), silicon (figure 4.4), and magnesium (figure 4.1) are definitely variable, while nitrogen (figure 4.5) and oxygen (figure 4.6) are only marginally so. H $\delta$  (figure 4.3) may be slightly variable but shows no indication of absorption by circumstellar material as is observed in  $\sigma$  Ori E.

Extensive photoelectric Zeeman analyzer observations of HD 64740 have been previously published (Borra and Landstreet 1979; Bohlender et al. 1987). Polarization measurements for HD 64740 have been obtained in the wings of H $\beta$  and He I  $\lambda$ 5876. These yield virtually identical sinusoidal longitudinal magnetic field curves, whose variations can be described by equation 2.2 with  $B_0$ ,  $B_1$ , and  $\phi_0$  given in table 2.2. The fit of this curve to the data yields a reduced chi-squared of 1.40, which suggests that the magnetic field configuration may be dominated by the dipole component. No information about the magnitude of the surface field,  $B_s$ , is given by these data. Of course, obtaining some constraints on the field geometry is one of the objectives of this work. The magnetic field observations are shown in figure 4.7 along with the helium strength R-index observations of Pedersen and Thomsen (1977). Maximum helium line strength occurs at  $\phi = 0.98 \pm 0.06$  and a secondary helium maximum occurs very close to the positive magnetic extremum. The helium line strength minima coincide closely with zero effective magnetic field. This suggests a possible geometry of two polar patches of enhanced helium abundances for HD 64740.

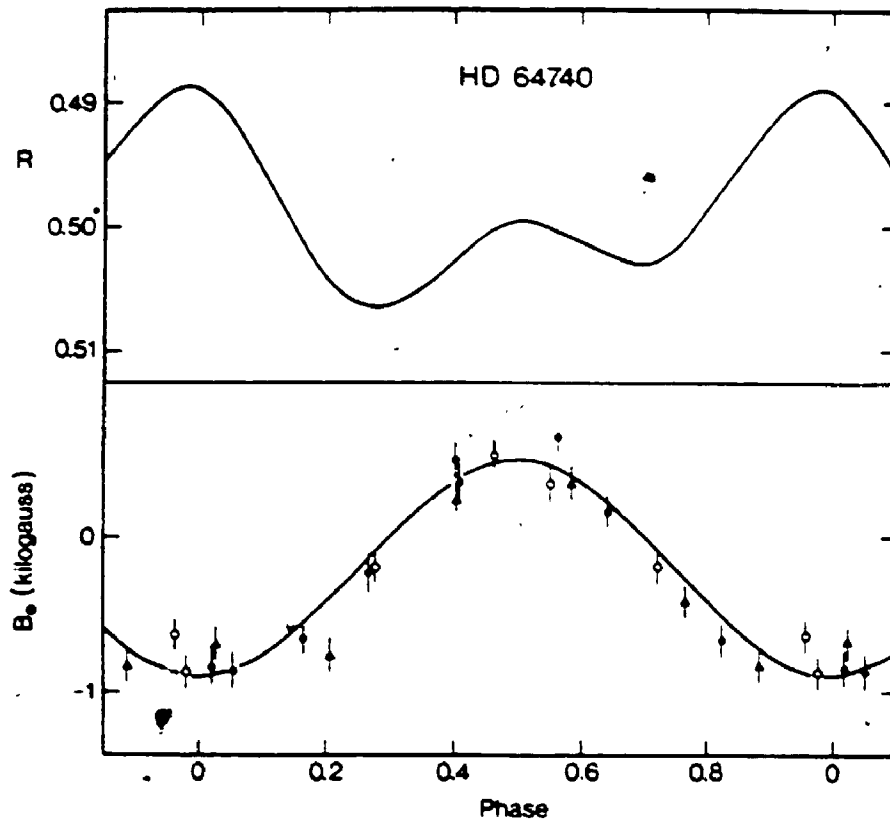


Figure 4.7 Helium line strength index,  $R$ , and magnetic field curves of HD 64740. The  $R$ -index curve is a hand-drawn fit to the data of Pedersen and Thomsen (1977) and Pedersen (1979). Magnetic data symbols: open circles -  $H\beta$  observations of Borra and Landstreet (1979); filled circles -  $H\beta$  observations of Bohlender et al. (1987); triangles - He I  $\lambda 5876$  observations of Bohlender et al. (1987). The curve through the magnetic observations is given in the text. (From Bohlender et al. 1987.)

From the observed maximum longitudinal field of 890 G, the minimum value of the polar field strength can be found from an expression first derived by Schwarzschild (1950). For a dipolar magnetic field geometry, he showed that the observed effective field is given by the expression

$$B_e = [(15 + u)/(15 - 5u)] B_p \cos \alpha / 4 \quad (4.2)$$

where  $u$  is the limb darkening constant,  $\alpha$  is the angle between the magnetic axis and the line of sight, and  $B_p$  the polar field strength. With  $\alpha = 0^\circ$ ,  $B_p$  is approximately 3000 G, assuming a limb darkening constant of 0.40. For a normal Zeeman triplet, a field of this magnitude would produce a Zeeman pattern with a separation between components of only 0.028 Å, while an element such as silicon at  $T_{\text{eff}} = 25000$  K has a Doppler width of approximately 0.05 Å. The magnetic field therefore, is not expected to have a large effect on line formation in the atmosphere of HD 64740. In particular, the Si III multiplet 2 lines are expected to be slightly strengthened because of the field, but differential intensification of the three lines in the multiplet, due to the desaturation of the various  $\sigma$  and  $p$  polarization components, will be negligible.

#### 4.3 Modelling

The effective temperature of HD 64740 has been estimated using data from three photometric systems. It is not practical to use the ionization equilibrium of Si II/Si III/Si IV as a temperature determinant for HD 64740.

Because of the star's high  $v \sin i$ , only the Si III multiplet 2 lines are strong enough to model with any confidence. In addition, previous studies have indicated possible problems in using Si II line strengths as a temperature diagnostic. For example, Peters (1976) has performed a fine analysis of the B2 standard Gamma Peg, and from a consideration of the continuous energy distribution and Balmer lines of the star, found an effective temperature of 21500 K and  $\log g = 3.70$  for the star. However, while the Si III/Si IV and S II/S III ionization equilibria give results consistent with this model, Si II/Si III line ratios do not. The Si II lines are much too strong and would require a silicon abundance of 0.5 dex lower than is derived from the higher ionization features. She suggests that the failure of the Si II lines to give abundances in agreement with those from Si III and Si IV could be a result of non-LTE effects, incorrect oscillator strengths, or an incorrect atmosphere. Similar behaviour has also been reported by Peters and Aller (1970), and Hardorp and Scholz (1970). Peters and Aller (1970) note that Si II forms high in the stellar atmosphere, where the assumption of LTE could be incorrect. However, the non-LTE analysis of silicon by Kamp (1973, 1978) does not completely solve the problem. For this reason Si II/Si III ionization equilibrium will not be used as a temperature determinant in this work. No other element has lines of more than one ionization state visible in the spectra of HD 64740, so broadband colours must be

used to determine the temperature.

Buser and Kurucz (1978) have published theoretical  $T_{\text{eff}}$  vs.  $UBV$  colour curves for early-type stars based on theoretical colours determined from Kurucz's (1979) blanketed model atmospheres. For B stars, the  $(U - V)_0$  index is most sensitive to changes in  $T_{\text{eff}}$ . Using  $(U - V)_0 = -1.20$  from table 1.2, and Buser and Kurucz's (1978) figure 5, the  $T_{\text{eff}}$  of HD 64740 ranges from 24550 K for  $\log g = 3.5$  to 26300 K for  $\log g = 4.5$ . In the Geneva photometric system, Cramer and Maeder (1979) and Cramer (1984) have determined a polynomial relation between the photometric index  $X$  (Cramer and Maeder 1979) and  $T_{\text{eff}}$ ,

$$\log T_{\text{eff}}(X) = 4.496 - 0.453X + 0.086X^2.$$

Using  $X = 0.2535$  from table 1.2 and the above relation,  $T_{\text{eff}} = 24360$  K in the Geneva system. The theoretical  $uvby\beta$  indices of Lester, Gray, and Kurucz (1986) have also been used to estimate the temperature of HD 64740. Using their solar composition results,  $\log g = 3.90$  (see below), and data from table 1.2, an approximate temperature of  $T_{\text{eff}} = 23750$  K is derived in the Strömgren system. An average  $T_{\text{eff}}$  of 24500 K has been adopted for HD 64740.

The next step in the analysis is to determine the relative abundances of helium and hydrogen. The helium singlet  $\lambda 4437$  is most suited for this purpose, being sensitive to  $\epsilon_{\text{He}}$ , free from blends, and relatively insensitive to the surface gravity. Helium lines are also not Zeeman sensitive. Preliminary models of the He I  $\lambda 4437$

profile of HD 64740 (which is fairly insensitive to the choice of model atmosphere) suggested that the helium abundance of this star is roughly normal over a large fraction of its surface and nowhere exceeds three times the solar abundance.

In determining the hydrogen and helium abundance geometry an inclination of  $40^\circ$  and a magnetic obliquity of  $75^\circ$  was first assumed for HD 64740. This represented a lower limit on  $i$  as determined by Bohlender et al. (1987) and proved to be an appropriate choice. By trial and error a preliminary abundance distribution for helium was determined which consisted of two helium-rich spots ( $c_{He} \approx 0.30$ , radii  $\approx 60^\circ$ ) near the magnetic poles, which fit the observed  $\lambda 4437$  variations adequately. The  $v \sin i$  of the best fit is  $140 \pm 5$  km s $^{-1}$ .

Once  $T_{eff}$  and the helium abundance geometry are known the surface gravity can be estimated by fitting the profiles of the gravity-sensitive lines H $\delta$  and He I  $\lambda 4471$ . Using the above helium abundance geometry, the best fit over all phases of both lines was found for a  $\log g$  of 4.0. Remembering that the surface gravity is most likely being overestimated by a small amount, a value of  $\log g = 3.90 \pm 0.15$  has been adopted.

With accurate values for  $T_{eff}$  and  $\log g$  the mass and radius of HD 64740 can be determined. In figure 4.8 the evolutionary track of Maeder and Mermilliod (1981) for a  $5 M_\odot$  star, and Maeder's (1981) evolutionary tracks for stars

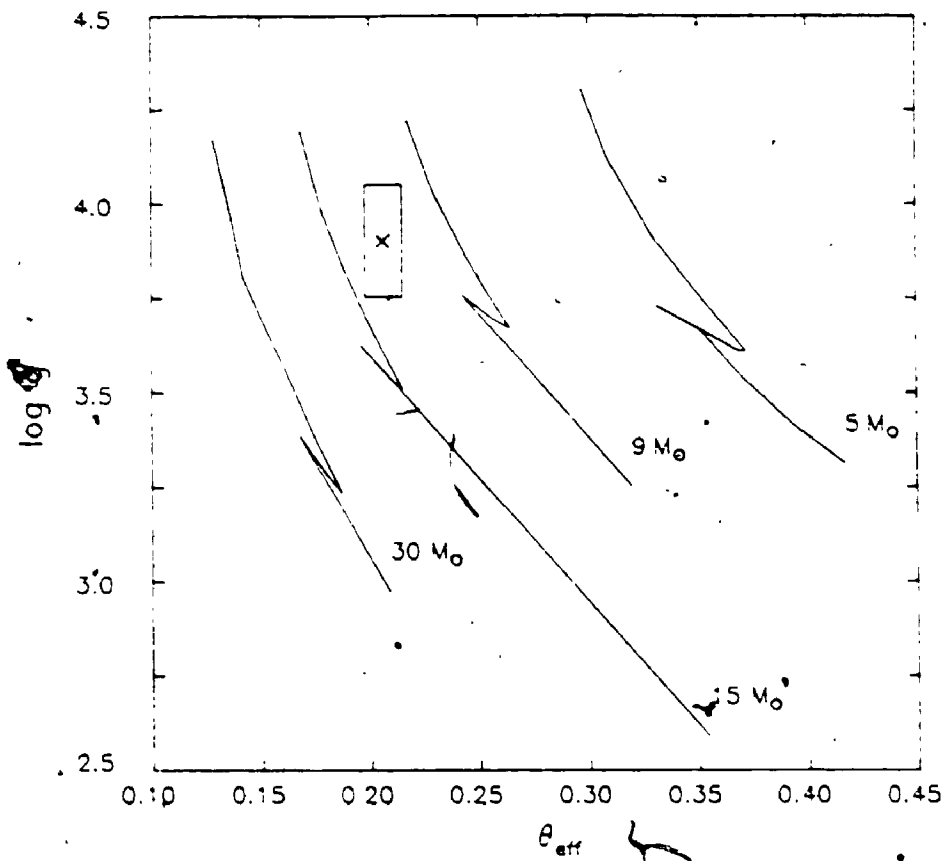


Figure 4.8 Location of HD 64740 in the  $\log g$  vs.  $\theta_{\text{eff}}$  plane. The cross indicates the derived parameters of HD 64740 as discussed in the text, and the error box gives the estimated uncertainty. The labelled curves are the evolutionary models of Maeder and Mermilliod (1981) and Maeder (1981), assuming no mass-loss.

with masses ranging from 9 to 30  $M_{\odot}$  and with no mass-loss have been plotted in the  $\log g$  vs.  $\theta_{\text{eff}}$  plane ( $\theta_{\text{eff}} = 5040/T_{\text{eff}}$ ). The location of HD 64740 is also plotted, with error bars indicating the estimates of the uncertainty in  $T_{\text{eff}}$  and  $\log g$ . From the star's position in the figure we arrive at an interpolated mass of  $11.5 \pm 2.0 M_{\odot}$ , and therefore a radius of  $6.3 \pm 1.8 R_{\odot}$ . It should be noted that the exact position of the theoretical evolutionary tracks is sensitive to the assumed metal abundance,  $Z$ , used in the evolutionary models. Maeder (1981) uses  $Z = 0.03$ , a value appropriate for young population I stars. An investigation by Alcock and Paczynski shows that for a 10  $M_{\odot}$  star, decreasing the metal abundance from  $Z = 0.03$  to  $Z = 0.01$  results in an increase of approximately 0.1 in  $\log g$ . This uncertainty has been taken into account when estimating the size of the error box in figure 4.8.

This additional information, along with the rotation period of 1.33026 days permits a determination of the inclination of HD 64740's rotation axis to the line of sight using the simple relation

$$\sin i = P v \sin i / (50.6 R/R_{\odot}) \quad (4.3)$$

where  $P$  is the period in days and  $v \sin i$  is in  $\text{km s}^{-1}$ . This gives a value for  $i$  of  $36 \pm 15^{\circ}$ . If the oblique rotator model is the correct interpretation of the spectrum and magnetic field variability, and the magnetic field geometry is predominantly dipolar, then the obliquity of the magnetic axis to the rotation axis,  $\beta$ , is given by (Preston, 1967)

$$\tan \beta = (1 - r) / [(1 + r) \tan i] \quad (4.4)$$

where  $r$  is the ratio of the magnetic extrema given by

$$r \equiv B_e(\text{min}) / B_e(\text{max}) = \cos(\beta + i) / \cos(\beta - i). \quad (4.5)$$

This argument still holds if there is a quadrupolar field component of equal or smaller magnitude than the dipole component. Given  $r = -0.55$  for HD 64740 (Bohlender *et al.* 1987), equation (4.5) gives  $\beta = 78 \pm 8^\circ$ . With this inclination and obliquity a polar field strength of 3700 G is needed to model the effective field variation with a centered dipole. A field of this strength is consistent with the lack of significant differential Zeeman intensification of the Si III lines. This magnetic geometry has been used in the final model of the abundance geometry of HD 64740.

The solid lines in figures 4.1 through 4.6 present the result of the final adopted best fit models for HD 64740. The model fits for He I  $\lambda\lambda 4471, 4437$ , and H $\delta$  are given in figures 4.1, 4.2, and 4.3 respectively. The derived abundance geometries are given in table 4.1, along with the solar abundances of Kurucz (1979). The abundance geometry for helium consists of two spots of enhanced helium near the magnetic poles: one spot with radius  $60^\circ$  centered at a point  $20^\circ$  from the positive pole at magnetic longitude  $180^\circ$  and with  $\epsilon_{\text{He}} = 0.30$ , the other at the negative pole with radius  $70^\circ$ , and  $\epsilon_{\text{He}} = 0.35$ . The helium abundance is normal ( $\epsilon_{\text{He}} = 0.10$ ) elsewhere. This surface distribution of helium is illustrated for several phases in figure 4.9. The  $20^\circ$  displacement of one of the helium-rich spots from the

Table 4.1. HD 64740 Abundance Geometries

Helium Spot Locations ( $\log \epsilon_0 = -1.0$ )

$\log \epsilon_{He}$	Colat.	Long.	Radius
-0.456	0°	0°	70°
-0.523	160°	180°	60°

Nitrogen Spot Location ( $\log \epsilon_0 = -3.99$ )

$\log \epsilon_N$	Colat.	Long.	Radius
-4.00	140°	0°	70°
-4.70	Remainder of Surface		

Silicon Geometry ( $\log \epsilon_0 = -4.50$ )

	<u>Magnetic Colatitude: 0°-110°</u>	<u>110°-140°</u>	<u>140°-180°</u>
$\log \epsilon_{Si}$	-4.30	-3.60	-6.00

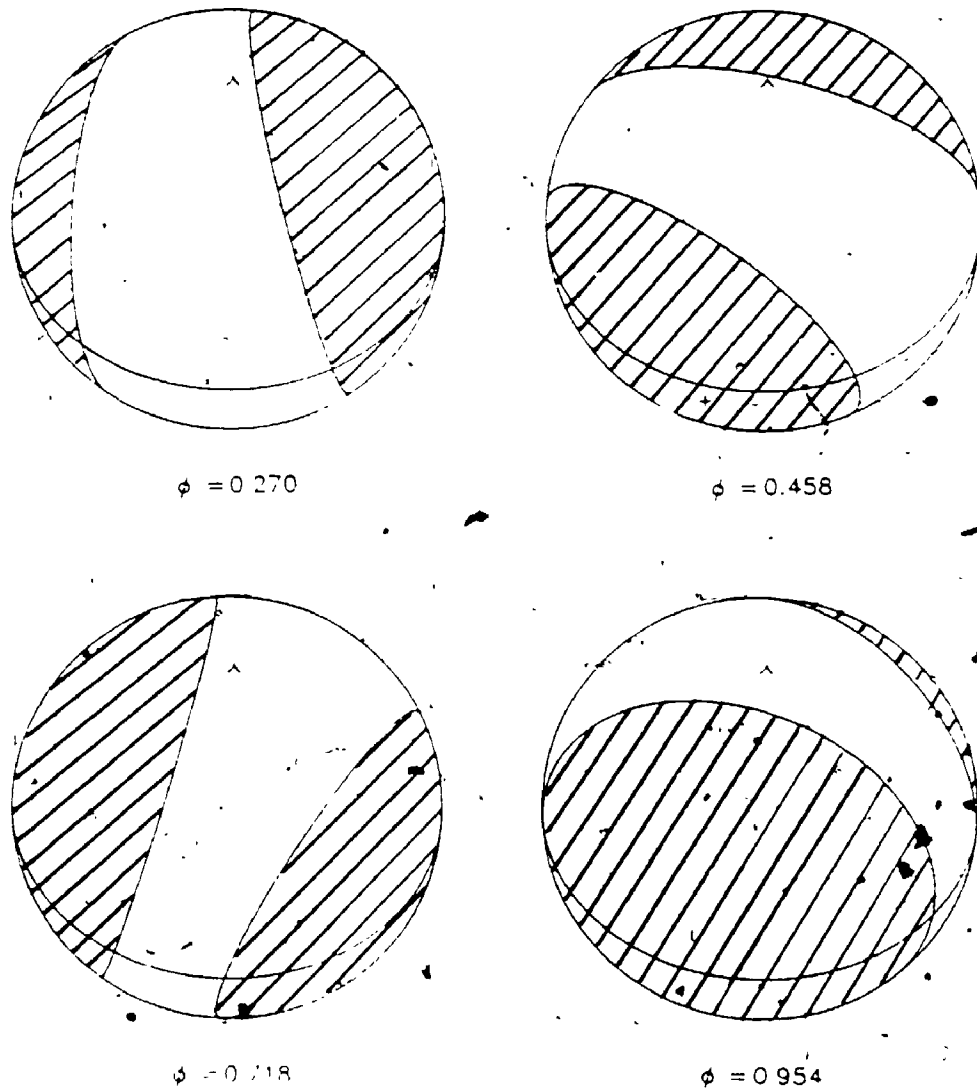
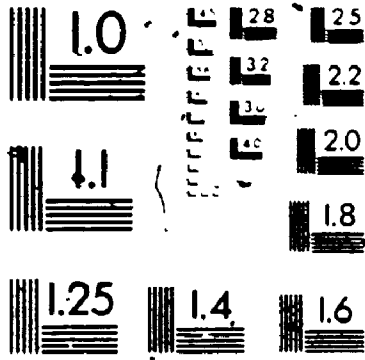


Figure 4.9 Illustration of the helium abundance geometry of HD 64740. The hatched areas represent the locations of the helium-rich regions on the stellar surface. The locations and signs of the magnetic poles are indicated by the symbols - and +. Details of the model are outlined in the text. The rotational phases are given below each figure.

2



**MICRO**

magnetic poles is significant: locating both helium-rich spots at the magnetic poles gives a poor fit for the line profile variations. It should be pointed out that a significant fraction of the stellar surface remains hidden from view because of the low inclination.

Figure 4.4 gives the fit for the Si III  $\lambda 4567$  line. Silicon appears to be overabundant ( $\log \epsilon_{\text{Si}} = -3.6$ ) in a band whose boundaries are  $40^\circ$  and  $70^\circ$  from the positive magnetic pole. Most of the remainder of the surface of HD 64740 has an approximately normal abundance of  $\log \epsilon_{\text{Si}} = -4.4$ . However, a very low silicon abundance of  $\log \epsilon_{\text{Si}} = -6.0$  in a  $40^\circ$  cap at the positive pole leads to an improved fit near  $\phi = 0.458$ . The silicon abundance distribution on the visible hemisphere of the star is shown at several phases in figure 4.10.

Model profiles for N II  $\lambda 3995$  and O II  $\lambda\lambda 4415$  and  $4417$  are given in figures 4.5 and 4.6. Nitrogen appears to be roughly uniform in abundance, although evidence of a nitrogen-rich patch may be present at  $\phi = 0.201$ . An abundance of  $\log \epsilon_{\text{N}} = -4.70$  is found over most of the surface; a  $60^\circ$  radius spot at the positive magnetic pole with  $\log \epsilon_{\text{N}} = 4.0$  improves the fit somewhat. The oxygen lines appear to vary in strength slightly, being strongest near  $\phi = 0.458$ , but problems with blends in the wings of the two lines shown in figure 4.6 have made it difficult to model the possible variation of these profiles. A uniform abundance of  $\log \epsilon_{\text{O}} = -3.5$  has been used for the fits in

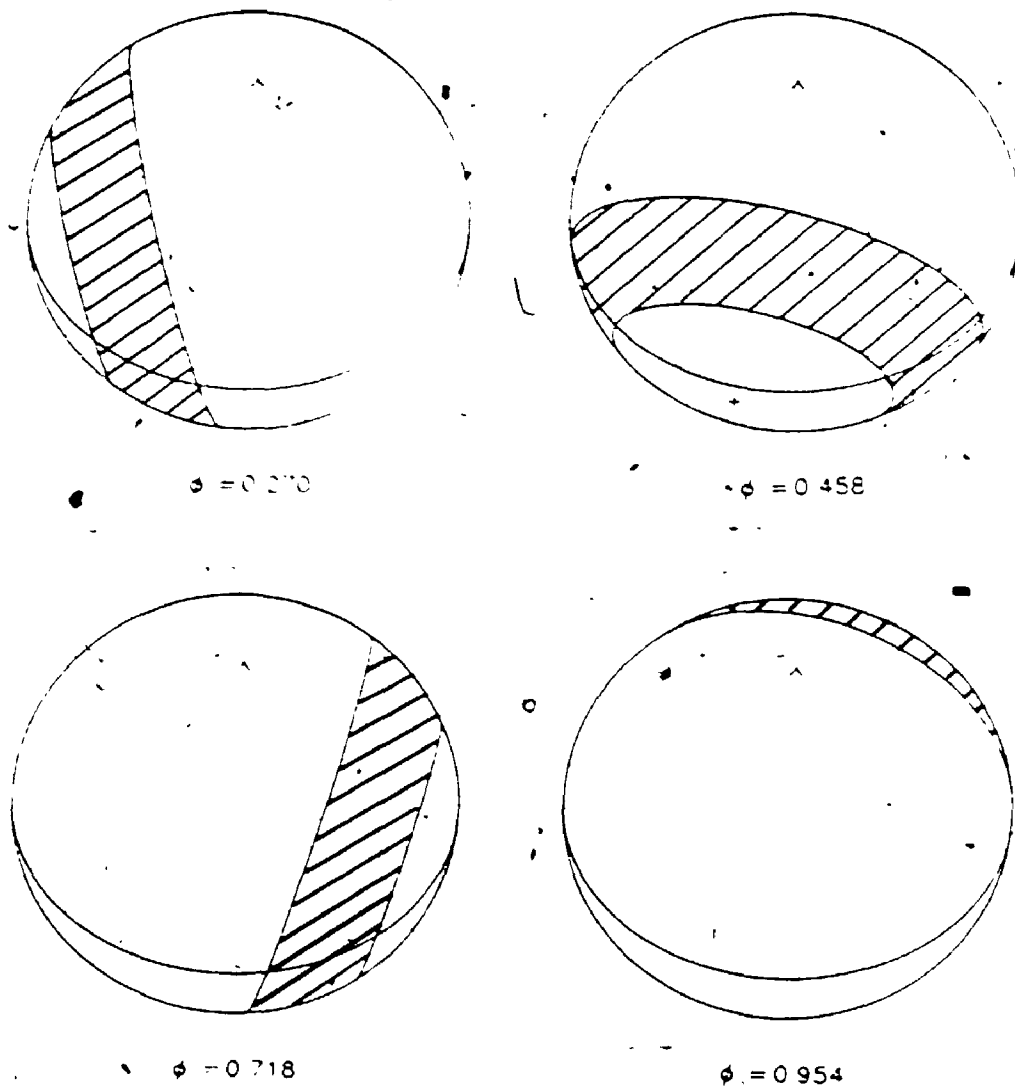


Figure 4.10 Illustration of the silicon abundance geometry of HD 64740. The hatched areas represent the locations of the silicon-rich regions on the stellar surface. The locations and signs of the magnetic poles are indicated by the symbols - and +. Details of the model are outlined in the text. The rotational phases are given below each figure.

figure 4.6.

#### 4.4 Discussion

The abundance geometries of HD 64740 suggest some interesting problems with current theories concerning the helium-strong stars. For example, helium is found to be overabundant at the magnetic poles of the star. Shore's (1987) model predicts that helium should be enriched at progressively lower magnetic latitudes for hotter helium-strong stars. In the simplest application of this model, the helium enrichment is caused by the interaction of a stellar wind with a dipolar magnetic field; for the cooler helium-strong stars, helium accumulates in the line forming region only where the field lines are vertical, near the magnetic poles, whereas the stronger winds expected for the hotter stars lead to a deficiency of helium at the magnetic poles and an overabundance at the magnetic equator. Since HD 64740 is one of the hottest helium-strong stars this interpretation is clearly in disagreement with the above observations, and might suggest that there is an undetected quadrupolar or higher order magnetic component present in the field of HD 64740.

Magnetic models of the Mg II  $\lambda 4481$  doublet have not been presented here, partly because the line is blended with the strong He I  $\lambda 4471$  profile, and partly because of the very complex Zeeman pattern of the two line components, and hence, very costly modelling. However, non-magnetic models

of the line profile suggest that magnesium has an abundance geometry very similar to that found for silicon. Bolton (1983) has suggested that the observed variations of lines from elements other than hydrogen and helium may be interpreted in terms of differences in temperature between regions with different helium abundances, rather than in terms of non-uniform distributions of the elements. The temperature is predicted to be lower in the helium-rich spots or bands. The observed variations of Mg II and Si III in HD 64740 do not appear to support this view. At  $T_{\text{eff}}$  of 24000 K, Si III will increase slightly in strength for increases in  $T_{\text{eff}}$  (Erhorn, Groote, and Kaufmann 1984), while Mg II line strengths will decrease. Instead, it seems preferable to assume that the observed line variations are caused by non-uniform surface abundances. Of course, variations in the continuous opacity over the surface of the star, resulting from the non-uniform helium abundance, could also contribute to the line profile variations.

In HD 64740 the abundances of silicon, oxygen, and nitrogen vary by a factor of approximately five at most over the surface of the star. According to Kamp (1978) the use of LTE in modelling Si III lines at  $T_{\text{eff}} = 24500$  K will result in overestimate of the silicon abundance by approximately 0.35 dex. The work of Dufton and Hibbert (1981) suggests an overestimate of 0.20 dex for nitrogen, while the recent study of Brown, Dufton, and Lennon (1988)

indicates a larger overestimate in the abundance of oxygen of 0.4 dex. With these corrections allowed for, the overall average surface abundances for HD 64740 would seem to be approximately solar. The relatively low-level abundance variation may be the reason for the lack of photometric variability of the star (Pedersen and Thomsen 1977).

The fact that the band of enhanced silicon (and magnesium) is closer to the positive magnetic pole of HD 64740 may suggest the presence of a quadrupole component to the surface field, if we adopt the models of Michaud et al. (1981). This pole, however, is never very close to the line-of-sight, so that it is not feasible to say anything quantitative about the importance of this possible complication to the field. The abundance geometries of the star are approximately axisymmetric with respect to the magnetic axis. The two helium-rich spots are, however, not both situated at the magnetic poles, as modelling the helium line profiles with the smaller spot moved  $20^\circ$  to the positive pole results in a large deterioration in the fit to the observed profiles.

Using the values for the radius and  $T_{\text{eff}}$  derived above, an estimate can be made of the distance to HD 64740. The temperature and radius give  $\log L/L_\odot = 4.1 \pm 0.3$ . The bolometric corrections of Code et al. (1976) and the observed  $E(B - V)$  of then leads to  $r = 350 \pm 80$  pc. From Maeder's (1981) evolutionary models, we find that HD 64740's properties are consistent with a main sequence star with an

age of approximately  $1.1 \times 10^7$  years.

## Chapter 5 HD 58260 and $\delta$ Ori C

### 5.1 Introduction

In this chapter observations and models are presented for the two sharp-lined helium-strong stars, HD 58260 and  $\delta$  Ori C. The non-variable spectra of these stars simplifies their analysis somewhat, since little can be said about the surface distributions of most elements with the data in hand at the present time. For most of the elements a uniform abundance will be assumed. The situation is complicated somewhat by the interesting helium line profiles of  $\delta$  Ori C. A brief summary of previous observations for each star follows.

#### 5.1.1 HD 58260

This star was identified as a helium-strong star by Garrison, Hiltner, and Schild (1977), who also noted that the helium line strengths might be variable. Walborn (1974) searched for, but failed to detect, H $\alpha$  emission in the star. Pedersen (1979) performed narrow-band photoelectric observations of the He I  $\lambda$ 4026 line and suggested that a 1.657 day periodicity might be present in the data, but the significance of the variation is low. IUE spectra of the star show strong and constant C IV emission (Barker 1986). HD 58260 has had a constant magnetic field of 2300 G (Borra and Landstreet 1979; Bohlender et al. 1987) for more than

nine years. Walborn (1983) suggested that the star has a  $v \sin i$  of less than  $30 \text{ km s}^{-1}$ , but Bohlender et al. (1987) have revised this value to  $18 \text{ km s}^{-1}$ . The latter authors provide a rather loose constraint on the inclination ( $> 4^\circ$ ) and magnetic obliquity ( $< 81^\circ$ ) of HD 58260. Drake et al. (1987) failed to detect radio emission from the star.

#### 5.1.2 $\delta$ Ori C = HD 36485 = HR 1851

This member of the Orion OB1 association was classified as helium-strong by Morgan, Abt, and Tapscott (1978). Abt and Levato (1977) had earlier classified it as B2 Vsn, the sn designation representing a class of stars that have both sharp and nebulous or diffuse lines in its spectrum. The diffuse lines are usually those of neutral helium (Jaschek and Jaschek 1987). Walborn (1982) also noted that  $\delta$  Ori C is sharp-lined, but has very pronounced helium line wings (he erroneously referred to the star as  $\delta$  Ori B [see Bohlender et al. 1987]). A short time later Walborn (1983) reported an observation of blue-shifted helium lines and suggested a mass ejection episode as an explanation. He also estimated a  $v \sin i$  of  $80 \text{ km s}^{-1}$ . IUE observations show no evidence of a stellar wind (Barker 1986). Bohlender et al. (1987) have recently reported the discovery of a strong, and apparently constant magnetic field for  $\delta$  Ori C. The average of six photoelectric magnetic field measurements made over a period of more than three years yields an effective field strength of  $-3400 \text{ G}$ , the largest observed in

the helium-strong stars to date (Bohlender et al. 1987). They measure a  $v \sin i$  of  $32 \text{ km s}^{-1}$ , and suggest that the inclination of the rotation axis of the star is  $i > 8^\circ$ , while the obliquity of the magnetic axis to the rotation axis,  $\beta$ , is poorly constrained, but probably less than  $63^\circ$ . Drake et al. (1987) have recently found that  $\delta$  Ori C is a nonthermal radio source.

### 5.2 Observations

In figure 5.1 the He I  $\lambda 4471$  profiles of HD 58260 and  $\delta$  Ori C are illustrated along with the same line for the normal B2IV-V star, 22 Ori. The effective temperatures of these stars, as determined from their broad band colours, do not differ by more than 1000 K. The peculiar nature of the line profile in the case of  $\delta$  Ori C is immediately obvious. The sharpness of the Mg II  $\lambda 4481$  line for each star indicates that both HD 58260 and  $\delta$  Ori C are relatively slow rotators. At temperatures appropriate for these stars, the strength of the magnesium line increases with decreasing temperature. Therefore, if magnesium is assumed to have the same abundance for the two peculiar stars, this suggests that  $\delta$  Ori C is the cooler of the two helium-strong stars. It will be argued below that this is the case.

The H $\delta$  profiles of each of these stars are shown in figure 5.2 along with another helium line, He I  $\lambda 4121$ . The substantial Stark broadened wings of H $\delta$  for  $\delta$  Ori C are indicators of a large surface gravity<sup>9</sup> for this star compared

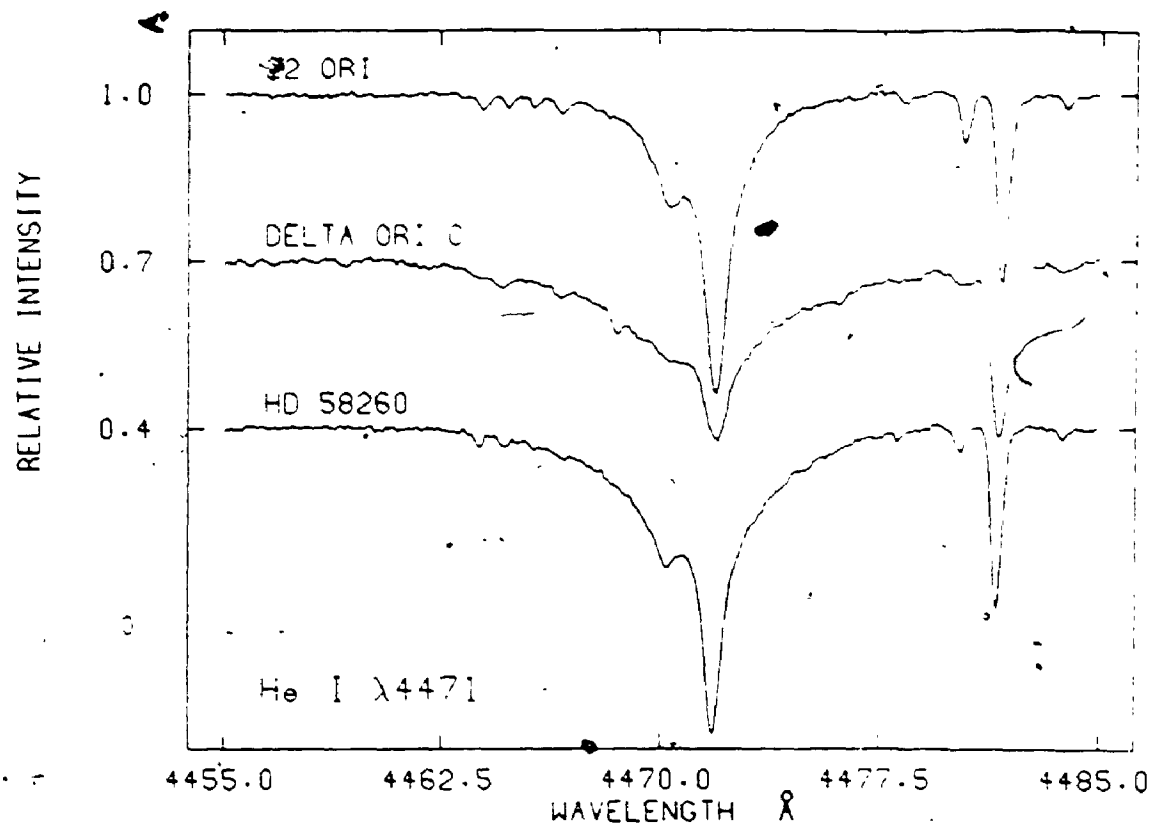


Figure 5.1. A comparison of the He I  $\lambda 4471$  line profiles of the normal B2 star, 22 Ori, and the helium-strong stars HD 58260 and  $\delta$  Ori C.

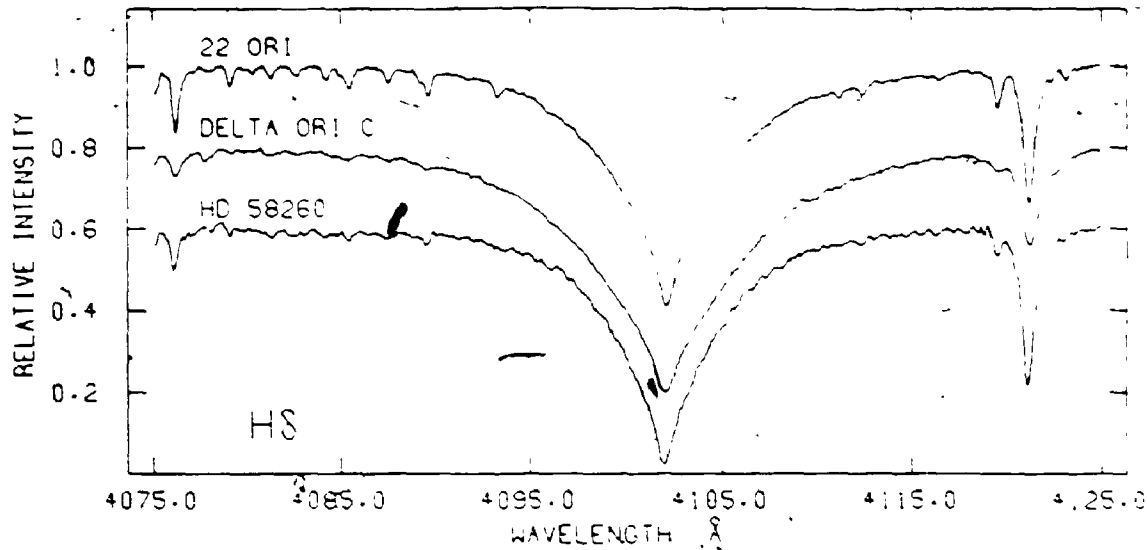


Figure 5.2 A comparison of the H $\delta$  line profiles of the normal B2 star, 22 Ori, and the helium-strong stars HD 58260 and  $\delta$  Ori C.

to HD 58260. The latter object appears to be somewhat more evolved than 22 Ori.

$\delta$  Ori C would seem to be an example of a small group of stars with peculiar helium line profiles of which the helium-weak star 3 Sco and the spectacular helium-variable  $\alpha$  Cen are members. The weak, but very broad lines of neutral helium in 3 Sco have been interpreted by Norris and Strittmatter (1975) as evidence of vertical or horizontal abundance gradients of helium in the atmosphere of the star. The latter model appears to be more appropriate after the discoveries of helium line variability by Pedersen and Thomsen (1977) and a variable magnetic field by Landstreet, Borra, and Fontaine (1979). Norris and Strittmatter (1975) are able to reproduce the He I  $\lambda\lambda$ 4026 and 4471 profiles of the star by assuming that two-thirds of the visible surface of the star has no helium while the remainder of the surface has a normal helium abundance. Landstreet, Borra, and Fontaine (1979) have demonstrated that helium is underabundant at the magnetic poles. Norris and Strittmatter also rule out the possibility of aspect effects of a rapidly rotating star and effects of non-LTE as explanations of the peculiar line profiles. This model is quite similar to that proposed for  $\alpha$  Cen (Norris and Baschek 1972), except here helium is overabundant in a small spot at one magnetic pole (Mihalas 1973; Borra, Landstreet, and Thompson 1983), and the star ranges from helium-rich to helium-poor over its surface.

Another peculiar object possibly related to  $\delta$  Ori C is HD 49333. Hunger (1986a,b) illustrated work by Kaufmann and Theil for this star, which suggests that helium is underabundant above  $\tau = 0.4$  ( $\epsilon_{\text{He}} \approx 0.001$ ) and has a normal abundance below this level. These peculiar line profiles might also be caused by a non-uniform distribution of helium on the star as discussed above. Hunger (1988, private communication) also reports that there are at least three other candidates with peculiar helium profiles.

### 5.3 Models

Because of the uncertainties involved in the formation of Si II and Si III lines discussed in Chapter 4, the temperatures of HD 58260 and  $\delta$  Ori C have been estimated from the photometric indices given in table 1.2, as was done for HD 64740. Geneva photometry is not available for HD 58260. Interpolating from Buser and Kurucz's (1978)  $T_{\text{eff}}$  vs.  $(U - V)_0$  relation, the  $(U - V)_0$  of -1.03 leads to a temperature of 20770 K for  $\log g = 4.0$ , or 20070 K for  $\log g = 3.5$ . As will soon be seen, the surface gravity of HD 58260 is close to  $\log g = 3.30$ . From the theoretical  $uvby\beta$  indices of Lester, Gray, and Kurucz (1986), a temperature of about 19300 K is estimated from the star's  $[u - b]$  index. A  $T_{\text{eff}}$  of 20000 K will be assumed for HD 58260. For  $\delta$  Ori C, the Geneva and  $UBV$  photometries, and the relations of Cramer (1984) and Buser and Kurucz (1978), yield temperature estimates of 19000 K and 19050 K

respectively. The  $[u - b]$  index gives a temperature of about 18000 K for a  $\log g$  near 4.0, appropriate for  $\delta$  Ori C. A  $T_{\text{eff}}$  of 19000 will be employed throughout the remainder of this work.

The helium abundance and surface gravity of HD 58260 are found by adjusting these two parameters and modelling the profiles of H $\delta$ , He I  $\lambda 4471$ , and He I  $\lambda 4437$  until a suitable fit is achieved for each line. A uniform abundance of helium is assumed. The effects of the star's surface magnetic field are ignored for this fitting. A  $v \sin i$  of  $16 \text{ km s}^{-1}$  is determined from the fit of the He I  $\lambda 4437$  line alone.

The best fit profiles of H $\delta$  and He I  $\lambda 4471$  for HD 58260 are shown in figures 5.3 and 5.4 respectively. They were obtained with a surface gravity of  $\log g = 3.30$  and  $\epsilon_{\text{He}} = 0.30$ . Figure 5.5 shows the resulting fit for the He I  $\lambda 4437$  line. A discussion of the success of the modelling presented here will be deferred until the next section. Allowing for the inherent problem in using solar abundance atmospheres in the above analysis, the final adopted  $\log g$  is 3.20.

The location of HD 58260 in the theoretical  $\log g$  vs.  $\theta_{\text{eff}}$  diagram is indicated in figure 5.6. Interpolating from Maeder's (1981) theoretical evolutionary tracks, a mass of  $16.0 \pm 4.0 M_{\odot}$  is found. This corresponds to a radius of  $16.6 \pm 4.0 R_{\odot}$ . The above model of HD 58260 suggests that the star is considerably evolved. An estimate of its age can be

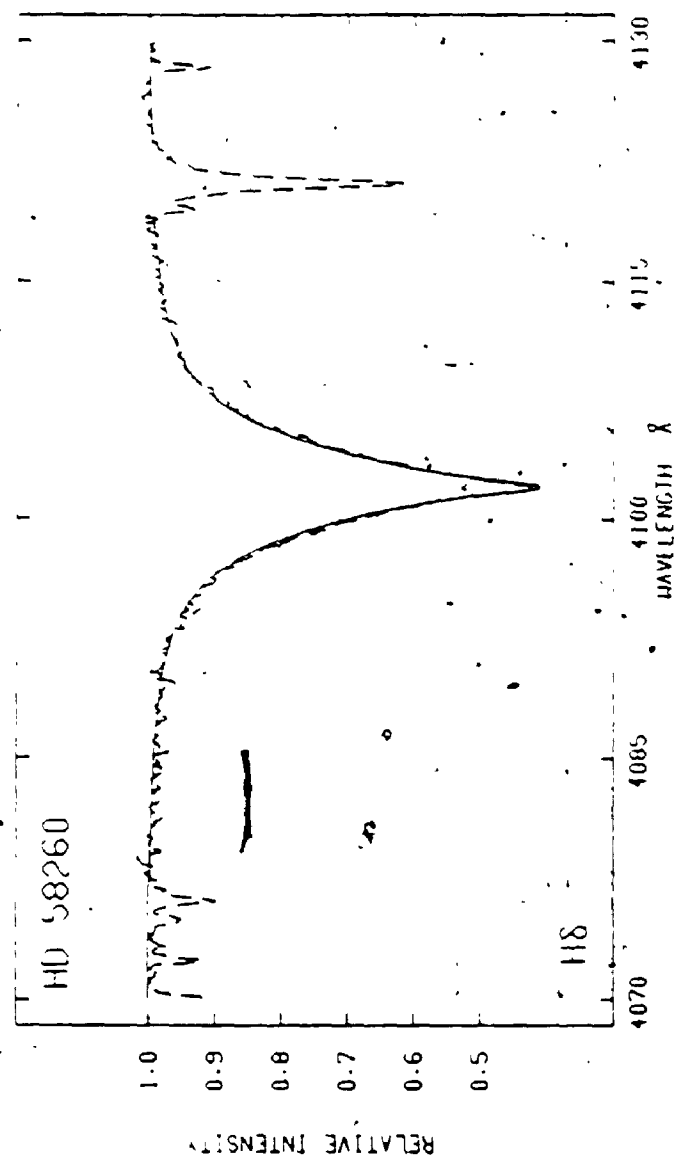


Figure 5.3 Observed (broken line) and modelled (solid line) H& line profiles of HD 58260 for a uniform hydrogen abundance of  $\epsilon_H = 0.70$ .

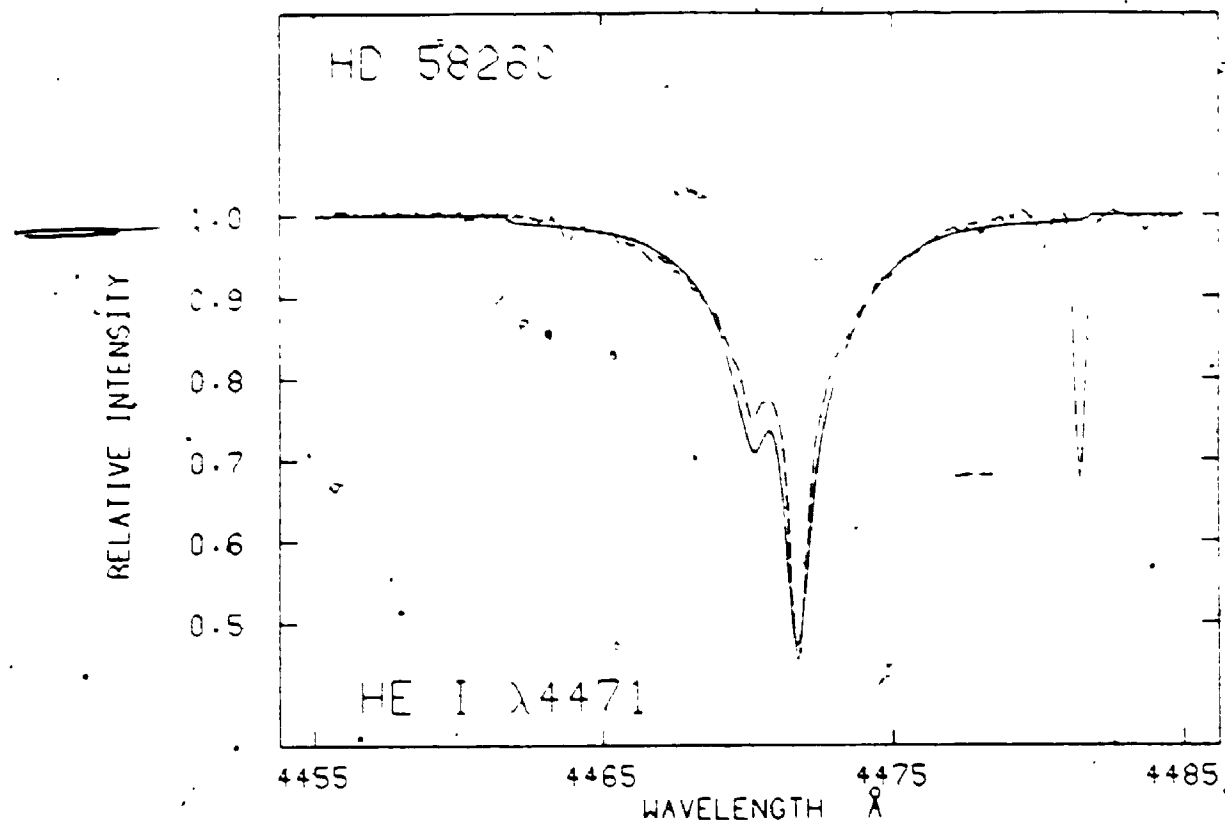


Figure 5.4 Observed (broken line) and modelled (solid line) He I  $\lambda 4471$  line profiles of HD 58260 for a uniform helium abundance of  $\epsilon_{\text{He}} = 0.30$ .

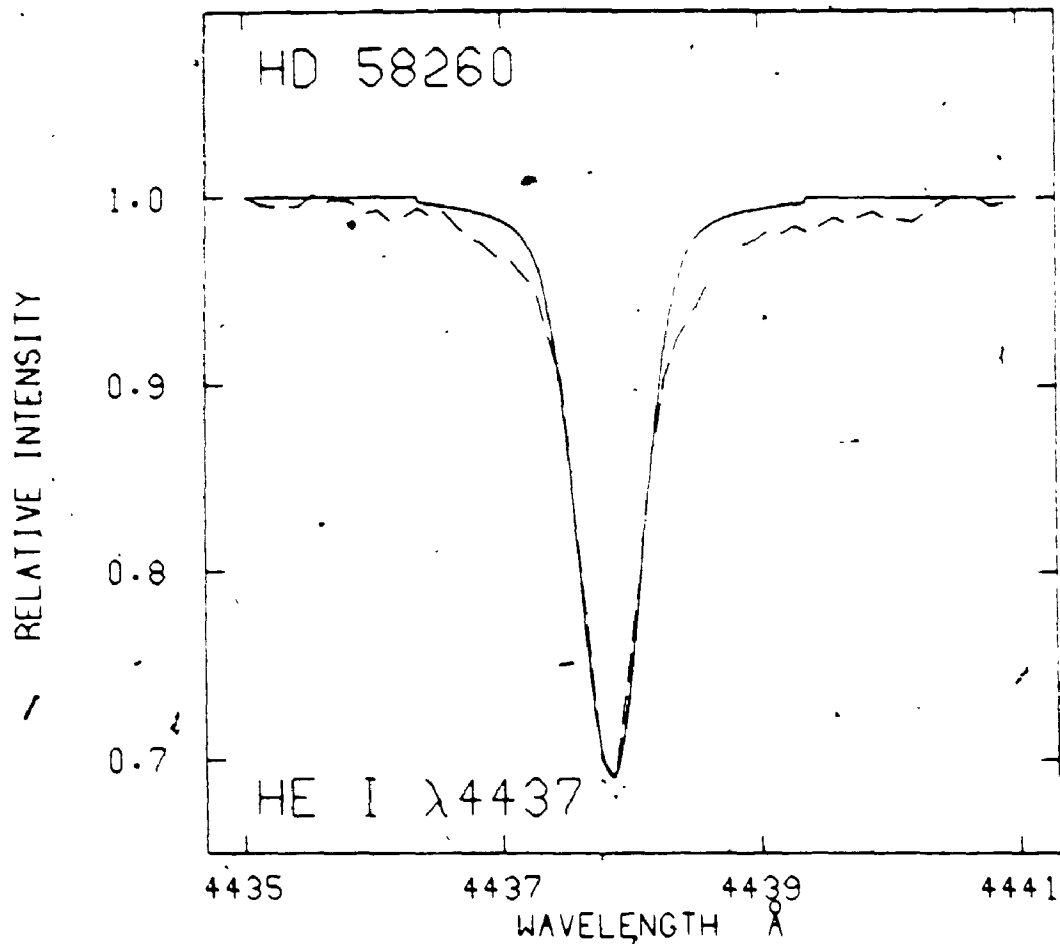


Figure 3.5 Observed (broken line) and modelled (solid line) He I  $\lambda$ 4437 line profiles of HD 58260 for a uniform helium abundance of  $\epsilon_{\text{He}} = 0.30$ .

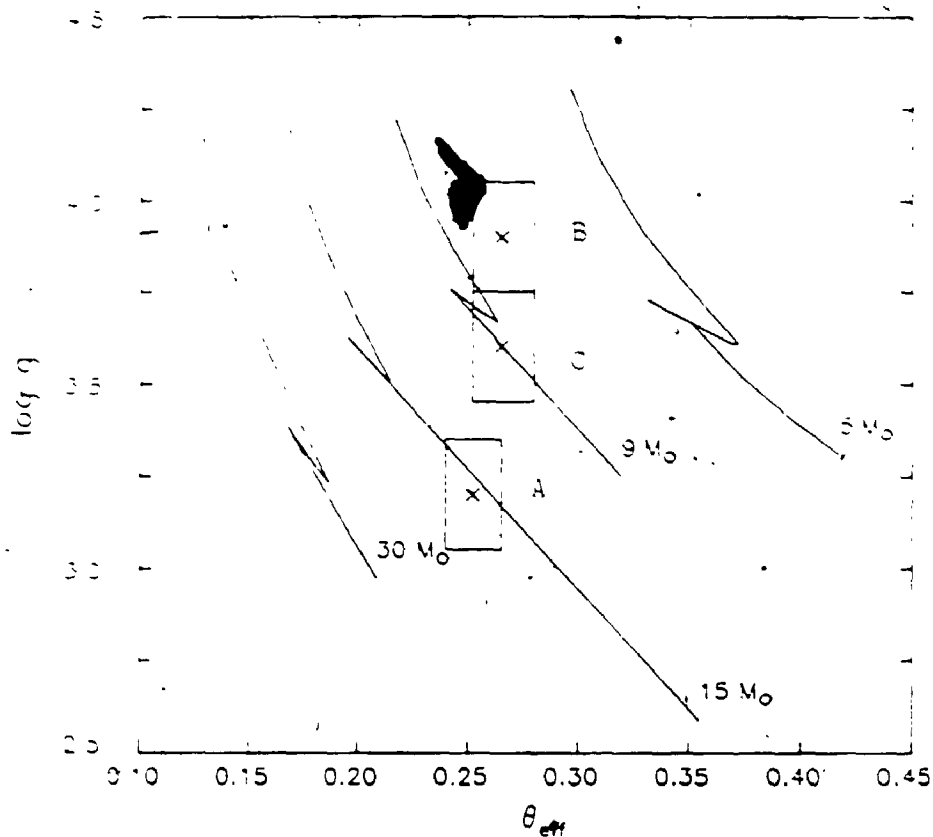


Figure 5.6 Locations of HD 58260 (A) and  $\delta$  Ori C (B for a spotted helium abundance geometry and C for a vertically stratified helium abundance geometry) in the  $\log g$  vs.  $\theta_{\text{eff}}$  plane. Symbols and evolutionary tracks are as in figure 4.8.

made from Maeder's (1981) calculations, and is found to be on the order of  $1.1 \times 10^7$  years. A possible error of 0.1 dex in  $\log g$  arising from uncertainty in the metallicity of the star (Alcock and Paczynski 1981) has been incorporated in the above errors.

Fitting the profiles of the Zeeman sensitive lines Si III  $\lambda\lambda 4567$  and  $4574$ , then yields constraints for the inclination, magnetic obliquity, and the polar field strength of HD 58260. The radius of  $16.6 R_{\odot}$ , as determined above, gives an upper limit of 52.5 days for the rotation period of HD 58260 using equation (4.3) and a  $v \sin i$  of  $16 \text{ km s}^{-1}$ . It is possible, but unlikely, that the constant magnetic field of the star is due to poor spacing of the observations. Since HD 58260 is somewhat evolved, its equatorial velocity,  $v_{\text{eq}}$ , should be considerably less than the maximum  $v \sin i$  of about  $240 \text{ km s}^{-1}$  observed in early B main sequence stars (Wolff, Edwards, and Preston 1982). If it is further assumed that the rotation velocities of the helium-strong stars are similar to normal early B stars, as seems to be the case (Walborn 1983, Bohlender et al. 1987), then the  $v \sin i$  of HD 58260 can be used to give a lower limit to the inclination of the star. Unfortunately, the low signal-to-noise of the magnetic observations gives little constraint to the value of  $\beta$  through equation (4.4) ( $r \approx 1.0$ ). An estimate of the value of  $r$  (equation [4.5]) can be made, if it is assumed that the extrema of the actual magnetic curve of HD 58260 are smaller than  $3160 \text{ G}$  (the

largest observed value of the magnetic field plus a  $2\sigma$  error) and larger than 1550 G (the smallest observation minus a  $2\sigma$  error). It can be shown that this gives a 95% probability of the value of  $r$  being greater than 0.4. Given lower limits for the inclination  $i$ , and  $r$ , equation (4.4) will then give an upper limit for the magnetic obliquity,  $\beta$ .

The relation of the polar magnetic field strength to the observed longitudinal field was given in equation (4.2) for the case of a dipolar field. The dipolar and quadrupolar polar field strengths,  $B_d$  and  $B_q$ ,  $i$ , and  $\beta$ , for a star can be determined uniquely only with observations of the extrema of the longitudinal and surface magnetic fields. If only the longitudinal field extrema are observed, then an independent determination of the inclination of the rotation axis is needed. The latter is usually determined through equation (4.3), which is of no use in this case, since no periodicity is seen in either HD 58260 or  $\delta$  Ori C. Because of the lack of variability of the magnetic fields, there will, however, remain an ambiguity in the values of  $i$  and  $\beta$  for these two stars; only the value of  $(i + \beta)$  can be uniquely determined. In this analysis, the initial assumption will be made that  $\beta = 0^\circ$  for these two stars. The inclinations of the rotation axes of HD 58260 and  $\delta$  Ori C are then determined by varying  $i$  and  $B_p$  in the models for the Si III line profiles until a suitable fit is obtained for both lines.

The Si III  $\lambda\lambda 4567$  and  $4574$  line profiles have been

modelled for various values of  $i$  and  $B_p$ , consistent with the observed constant longitudinal magnetic field of +2300 G. The silicon abundance is adjusted to give the best fit for the  $\lambda 4574$  line and the same model is then used to synthesize the  $\lambda 4567$  profile. It is found that suitable fits can be found simultaneously for both profiles for  $10^\circ < i < 50^\circ$ . For  $i < 10^\circ$  the  $\lambda 4567$  profile is slightly weak, while for  $i > 50^\circ$  the same line is too strong, and both line profiles are too broad, even for  $v \sin i = 0$ . An inclination of  $i = 40^\circ$  will be assumed for the remainder of the models. This gives a polar field strength of  $B_p = 8.1$  kG for HD 58260. Since the He I  $\lambda 4437$  line may be broadened to a small extent by such a field, this line was remodelled utilizing the derived magnetic geometry. The helium abundance is not affected, but a slightly lower  $v \sin i$  is found. Profiles of other metallic lines are modelled in a similar way. Most of the broadening of the metal line profiles results from the Zeeman effect. An upper limit to  $v \sin i$  is about  $12 \text{ km s}^{-1}$ , but the majority of the lines suggest a  $v \sin i$  near 0. Note, however, that the minimum velocity resolution of the spectrograph is on the order of  $10 \text{ km s}^{-1}$ , so that little can be said about rotation velocities below this limit. If  $i = 0^\circ$  is adopted, then from the above considerations,  $\beta = 40^\circ$ .

The derived abundances for silicon and some of the other elements seen in the spectra of HD 58260 are summarized in table 5.1. Included in the table are the

Table 5.1 HD 58260 and  $\delta$  Ori C Abundance Results

Ion/Mult.	$\lambda$ (A)	log gf	Ref.*	log $\epsilon$		
				HD 58260	$\delta$ Ori C	Solar
N II	12 3995	+0.28	WSG	-5.0	-4.5	-3.99
O II	5 4415	+0.305	WSG	-4.2	-3.4	-3.22
	5 4417	+0.044	WSG	-4.2	...	
Mg II	4 4481	+0.97	WM	-4.8	-4.0	-4.51
Al III	3 4529	+0.67	WSG	-6.2	-5.6	-5.65
Si II	3 4128	+0.31	WSG	-5.4	-5.0	-4.50
	4130	+0.46	WSG	-5.5	-5.3	
Si III	2 4567	-0.07	WM	-5.0	-4.4	
	4574	-0.41	WM	-5.0	-4.4	
Fe II	38 4549	-2.14	A	...	-3.0	-4.50
Fe III	4 4419	-2.33	A	-5.3	-4.3	

\*WSG = Wiese, Smith, and Glennon (1966)

WM = Wiese and Martin (1980)

A = Adelman (1988)

wavelengths of the lines considered, adopted oscillator strengths and their sources and the derived logarithmic abundances. In all cases, the element in question is assumed to be uniformly distributed over the surface. Solar abundances for each element are also indicated and are adopted from Kurucz (1979). Typically, the adopted abundances are 0.2 dex lower than would be needed, if the effects of the strong surface magnetic field were neglected. Effects of NLTE should be small for both HD 58260 and  $\delta$  Ori C.

The modelling approach for  $\delta$  Ori C proceeds in much the same manner as for HD 58260, except for the complication added by the peculiar nature of the star's helium profiles: the He I  $\lambda 4471$  line profile cannot be reproduced with a uniform atmospheric abundance of the element. Attempts at modelling this line with a high surface gravity and uniform helium abundance result in reasonable fits to the wings of  $\lambda 4471$ , but the core of the line is then much too strong. The H $\delta$  profile also does not support a high surface gravity interpretation.

After extensive trial and error it has been found that the helium and H $\delta$  profiles of  $\delta$  Ori C can be reproduced reasonably well if one of two possible assumptions is accepted: 1) the helium abundance is not uniform, but instead most of the helium is concentrated in only a small portion of the star's surface, or 2) helium is distributed uniformly, but there is a vertical stratification of helium

$c_{He} = 0.005$  above  $\tau = 0.35$  and no helium below, and  $c_{He} = 0.40$  below  $\tau = 0.35$  and no helium above, are given to demonstrate the fitting procedure.

As was done for HD 58260, the possible positions of  $\delta$  Ori C in the  $\log g$  vs.  $\theta_{eff}$  diagram are indicated in figure 5.6, after adjusting the derived gravities by  $-0.1$  dex, because of the inconsistency in Kurucz's atmospheres. The above models give two possible values of the surface gravity, and hence the mass and radius of the star. The error boxes shown include an additional uncertainty because of metallicity effects. The resulting interpolated masses for  $\delta$  Ori C are  $7.5 \pm 2.0 M_{\odot}$  for the spotted model and  $9.0 \pm 2.5 M_{\odot}$  for the stratified model of the star. Again (equation [4.3]), a  $v \sin i$  of  $32 \text{ km s}^{-1}$  (found from the He I  $\lambda 4437$  profile), and the resulting radii of  $5.1 \pm 1.6 R_{\odot}$  and  $7.9 \pm 2.5 R_{\odot}$  give upper limits of 8.1 and 12.5 days for the rotation period of  $\delta$  Ori C. As for HD 58260, the constant magnetic field of  $\delta$  Ori C is unlikely to be due to poor spacing of the observations. Assuming a maximum  $v_{eq}$  of  $240 \text{ km s}^{-1}$ , the inclination must be greater than  $7^{\circ}$ . Once again,  $\beta$  is poorly constrained by the observations. Proceeding as was done for HD 58260, a lower limit to  $r$  of 0.57 can be determined which, along with the above limit on the inclination and equation (4.4), gives the result  $\beta < 63^{\circ}$ .

Modelling of the Si III  $\lambda\lambda 4567$  and  $4574$  lines, then again leads to an upper limit on the inclination  $i$  (if  $\beta$  is

determined from the fit of the core for the remainder of the star's surface. The size of the spot and the abundances inside and outside of the spot were then adjusted until the best fit to the observed  $\lambda 4471$  profile was obtained. The resulting model was then used to produce synthetic profiles of He I  $\lambda 4437$  and H $\delta$ . The surface gravity was also a free parameter.

The adopted model consists of a helium-rich spot ( $\epsilon_{\text{He}} = 0.50$ ) with radius  $45^\circ$  on an otherwise extremely helium-poor surface ( $\log \epsilon_{\text{He}} = -3.6$ ). A surface gravity of  $\log g = 4.00$  gives the best results for the model profiles which are presented in figures 5.7 to 5.9. Also indicated in figure 5.8 are the model profiles for uniform helium abundances of  $\epsilon_{\text{He}} = 0.50$  and  $\log \epsilon_{\text{He}} = -3.6$ , which illustrate the general idea behind the fitting procedure discussed above. Simultaneous fitting of H $\delta$  and a strong and weak helium profile provide fairly tight constraints on the proposed model. For example, the relative strengths of the core and wings of the He-I  $\lambda 4471$  line are very sensitive to the helium abundance outside the helium-rich spot. Varying the 'background' helium abundance by 0.3 dex seriously degrades the model fit for this profile. Changing the size or helium abundance of the helium-rich spot results in poor fits to the He I  $\lambda 4437$  line and the wings of the He I  $\lambda 4471$  line. H $\delta$  gives an additional constraint for the surface gravity of the model.

The stratified model of  $\delta$  Ori C was determined in a

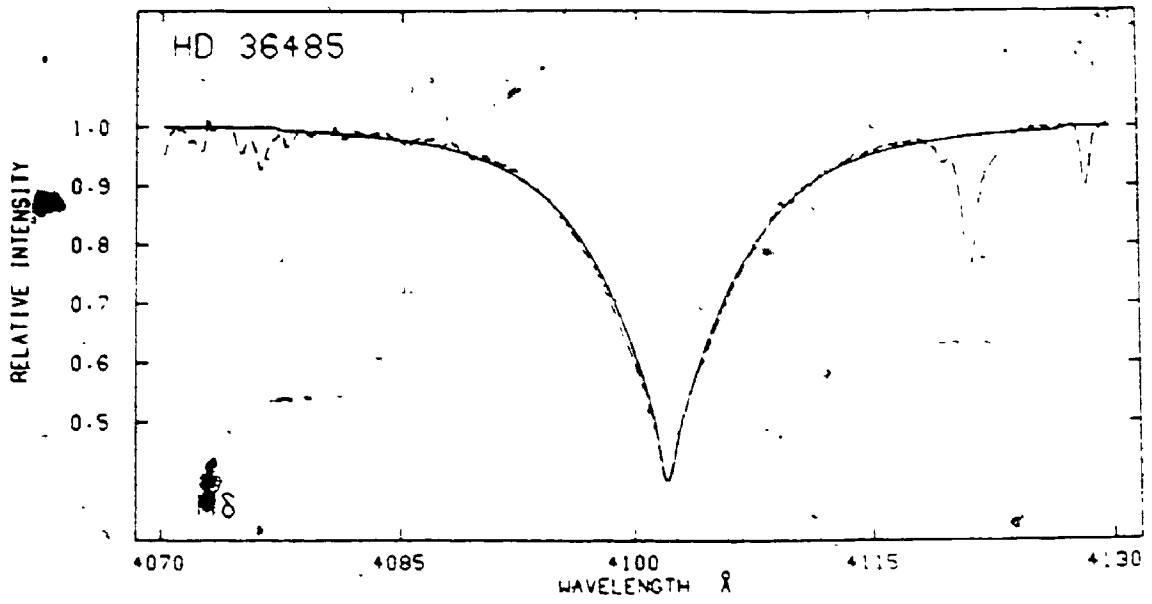


Figure 5.7 Observed (broken line) and modelled (solid line) H6 line profiles of  $\delta$  Ori C for a spotted helium abundance geometry.

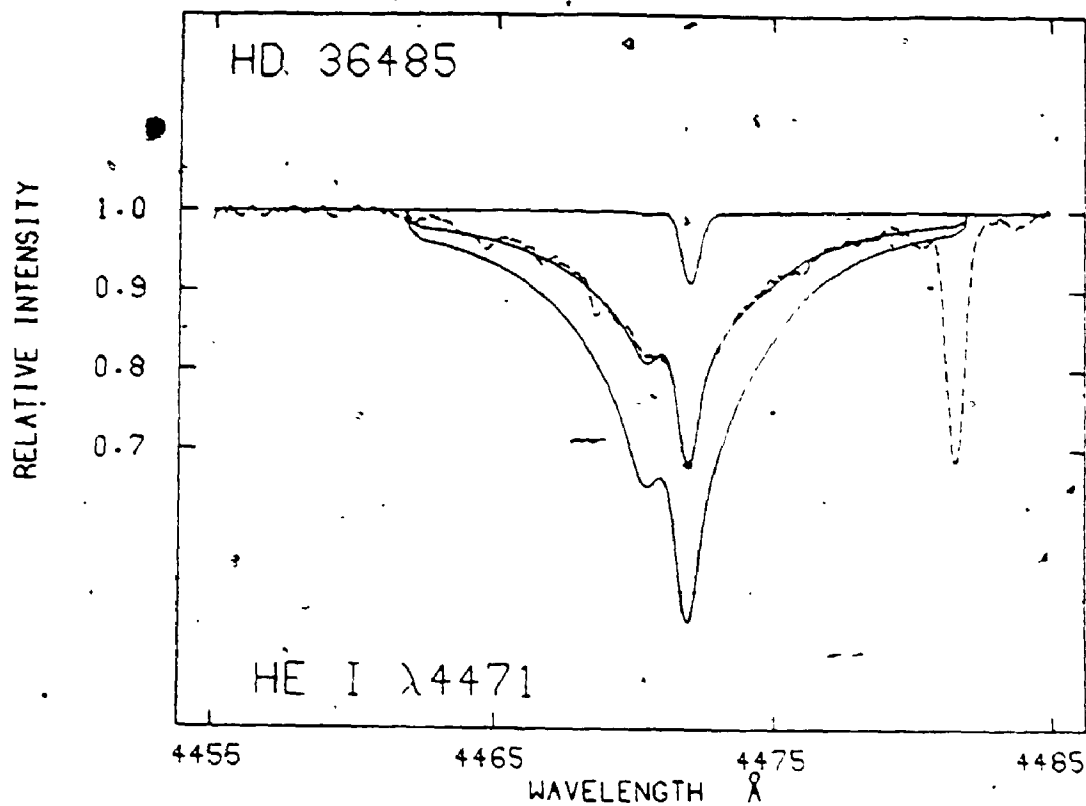


Figure 5.8 Observed (broken line) and modelled (solid lines) He I  $\lambda 4471$  line profiles of  $\delta$  Ori C for a spotted helium abundance geometry. Three model profiles are shown. From top to bottom: i) profile for uniform helium abundance of  $\log \epsilon_{\text{He}} = -3.6$  ii) adopted model profile iii) profile for uniform helium abundance of  $\epsilon_{\text{He}} = 0.50$ .

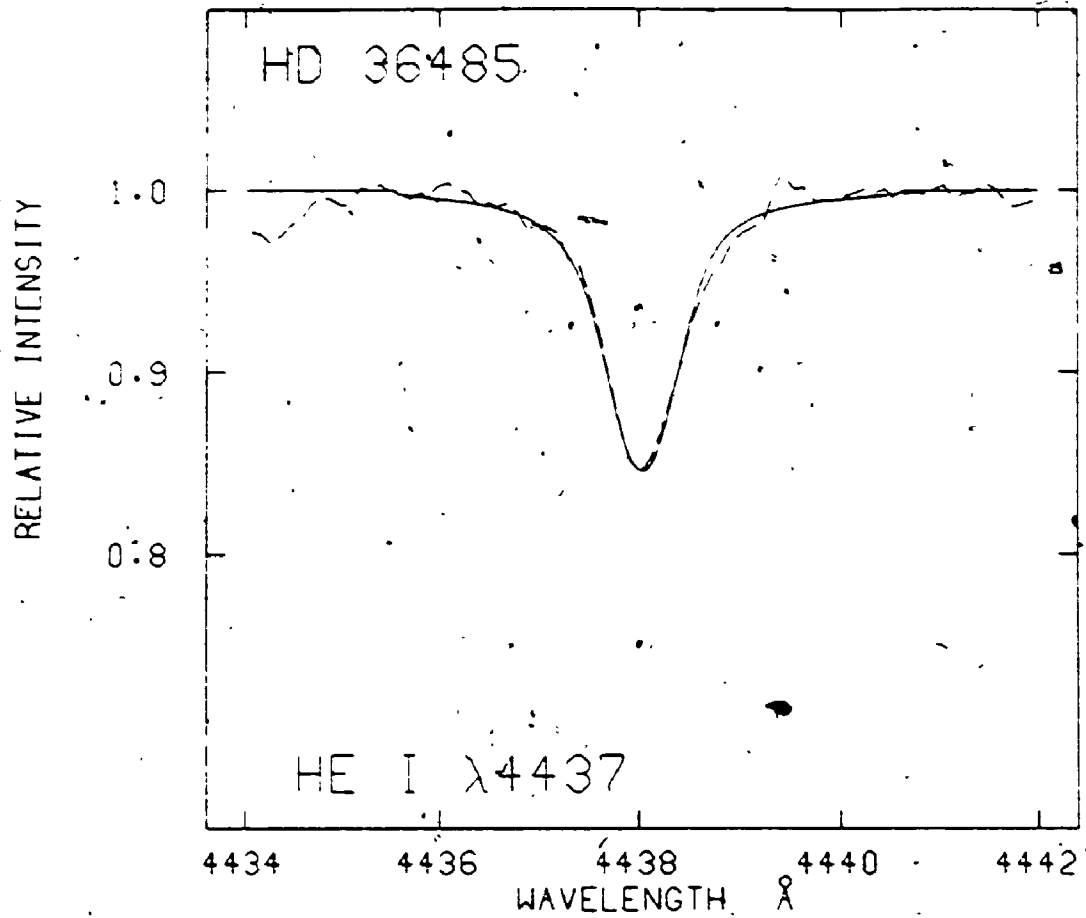


Figure 5.9 Observed (broken line) and modelled (solid line) He I  $\lambda 4437$  line profiles of  $\delta$  Ori C for a spotted helium abundance geometry.

similar manner. First, the He I  $\lambda 4471$  line core is fitted with a uniform, unstratified helium abundance. Then, a vertical abundance gradient of helium is incorporated into the model by using a simple step function at a specified optical depth,  $\tau_s$ . Since the line wings are formed deep in the atmosphere where the pressure broadening is large, the helium abundance is increased at optical depths greater than  $\tau_s$  in an attempt to fit the line wings. A step function for the helium stratification is probably justified when the rapid change in the radiative acceleration of helium with depth is considered. More complicated treatments of the stratification were not considered, because of the lack of a sufficiently well developed theory of helium stratification in stellar atmospheres, as well as because of the additional free parameters more sophisticated treatments would introduce. Giannone and Rossi (1980) have discussed some of the observed effects of such a helium stratification in stellar atmospheres. Here, the best fit model is found by varying  $\tau_s$ , the helium abundance above and below  $\tau_s$ , as well as the surface gravity, until a satisfactory fit is found for H $\delta$ , and the He I  $\lambda\lambda 4471$  and  $4437$  lines simultaneously.

The resulting stratified model for the helium abundance of  $\delta$  Ori C is presented in figures 5.10 through 5.12. The final model has a surface gravity of  $\log g = 3.70$  and  $\tau_s = 0.35$ . Above  $\tau_s$ ,  $\epsilon_{He} = 0.005$  and below  $\tau_s$ ,  $\epsilon_{He} = 0.40$ , a factor of 80 enhancement in helium abundance. Again, in figure 5.11 the profiles for uniform helium abundances of

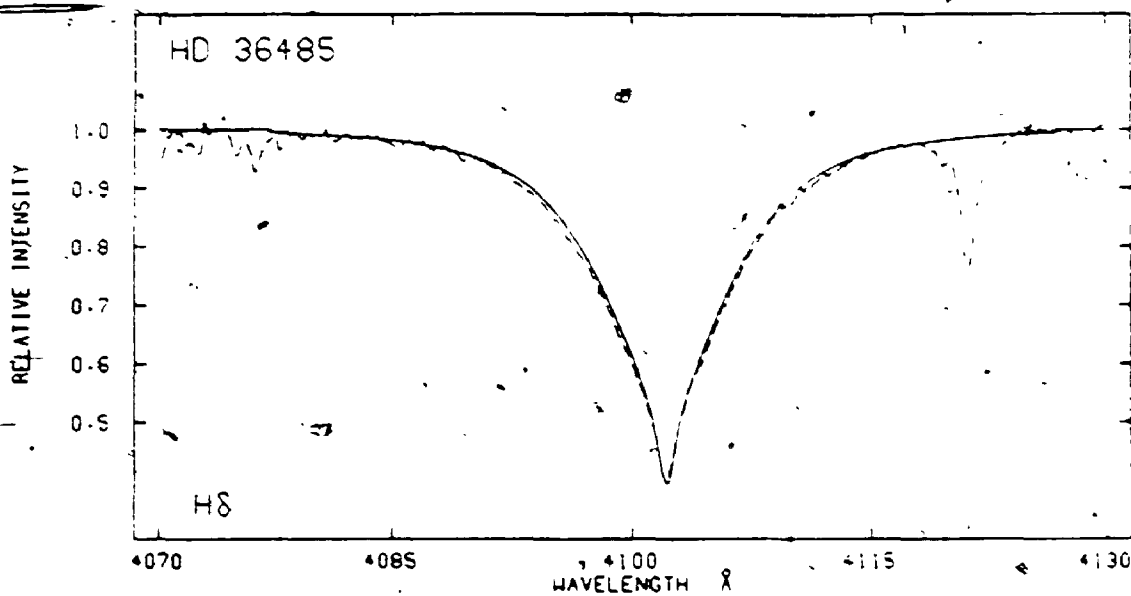


Figure 5.10 Observed (broken line) and modelled (solid line) H $\delta$  line profiles of  $\delta$  Ori C for a vertically stratified helium abundance geometry.

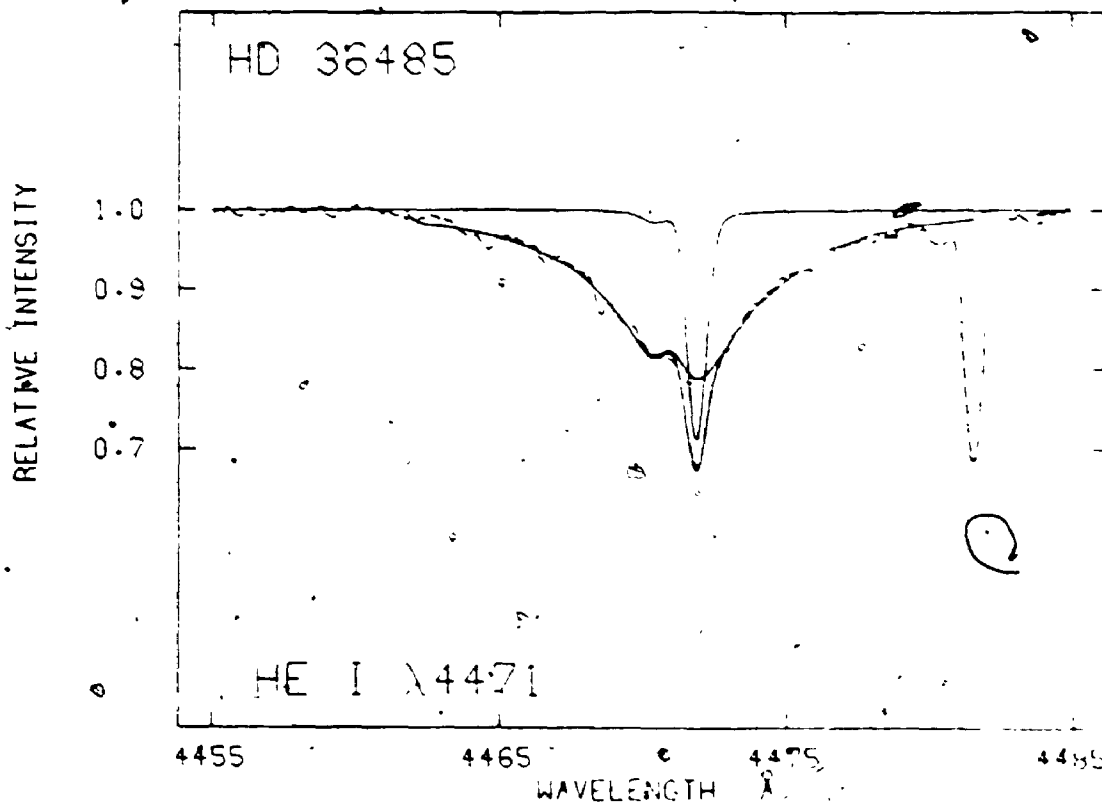


Figure 5.11 Observed (broken line) and modelled (solid lines) He I  $\lambda 4471$  line profiles of  $\delta$  Ori C for a vertically stratified helium abundance geometry. Three model profiles are shown. From top to bottom: i) profile for uniform helium abundance of  $\epsilon_{\text{He}} = 0.005$  above  $\tau = 0.35$ , no helium below ii) profile for uniform helium abundance of  $\epsilon_{\text{He}} = 0.40$  below  $\tau = 0.35$ , no helium above iii) adopted model profile.

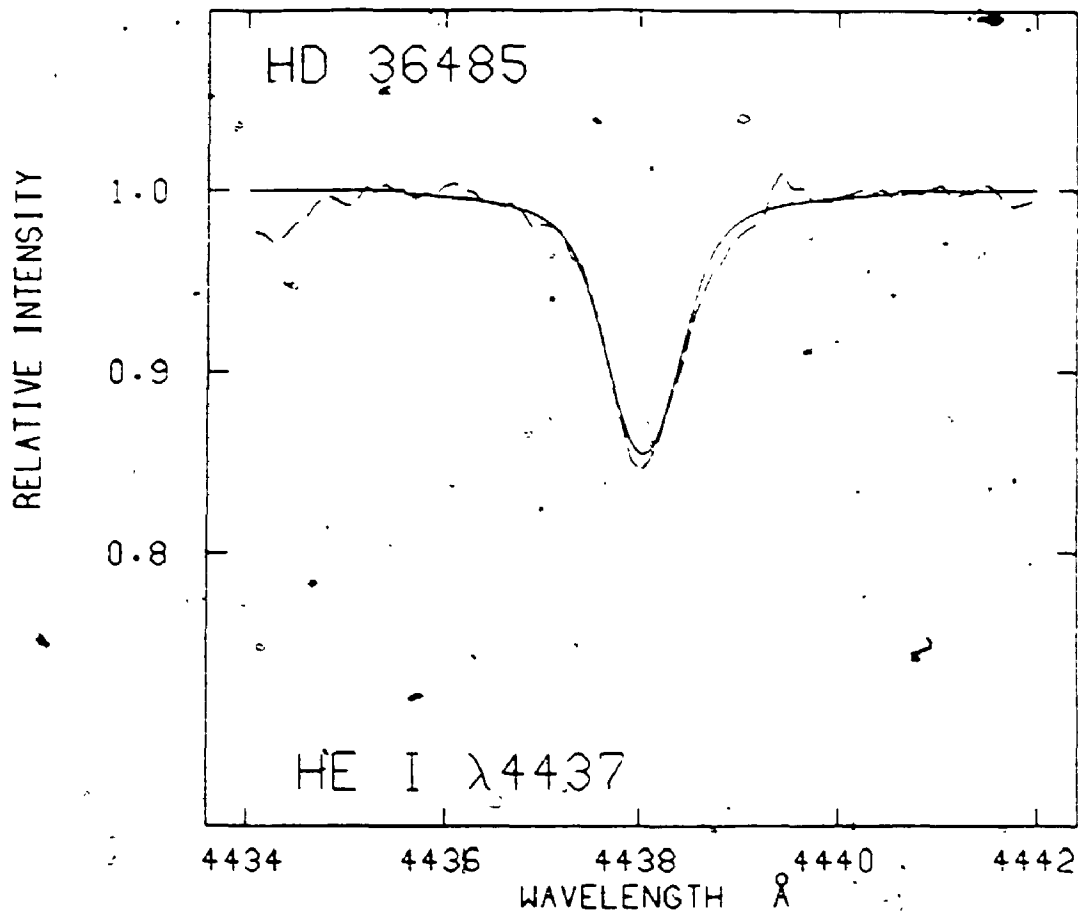


Figure 5.12. Observed (broken line) and modelled (solid line) He I  $\lambda$ 4437 line profiles of  $\delta$  Ori C for a vertically stratified helium abundance geometry.

$c_{He} = 0.005$  above  $\tau = 0.35$  and no helium below, and  $c_{He} = 0.40$  below  $\tau = 0.35$  and no helium above, are given to demonstrate the fitting procedure.

As was done for HD 58260, the possible positions of  $\delta$  Ori C in the  $\log g$  vs.  $\theta_{eff}$  diagram are indicated in figure 5.6, after adjusting the derived gravities by  $-0.1$  dex, because of the inconsistency in Kurucz's atmospheres. The above models give two possible values of the surface gravity, and hence the mass and radius of the star. The error boxes shown include an additional uncertainty because of metallicity effects. The resulting interpolated masses for  $\delta$  Ori C are  $7.5 \pm 2.0 M_{\odot}$  for the spotted model and  $9.0 \pm 2.5 M_{\odot}$  for the stratified model of the star. Again (equation [4.3]), a  $v \sin i$  of  $32 \text{ km s}^{-1}$  (found from the He I  $\lambda 4437$  profile), and the resulting radii of  $5.1 \pm 1.6 R_{\odot}$  and  $7.9 \pm 2.5 R_{\odot}$  give upper limits of 8.1 and 12.5 days for the rotation period of  $\delta$  Ori C. As for HD 58260, the constant magnetic field of  $\delta$  Ori C is unlikely to be due to poor spacing of the observations. Assuming a maximum  $v_{eq}$  of  $240 \text{ km s}^{-1}$ ; the inclination must be greater than  $7^{\circ}$ . Once again,  $\beta$  is poorly constrained by the observations. Proceeding as was done for HD 58260, a lower limit to  $r$  of 0.57 can be determined which, along with the above limit on the inclination and equation (4.4), gives the result  $\beta = 63^{\circ}$ .

Modelling of the Si III  $\lambda\lambda 4567$  and  $4574$  lines, then again leads to an upper limit on the inclination  $i$  (if  $\beta$  is

assumed equal to zero) of approximately  $40^\circ$ . The final adopted model has  $i = 10^\circ$ , and a polar field strength of  $-9$  kG. The subsequent use of this value of the inclination has no effect on the helium abundance models. The He I  $\lambda 4437$  line is not significantly affected by the surface field.

Table 5.1 contains the derived abundances for elements, other than helium, modelled in the spectra of  $\delta$  Ori C using the above magnetic model. Once again, it is assumed that the elements have uniform surface abundances. An average  $v \sin i$  of  $32 \text{ km s}^{-1}$  is found from the entire set of profiles.

#### 5.4 Discussion

Both models of the helium abundance geometry for  $\delta$  Ori C give very good fits to the H $\delta$  and helium line profiles. The results of the simple uniform abundance model for HD 58260 are reasonably good, but the wings of  $\lambda 4437$  are too weak in the model profile, while the forbidden component of the  $\lambda 4471$  line is too strong. This is similar to the more exaggerated behaviour of  $\delta$  Ori C, which suggests that HD 58260 may also have a vertical or horizontal stratification of helium.

To investigate this possibility, spot and stratified models of the helium abundance have been attempted for HD 58260 following the procedure outlined above for  $\delta$  Ori C. Figure 5.13 shows the results of modelling the He I  $\lambda 4471$

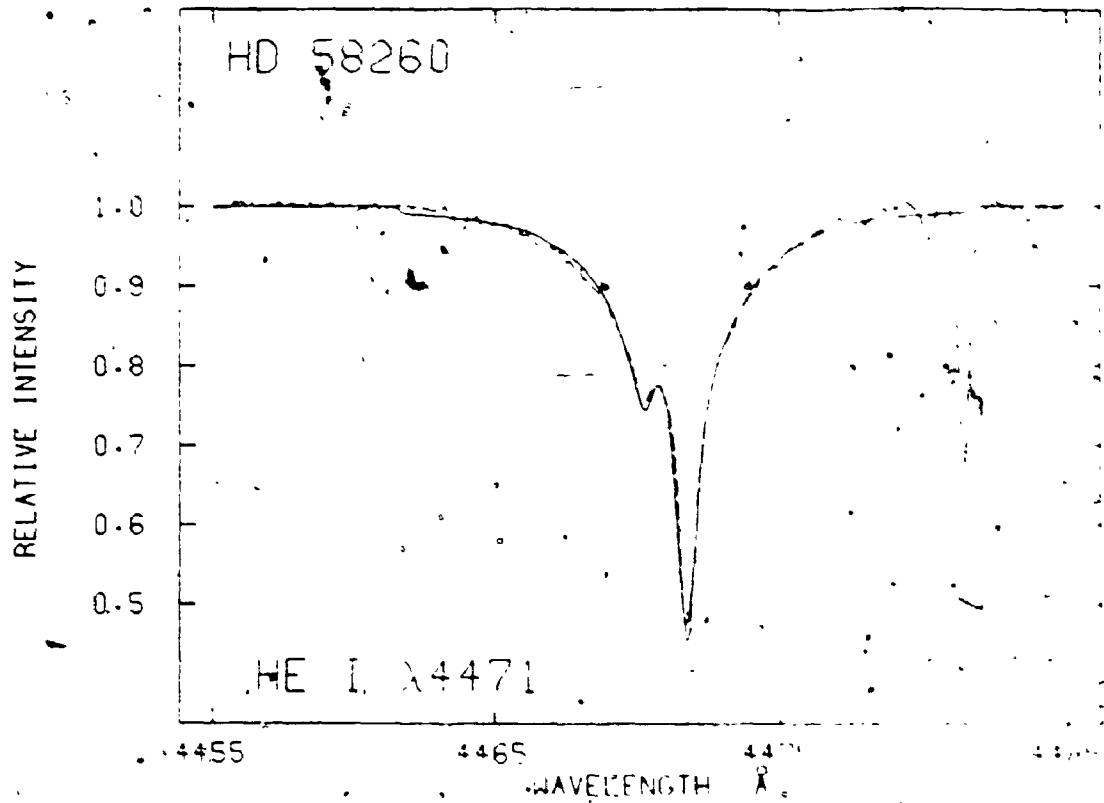


Figure 5.13 Observed (broken line) and modelled (solid line) He I  $\lambda$ 4471 line profiles of HD 58260 for a spotted helium abundance geometry described in the text.

profile using a  $60^\circ$  radius helium-rich spot ( $\epsilon_{\text{He}} = 0.50$ ) at the visible magnetic pole of HD 58260 ( $\log g = -3.30$  and  $T_{\text{eff}} = 20000$  K). The remainder of the surface has  $\epsilon_{\text{He}} = 0.03$ .

The fit to the observed profile is much better, and H $\delta$  (not shown) is also well represented by the model. However, the wings of the  $\lambda 4437$  line are still not reproduced. The results are similar for the stratified models. Adjusting the free parameters of either model (spot size, abundance, step function of vertical helium stratification, etc.) do not improve the results. For now, the peculiar profile of this line must remain an unanswered problem.

An examination of table 5.1 indicates that  $\delta$  Ori C is more metal-rich than HD 58260 by a factor of between 5 and 10 for the limited sample of elements for which abundances have been determined. HD 58260 is almost certainly metal-deficient. Relative to the sun,  $\delta$  Ori C is overabundant in magnesium. Oxygen and nitrogen are underabundant in the star. Silicon and aluminum have roughly solar abundances. Iron presents an interesting case. The difference in derived abundances between Fe II and Fe III suggests that the temperature of  $\delta$  Ori C, as determined from its colour indices, has been overestimated by a substantial amount. The two lines in table 5.1 yield an identical abundance of  $\log \epsilon_{\text{Fe}} = -3.3$  (10 times the solar abundance) for a  $T_{\text{eff}}$  of 16500 K, 2500 K lower than the temperature derived above. It is difficult to estimate how much weight to give to this ionization equilibrium temperature, given the uncertainties

in the oscillator strengths of iron, errors in the outer atmosphere structure, or possible non-LTE effects, but the discrepancy should be investigated further. If the star is indeed this cool, then the abundances given in table 5.1 will all be too small, with the exception of magnesium. The star in this case would be metal-rich, and probably more closely related to the helium-weak stars than the helium-strong class. Indeed, this might be supported by the spotted helium geometry discussed earlier, since the star can be modelled by assuming that it is very helium-weak over much of its surface.

If  $\delta$  Ori C is assumed to be a member of the Orion OB1 association, then its distance is on the order of  $450 \pm 50$  parsecs. The visual magnitude may then be used to estimate the luminosity, and hence radius of the star. The distance and apparent magnitude give  $M_v = -1.54$ . The tables of Code et al. (1976) give a bolometric correction of  $-1.91$  using a temperature of 19000 K. This gives  $\log L/L_\odot = 3.28$  and a radius of  $4.04 R_\odot$ . This independent determination of the radius of  $\delta$  Ori C would seem to support the spotted helium geometry of the star, although the result depends heavily on the assumption that the star is a member of the Orion association. Obviously, if the star was at a greater distance, the derived radius would be in better agreement with the stratified model for the star derived earlier. A suggestion for how to determine which of the above two

scenarios is the correct interpretation for  $\delta$  Ori C will be given in chapter 8.

## Chapter 6 $\sigma$ Orionis E

### 6.1 Introduction

As was pointed out in the introductory chapter,  $\sigma$  Ori E is the prototype of the helium-strong stars, and also the most extensively studied. A roughly chronological history of the investigations of this star is given below.

The discovery of the star's peculiar nature by Berger (1956), and the analyses of Greenstein and Wallerstein (1958), and Klinglesmith et al. (1970) have already been touched upon (chapter 1). Lester (1972) modelled photographic spectra of  $\sigma$  Ori E and found  $T_{\text{eff}} = 22750$  K,  $\log g = 4.15$ , and  $N_{\text{He}}/N_{\text{H}} = 0.36$  from an average of four helium line profiles. His best fit  $v \sin i$  ranges from 142 to 180 km s<sup>-1</sup>. Osmer and Peterson (1974) used the equivalent width ratios of the He I  $\lambda 4143$  and H $\delta$  lines, as well as He I  $\lambda 4471$  and H $\gamma$ , to determine a helium abundance of  $x_{\text{He}} = 0.52$ , and found  $\log g = 4.31$  from the hydrogen profiles, as well as an effective temperature of 24500 K from uvby $\beta$  colour indices.

Walborn (1974) discovered variable H $\alpha$  emission in  $\sigma$  Ori E. The emission has a maximum width of 1800 km s<sup>-1</sup> (about 40Å) and rises to 30% above the continuum. He noted that whenever the emission is strong the absorption is weak, and that the sum of the maximum emission intensity and maximum absorption intensity with emission strong is approximately equal to the maximum absorption intensity, when there is no

emission. Walborn (1974) suggested that this indicates that the emission is a single, broad emission profile superposed on the absorption feature. (Higher quality observations have altered this picture; see below.) The emission is variable on a time scale of a few hours.

Searches for radial velocity variations in the helium and metal line spectrum of  $\sigma$  Ori E have given negative results (Wallerstein 1959; Bolton 1974). Bolton (1974) estimates an upper limit of  $4 \text{ km s}^{-1}$  for the velocity semi-amplitude. He did, however, report variations in the Ca II K line, which are possibly circumstellar in origin.

Hunger (1974) discovered spectrum variability in  $\sigma$  Ori E. Helium lines vary with an amplitude of up to 48%, and silicon lines up to 54%.  $H\gamma$  and  $H\delta$  are constant within 12%, and Mg II and C II appear constant as well. The time scale of the variability is again on the order of an hour. Prior to this work (although published later), Nissen (1974) had noted that the He I  $\lambda 4026$  line appeared variable in his narrow-band photoelectric measurements. Thomsen (1974) obtained photoelectric observations of variations of the He I  $\lambda 4471$  line and obtained a best fit to the data for a period of just under 6 days. Shorter periods of 29 and 21 hours are also consistent with his observations. These short periods are appropriate for an oblique rotator interpretation for  $\sigma$  Ori E, as first suggested for the helium-strong stars in general by Osmer and Peterson (1974).

Broad-band light variability in the star was first

observed by Walborn and Hesser (1976), who obtained simultaneous uvby $\beta$  photometry, H $\alpha$  emission, and helium equivalent width measurements. A period of 1.19 days was found from the photometry and the H $\alpha$  data, including Walborn's (1974) earlier observations. Again, no radial velocity variations were detected. When plotted on this period, the H $\alpha$  and helium line data suggested a possible double wave variation, similar to the behaviour seen in the equivalent widths of elements in Ap stars. The simultaneous data acquisition also gave much information concerning the relative phasing of the various data. For example, the primary H $\alpha$  emission and helium absorption maxima coincide. In addition, the sharp light minimum observed coincides with H $\alpha$  emission and helium absorption minima. The light variations are remarkably eclipse-like, rather than the smooth, low-amplitude photometric variability observed for many Ap stars. However, the authors caution that Bolton's (1974) upper limit to the radial velocity variations imposes a mass of less than 0.1  $M_{\odot}$  for any companion for an orbital inclination greater than 45°.

Further photometric observations (Hesser, Walborn, and Ugarte P. 1976; Hesser, Moreno, and Ugarte P. 1977) led to a very accurate determination of the period of  $\sigma$  Ori E. Hesser, Moreno, and Ugarte P. (1977) find  $P = 1.19081 \pm 0.00001$  days. This remains the definitive period. Better phase coverage of the photometry shows that a secondary light minimum, also eclipse-like, follows the primary by 0.43 P.

The amplitude of the variation is greatest in the ultraviolet. The two minima are asymmetrical and the light level outside the minima is not constant. The  $H\beta$  observations show behaviour similar to previous  $H\alpha$  data (Walborn and Hesser 1976), and suggest that there is also emission present at  $H\beta$ .

Shortly thereafter, Groote and Hunger (1976) observed a variable shell spectrum in the star. The number of Balmer lines visible,  $n$ , varies from 15 to 21, with the star being faintest when  $n$  reaches a maximum. Groote and Hunger proposed that the additional absorber could consist of a ring or two clouds of material located at two magnetic poles of a magnetic star. The suggested magnetic field had yet to be observed. Further observations (Groote and Hunger 1977) showed that the radial velocities of the additional shell lines are shifted by  $-60 \text{ km s}^{-1}$  immediately before, and  $+50 \text{ km s}^{-1}$  immediately following each eclipse. A ring model for the absorbing material would then require a retrograde rotation for the ring.

Kemp and Herman (1977) added yet another observation to the plethora of data for  $\sigma$  Ori E. Thirty-three nights of linear polarization measurements showed a 0.10% peak-to-peak variation of linear polarization in the B-band on the above 1.19 day period. Lower quality U band data showed somewhat more complicated polarization structure.

Pedersen and Thomsen (1977) and Pedersen (1979) performed narrow-band photometry of the He I  $\lambda 4026$  line as

well as uvby $\beta$  photometry for  $\sigma$  Ori E. Their  $R$  index data indicate a definite double wave variation in the helium line strength on the 1.19 day period. The primary minimum in the light curve follows the phase of maximum helium line strength by 0.12 P. Pedersen (1979) also made extensive additional H $\alpha$  scans of the star.

The observations of  $\sigma$  Ori E were very suggestive of an oblique rotator explanation for the star, and this interpretation was strengthened by the observation of a strong, variable longitudinal magnetic field on the star by Landstreet and Borrå (1978). More magnetic field observations, including measurements obtained using the He I  $\lambda$ 5876 line, have been reported by Bohlender et al. (1987). Both the H $\beta$  and helium line polarization data show that the field varies between -1500 and +2800 G with the 1.19 day period of the spectroscopic and light variations of the star. The shell lines and eclipses of the star occur when the line of sight is close to the plane of the magnetic equator. Landstreet and Borrå (1978) suggested that the variable phenomena of  $\sigma$  Ori E can be understood in terms of an oblique rotator model with hot ( $T = 10000$  K) gas trapped in a magnetosphere above the magnetic equator. The  $R$  index observations of Pedersen and Thomsen (1977) and Pedersen (1979) also suggest that helium is most overabundant around the magnetic equator of the star.

Groote, Hüngrer, and Schultz (1980) and Groote and Kaufmann (1981) measured the infrared fluxes of several

helium-variable stars and reported a possible variable infrared excess of more than 150% in  $\sigma$  Ori E. The infrared emission appears to be strongest during the shell phases of the star, although the data are quite limited in phase coverage. Free-free emission due to ionized gas trapped in the magnetosphere of the star is suggested as the source of the emission. Bonsack and Dyck (1983) however, have carried out infrared photometry of several chemically peculiar stars and have failed to confirm the above results for  $\sigma$  Ori E (or for any of the stars measured by Groote and his collaborators), although one of their measurements for the star shows a statistically significant infrared excess. They point out that the infrared excesses reported by Groote, Hunger, and Schultz (1980) are correlated with the visual magnitudes of their program stars, and believe the earlier measurements were affected by systematic errors. Groote and Kaufmann (1984) counter this argument by suggesting periodic variations of the infrared fluxes and systematically fainter magnitudes measured by Bonsack and Dyck (1983), either because of poor weather conditions or because calibration errors are the source of the discrepancy between the two sets of observations. More recently however, Kroll (1987) has demonstrated that there is indeed a non-linearity present in the ESO infrared photometry, and by carefully correcting his data for this non-linearity, confirms the results of Bonsack and Dyck.

Shore and Adelman (1981) have carried out IUE

observations of several helium-strong stars, including  $\sigma$  Ori E. Ultraviolet line profiles of C II, C III, C IV, Si III, Si-IV, and Al III all vary on the rotational period in antiphase with helium. . Barker et al. (1982) have presented additional IUE data. The C IV profiles have a persistent shortward absorption extending to  $-600 \text{ km s}^{-1}$ , which is suggestive of a stellar wind, but show no evidence for fully developed P Cygni profiles. The cores of these lines vary in depth by a factor of about two, but only near the line center. It is uncertain whether this line variability arises in the wind of the star or in the photosphere. One maximum of the C IV absorption occurs near maximum negative magnetic field strength, which suggests that the stellar wind might be confined to a cone above this pole. The second C IV absorption maximum, on the other hand, leads the positive pole in rotation by about  $0.2 P$  (Barker 1986).

The work of Groote and Hunger (1982) is the most comprehensive modelling that has been performed for  $\sigma$  Ori E, prior to the current investigation. . From the continuum fluxes they derived a  $T_{\text{eff}} = 22500 \text{ K}$ , and angular diameter of  $0.079 \pm 0.002$  milliarcsec. A surface gravity of  $\log g = 3.85 \pm 0.1$  was found from the optical spectrum, as was the helium abundance on the visible hemisphere of the star as a function of phase. The helium abundance ranges from  $\epsilon_{\text{He}} = 0.75$  to  $\epsilon_{\text{He}} = 0.38$  (note that this abundance refers to an average over the disk as a whole at each phase; the actual range in helium abundance could be considerably higher).

The 400 pc distance to  $\sigma$  Ori AB then yields a mass of  $3 \pm 1 M_{\odot}$  for the star. Since the mass and temperature are consistent with a star of this mass with hydrogen mass fraction  $X = 0.3 \pm 0.2$ , the authors conclude that the helium enrichment is not confined to the surface. In their model, the H $\alpha$  emission and shell lines arise from two more or less isolated clouds located near the intersections of the magnetic and rotational equators at a distance of about two stellar radii from the center of the star. A temperature of 15000 K and a total mass of the order of  $10^{-10} M_{\odot}$  is estimated for the clouds. The clouds appear in emission when the Doppler effect is large enough to shift their emission away from the photospheric absorption line. Barker (1986) has extended this model to incorporate the observed behaviour of the C IV resonance lines observed by IUE. Groote and Hunger (1982) were also able to explain the lack of observed radial velocity variations in the helium lines, despite the obviously non-uniform helium abundance. Landstreet and Borra (1978) had earlier argued that since the strong helium lines that are normally used for radial velocity measurements have saturated cores, even for normal helium abundances, the radial velocity variations for these lines would occur only in the damping wings and hence escape detection using conventional techniques. In fact, Groote and Hunger (1982) have shown that the cores of the strong helium lines should show opposite radial velocity shifts to the cores of weak helium lines, and present observational

evidence in favour of this. This effect will be encountered again below and in the next chapter.

Walborn (1982) and Bolton et al. (1986) have demonstrated that the H $\alpha$  emission variability of  $\sigma$  Ori E is stable over more than 3400 rotation periods of the star. The latter data will be presented in more detail below. Emission has now also been observed in high quality spectra of the H $\beta$  line (Hunger 1986). Nakajima (1981, 1985) has developed a theory for the Balmer line emission in which the circumstellar gas is trapped by the stellar magnetic field and forced to corotate with the star. The position and extent of the circumstellar cloud(s) are determined by the balance between centrifugal and gravitational forces.

Walborn (1983) measured a  $v \sin i$  of 170 km s<sup>-1</sup> for  $\sigma$  Ori E using the He I  $\lambda 4121$  line. Adelman and Pyper (1985) have performed additional  $uvby\beta$  photometry and optical spectrophotometry of the star, and using Kurucz's  $\log g = 4.0$ , solar abundance model atmospheres find  $T_{\text{eff}} = 23400$  K. Drake et al. (1985, 1987) have found  $\sigma$  Ori E to be a variable, non-thermal, radio source at 2, 6, and 20 cm. The emission is consistent with gyrosynchrotron emission from mildly relativistic particles trapped in the magnetosphere of the star. Phillips and Lestrade (1988) have confirmed these observations using Very Long Baseline Interferometry (VLBI), and have determined an upper limit of 6 stellar diameters for the extent of the emitting region.

## 6.2 Observations

The magnetic field measurements of  $\sigma$  Ori E are presented in figure 6.1 along with smoothed curves representing the helium line strength index R (Pedersen and Thomsen 1977; Pedersen 1979), the number,  $n$ , of the last visible Balmer line (Groote and Hunger 1976), and the photometric measurements of Hesser, Walborn, and Ugarte (1976). The data are plotted according to the ephemeris determined by Hesser, Moreno, and Ugarte (1977):

$$\text{JD (primary minimum)} = 2442778.819 + 1.19081(\pm 0.00001)E.$$

The phasing of the various data discussed in the preceding section is clearly seen in the figure.

As for HD 64740, circular polarization measurements of  $\sigma$  Ori E have been obtained in the wings of  $H\beta$  and He I  $\lambda 5876$  (Landstreet and Borra 1978; Bohlender et al. 1987). The results for both lines again yield identical sinusoidal longitudinal magnetic field curves. The curve through the magnetic data in figure 6.1 is given by equation (2.2) and data given in table 2.2. Once more, the dipole component of the field configuration appears to dominate, as is reflected by the goodness of fit (the reduced chi-squared is 1.48) of the curve to the data. Equation (4.2) gives a lower limit of about 9.5 kG for the dipole polar field strength. From the arguments in chapters 3 and 4, a surface magnetic field of this order might be expected to manifest itself through differential intensification of the Si III multiplet 2 lines. This will be discussed below.

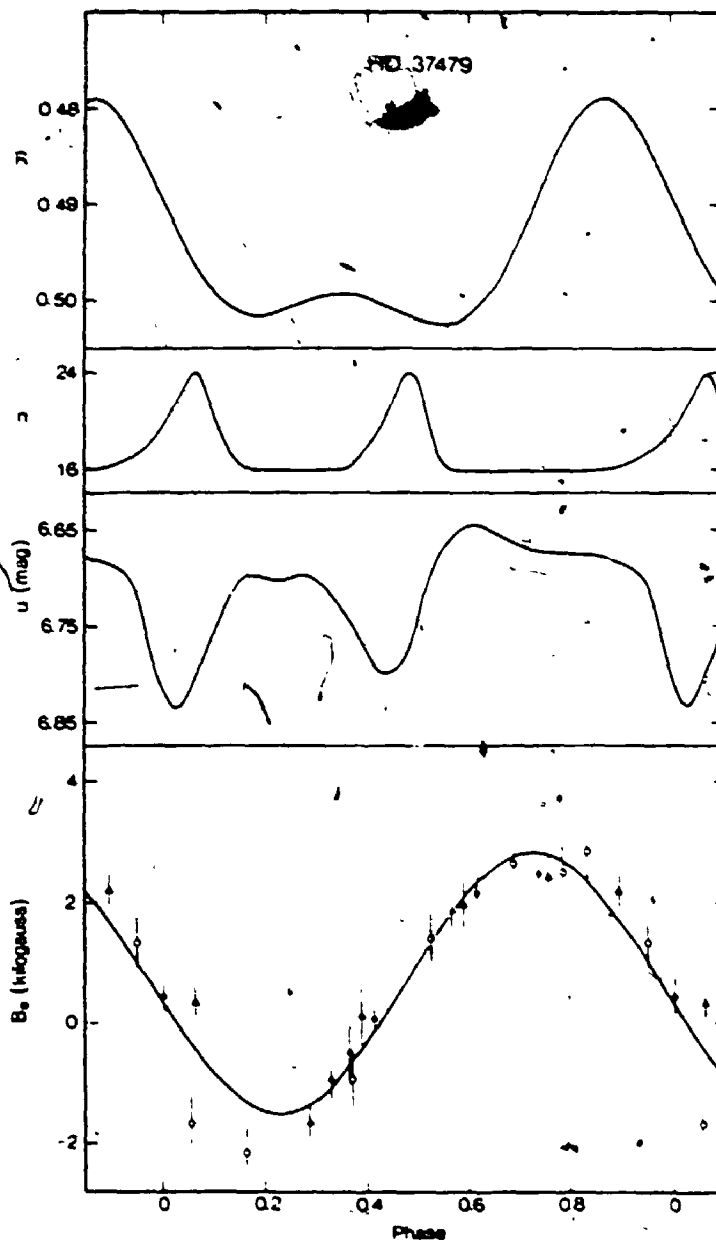


Figure 6.1 Helium line strength index,  $R$ , shell line, and photometric and magnetic curves of  $\sigma$  Ori E = HD 37479. The first three curves are hand-drawn fits to the data. Magnetic data symbols are as in figure 4.7, except that open circles represent  $H\beta$  observations of Landstreet and Borra (1978). The curve through the magnetic observations is given in the text. (From Bohlender et al. 1987.)

The CFHT observations are given in table 2.1, where the phases have been determined to a high degree of accuracy using the above ephemeris. In figures 6.2 and 6.3, the complete set of CFHT H $\alpha$  and H $\delta$  profiles are presented. These data represent the highest quality observations of the phenomena associated with the circumstellar material of  $\sigma$  Ori E. Bolton et al. (1986) have summarized these observations (supplemented with additional spectra obtained at McDonald Observatory). By comparing these figures with figure 6.1, it can be seen that the disappearances of the H $\alpha$  emission coincide with the appearances of shell absorption at H $\delta$ , and the photometric minima (near phases 0.00 and 0.45). In addition, the depths of the photometric minima are correlated with both the strengths of the violet emission seen at phases approximately 0.20 P prior to the shell phases, and with the depth of the shell absorptions at the time of the minimum (e.g. the violet emission near  $\phi = 0.75$  is stronger than the violet emission at  $\phi = 0.20$ ). This suggests that most of the light variations are produced by eclipses of the star by the circumstellar material. The emission variations support a model with two distinct regions of emitting gas co-rotating with the star near the intersections of the magnetic and rotational equators. According to Bolton et al. (1986), the maximum width of roughly 4 A for the Balmer shell lines and the widths of the minima in the light curve indicate that the emission regions subtend an angle of 18° to 40° at the center of the star.

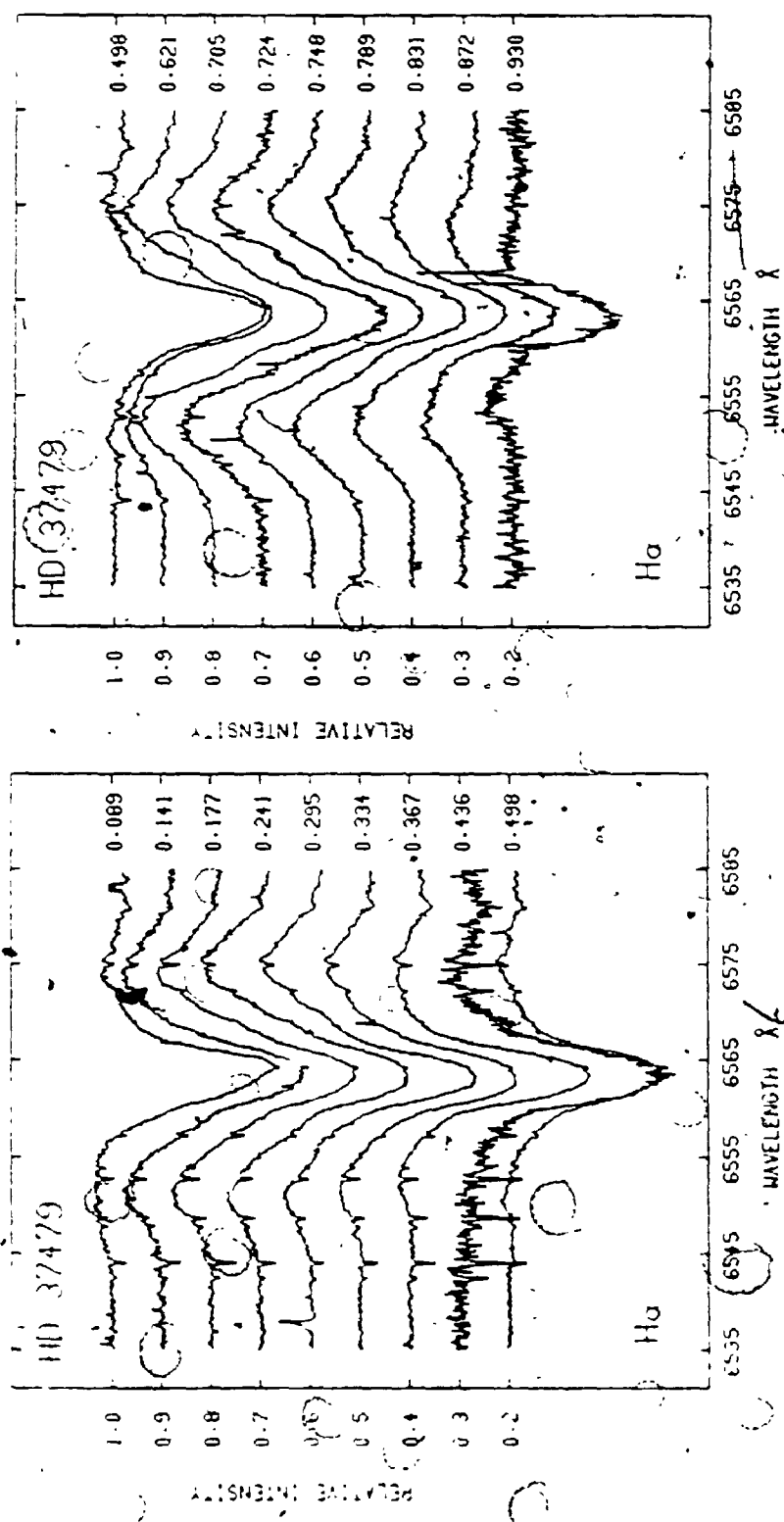


Figure 6:2 Observed H $\alpha$  line profiles of  $\alpha$  Ori E. Rotational phases are given above each line profile and are calculated from the ephemeris given in the text.

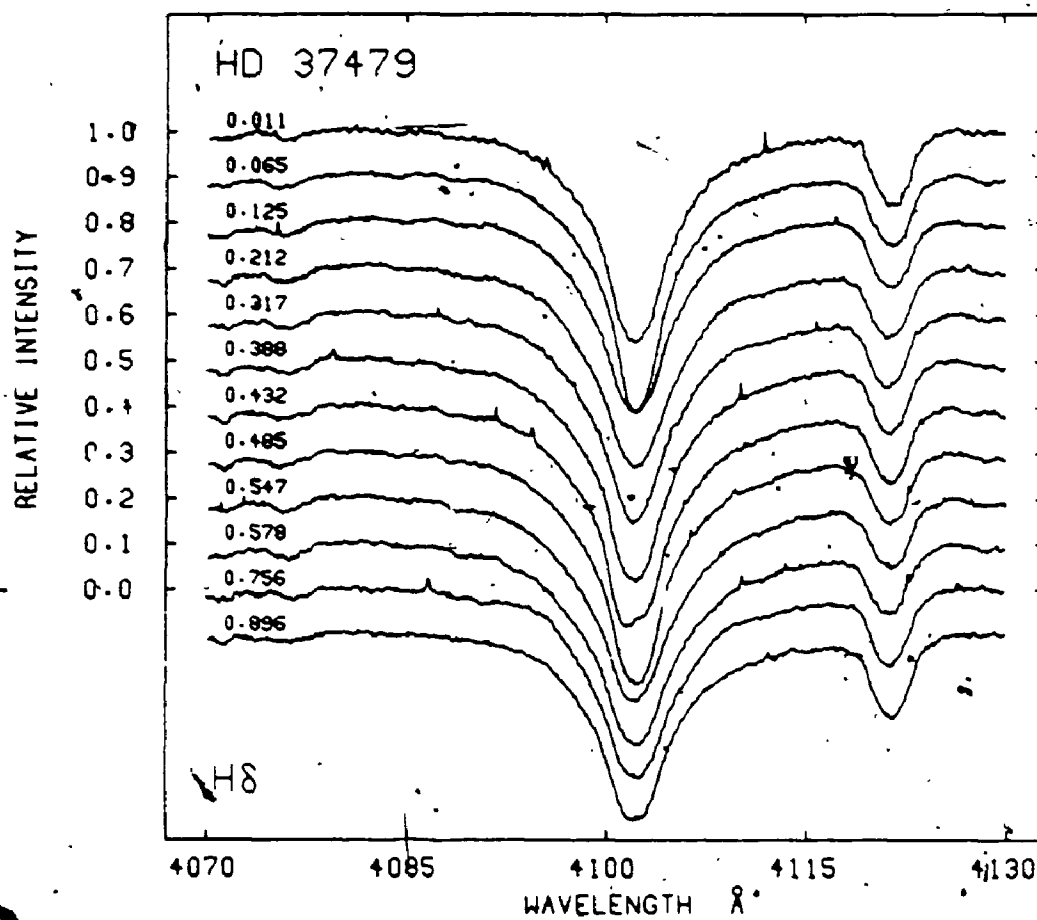


Figure 6.3 Observed H $\delta$  line profiles of  $\sigma$  Ori E. Note the appearance of shell episodes near  $\phi = 0.065$  and  $\phi = 0.485$ .

The emission has a sharp inner boundary about  $285 \text{ km s}^{-1}$  from the velocity of the star and extends to approximately  $1000 \text{ km s}^{-1}$ , which constrains the emission region to between  $1.76$  and about  $6 R_*$ . Bolton et al. (1986) do not comment on the presence of possible emission features in the  $H\delta$  line, but an examination of this profile in figure 6.3, especially at  $\phi = 0.756$  and phases near  $\phi = 0.200$ , reveals evidence of emission at  $\pm 10 \text{ \AA}$  from the core of the line, precisely when, and where, the emission is strongest in  $H\alpha$ .

A sample of helium profiles of  $\sigma$  Ori E at two different phases are given in figure 6.4 to illustrate the peculiar radial velocity behaviour of these lines alluded to earlier. Previous observations have suffered from considerable plate noise (Groote and Hunger 1982). The entire set of  $\lambda 4437$  and  $\lambda 4471$  profiles are shown in figures 6.5 and 6.6 respectively (dashed lines). The  $\lambda 4437$  line displays a wide range in equivalent width as well as radial velocity variations. By comparing profiles of the  $\lambda 4437$  and  $\lambda 4471$  lines in figure 6.4 it is immediately apparent that, when a helium-rich spot is approaching the line of sight ( $\phi = 0.662$ ), the  $\lambda 4437$  line shows a pronounced blueward asymmetry, while the core of the  $\lambda 4471$  line is redshifted. The opposite occurs when a helium-rich region is receding from the observer ( $\phi = 0.454$ ). This is the exact behaviour modelled (and less convincingly illustrated) by Groote and Hunger (1982), and first suggested as a reason for the lack of observed radial velocity variations by Landstreet and Borra (1978). These

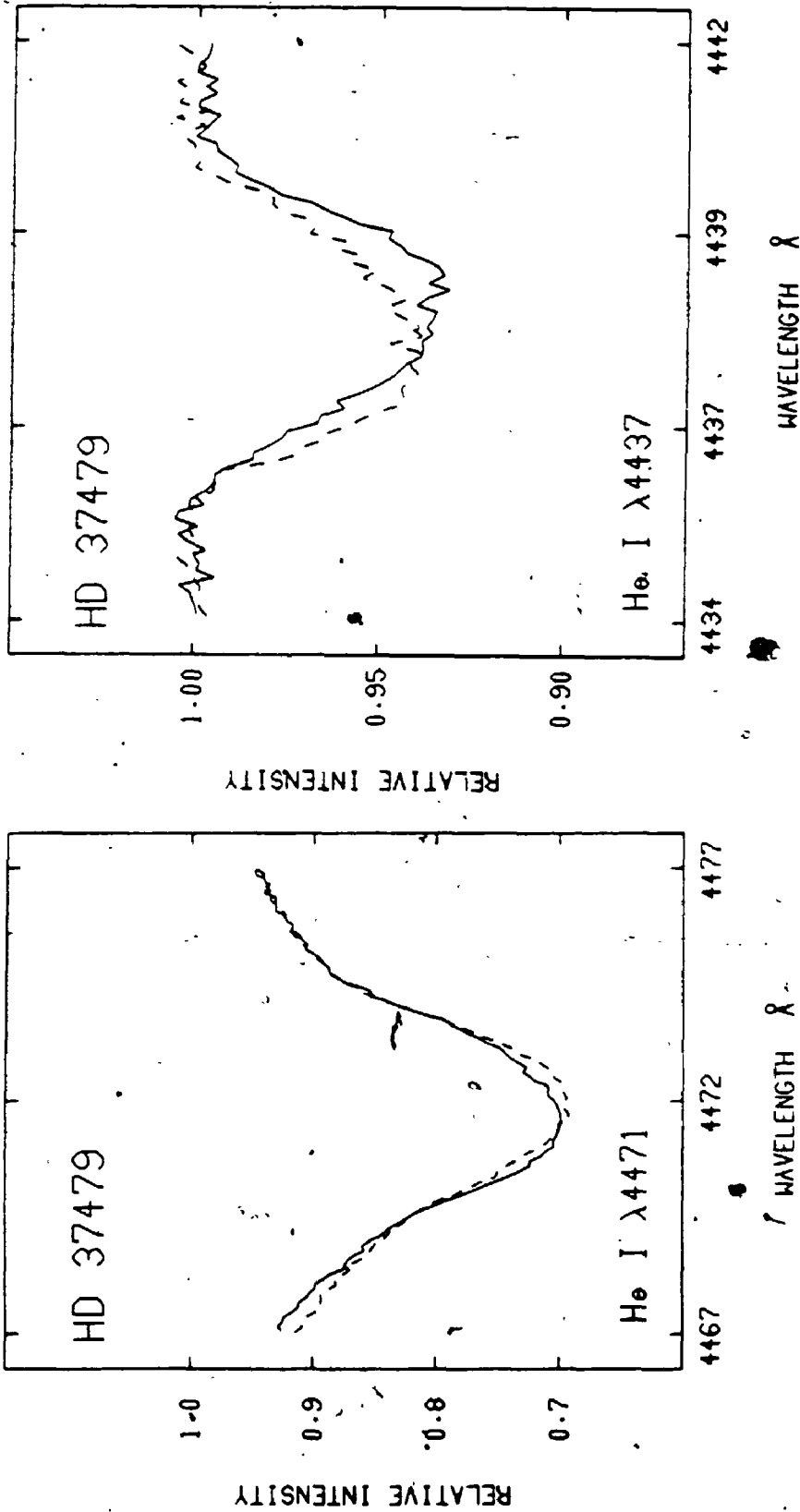


Figure 6.4 Illustration of the radial velocity variations of the helium line profiles of  $\sigma$  Ori E. Note, for example, that the  $\lambda 4471$  profile is blue-shifted when the  $\lambda 4437$  profile is red-shifted.

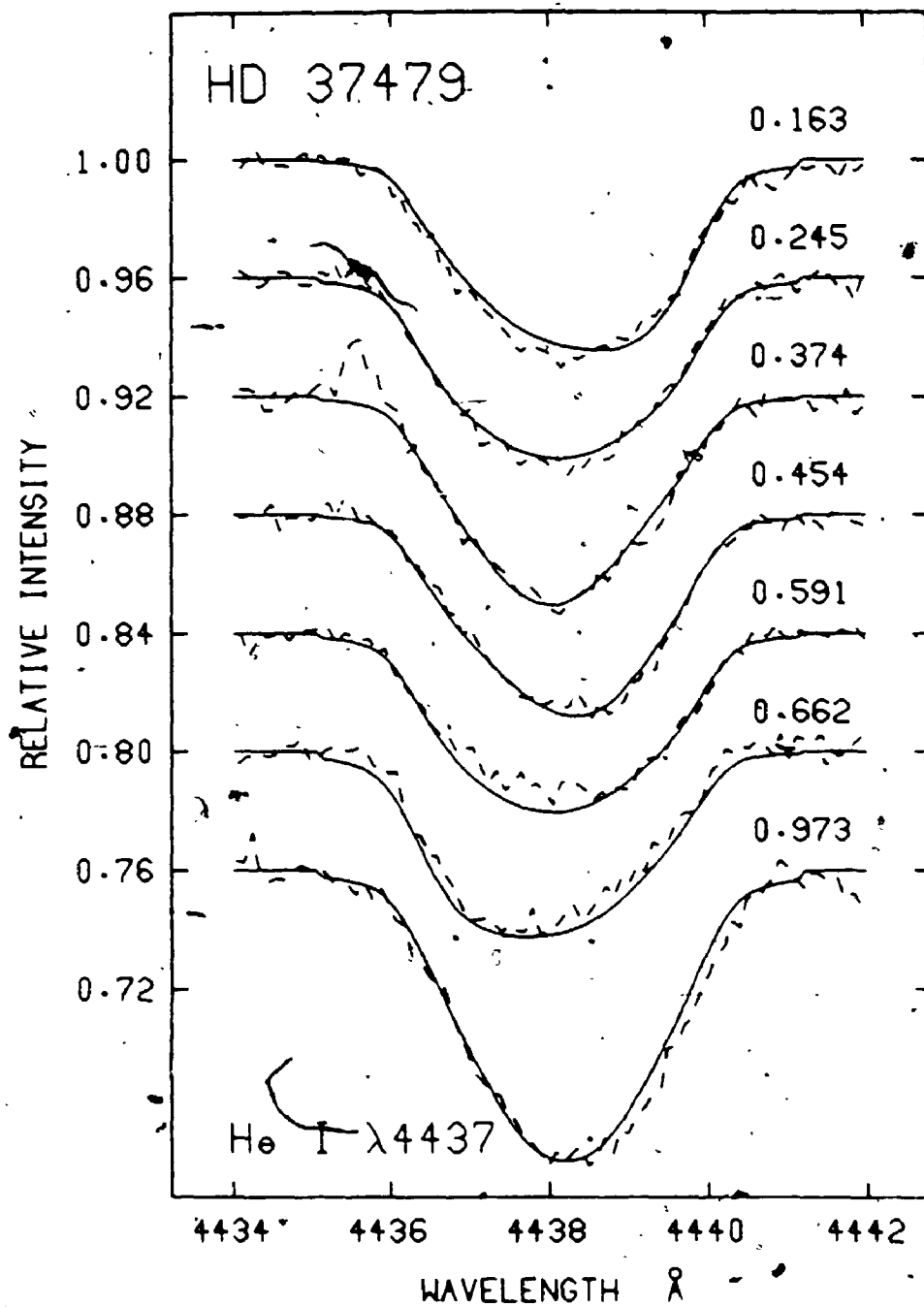


Figure 6.5 Observed (broken line) and modelled (solid line) He I  $\lambda 4437$  line profiles of  $\sigma$  Ori E. The helium abundance geometry is described in the text.

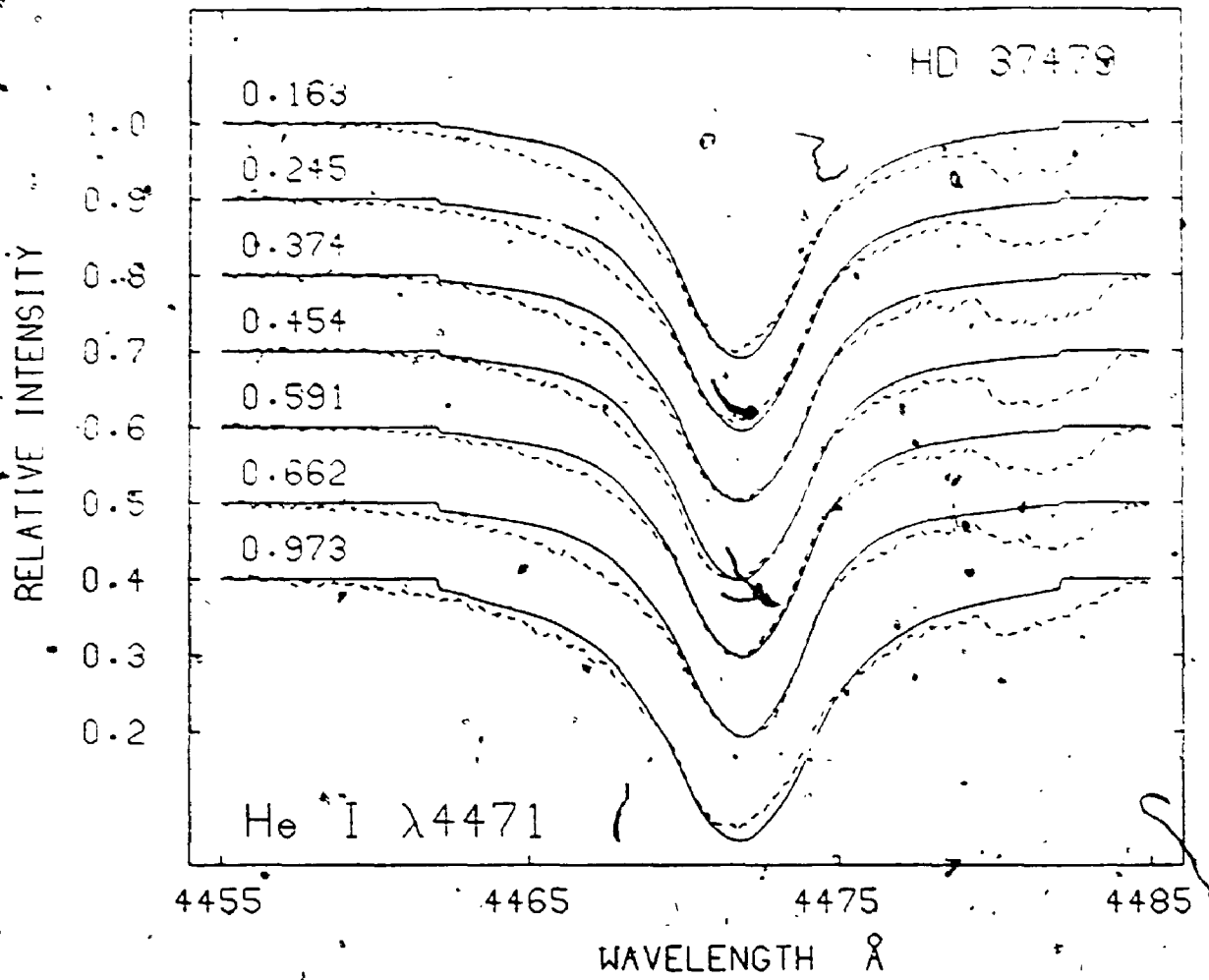


Figure 6.6 Observed (broken line) and modelled (solid line) He I  $\lambda$ 4471 line profiles of  $\sigma$  Ori E. The helium abundance geometry is described in the text.

radial velocity variations are an important confirmation of the correctness of the oblique rotator interpretation of the helium-strong stars. The variations are even more pronounced in HD 37776 (chapter 7).

Finally, variations of the Si III  $\lambda 4567$  line are indicated by the dashed lines in figure 6.7. The Mg II  $\lambda 4481$  line shows a similar phase variation, but is blended with He I  $\lambda 4471$ . Lines of O II and N III also give evidence of this type of phase behaviour, but are too weak to model with any confidence.

### 6.3 Modelling

Groote and Hunger (1982) have derived a  $T_{\text{eff}}$  of  $22500 \pm 600$  K for  $\sigma$  Ori E by matching its continuous energy distribution from 1000 Å to 50000 Å with theoretical fluxes from Kurucz's solar abundance model atmospheres. There is an inconsistency in their derivation because of the use of solar helium abundances. However, currently available helium-rich model atmospheres do not include metal line blanketing, which is very important in the ultraviolet spectra of hot stars. Groote and Hunger (1982) justify their result by claiming that at the relevant temperature and helium abundance, line blanketing is hardly affected by the abnormal helium abundance. Since this is probably the most physically reasonable method for determining the temperatures of the helium-strong stars, the effective temperature of Groote and Hunger will be adopted here.

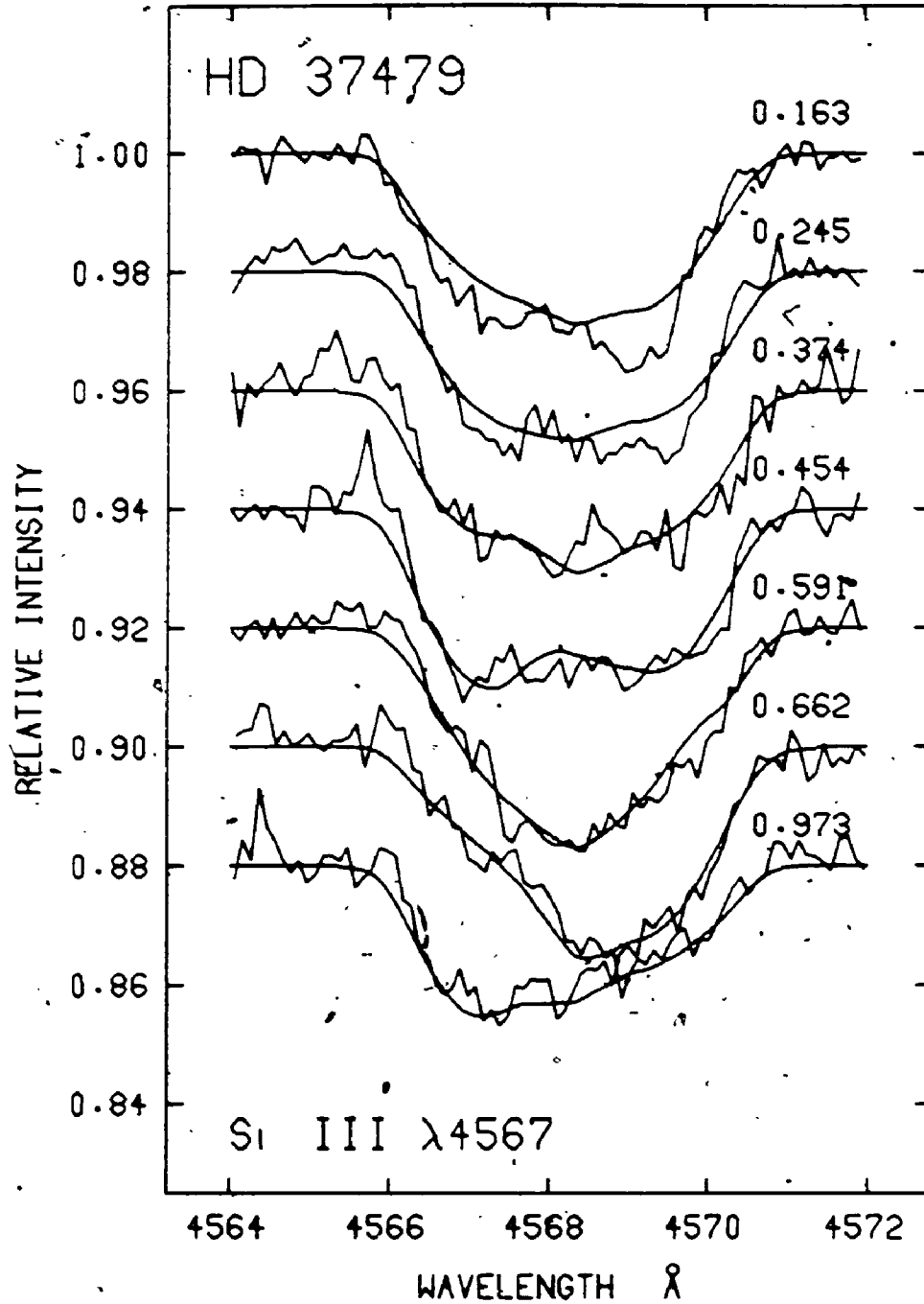


Figure 6.7. Observed (broken line) and modelled (solid line) Si III  $\lambda$ 4567 line profiles of  $\sigma$  Ori E. The silicon abundance geometry is described in the text.

An extra problem to consider, however, is that in dereddening the observed flux of  $\sigma$  Ori E, Groote and Hunger (1982) assume that the star is at the same distance as  $\sigma$  Ori AB, and adopt the colour excess,  $E(B - V)$ , of the latter system for the peculiar star. However, in the course of this work, it will be suggested that  $\sigma$  Ori E is not a member of this multiple star system, but in fact lies at a significantly greater distance. The above temperature estimate may then be somewhat low depending on the amount of interstellar reddening beyond Orion.

To obtain an indication of the accuracy with which the temperatures of HD 64740, HD 58260, and  $\delta$  Ori C have been determined in the previous two chapters, the various colour indices of  $\sigma$  Ori E have also been used to provide an estimate of the star's temperature. Following the same procedure used for the above three stars, and assuming a surface gravity of  $\log g = 4.0$  for  $\sigma$  Ori E, effective temperatures of 23850 K, 23950 K, and 23600 K, are found from the  $UBV$ , Geneva, and  $uvby\beta$  photometric systems respectively. These values are consistent with the  $T_{\text{eff}} = 23500$  K determined by the fine analysis of Klinglesmith et al. (1970), and with  $T_{\text{eff}} = 23400$  K found by Adelman and Pyper (1985) from fitting the visible continuous energy distribution of the star. The estimated uncertainty of 1000 K for the temperatures derived for the other program stars therefore seems appropriate.

The remainder of the analysis for  $\sigma$  Ori E proceeds in a

manner similar to that carried out for HD 64740.

Preliminary modelling of the silicon lines, as well as He I  $\lambda 4437$ , suggested a  $v \sin i$  on the order of  $140 \text{ km s}^{-1}$  for  $\sigma$  Ori E. A distance to the star of about 450 pc and the angular diameter measurement of Groote and Hunger (1982) then gives a radius of  $3.9 R_{\odot}$  (Bohlender et al. 1987). An initial estimate of  $i = 58^{\circ}$  and  $\beta = 64^{\circ}$  was then obtained using equations (4.3) through (4.5) and the longitudinal magnetic field curve extrema.

An initial model of the helium abundance geometry was found by modelling the variations of the He I  $\lambda 4437$  line, ignoring any influences from the surface magnetic field. The  $R$  index measurements of Pedersen and Thomsen (1977) and Pedersen (1979) shown in figure 6.1 indicate that helium is most abundant near the magnetic equator. Accordingly, a first attempt to model the observed line variations was made using a geometry consisting of a helium-rich equatorial region surrounding the star. Models were tried with various abundance contrasts between the helium-rich belt and the rest of the surface, as well as various widths of the helium-rich region, but none of the models reproduced the large variations in line strength observed. Instead, the model that fits the observations best consists of two patches of large helium abundances located near the two intersections of the magnetic and rotational equators. The remainder of the surface of the star also requires a helium abundance approximately twice the solar value. A  $v \sin i$  of

about  $130 \text{ km s}^{-1}$  gives the best fit to the profiles.

Next, the surface gravity was determined by synthesizing the profiles of the H $\delta$  and He I  $\lambda 4471$  lines using the above tentative solution for the relative abundances of hydrogen and helium. A problem immediately arose in this modelling. The H $\delta$  profiles are reproduced best with a surface gravity of  $\log g = 3.7$ . This value for the gravity reproduces the cores of the He I  $\lambda 4471$  lines, (for a somewhat higher  $v \sin i$  of  $150 \text{ km s}^{-1}$ ), but gives line wings that are too weak. Also, this gravity gives an uncomfortably high mass and radius, and hence a low inclination of about  $20^\circ$  for  $\sigma$  Ori E. The appearance of the very distinct phenomena observed in the star, such as the shell lines, would then be very difficult to understand, since in this case  $\beta \approx 80^\circ$ , and the magnetic equator of the star would never be far from the line of sight. The wings of the  $\lambda 4471$  lines can be reproduced nicely for a  $\log g$  of 4.1 and for an abundance geometry that matches the  $\lambda 4437$  variations. However, the  $\lambda 4471$  cores are then much too deep.

There are at least two possible reasons for this discrepancy. Firstly, as has already been mentioned, H $\delta$  does show some evidence of emission at certain phases. This would have the effect of raising the wings of the line, and hence, reduce the apparent surface gravity if the contribution of the emission is ignored, as it is here. Secondly, the He I  $\lambda 4437$  profile variations suggest very

band centered about  $60^\circ$  from the negative magnetic pole and in a spot located near the line of sight at  $\theta = 0.591$ . With the above dipolar field strength, the relative strengths of the Si III  $\lambda\lambda 4567$  and  $4574$  lines are in good agreement. Models of these profiles without a magnetic field result in  $\lambda 4567$  profiles that are too weak in relation to  $\lambda 4574$ . Unfortunately, the inclination can not be constrained any further by this marginal differential magnetic intensification.

#### 6.4 Discussion

Until now, the large range of masses found for  $\sigma$  Ori E by various investigators (see section 6.1) has posed a serious problem in that a low mass suggests the uncomfortable idea of a global enrichment of helium in what must be a young star, while a large mass points to the peculiar helium abundance being confined to the atmosphere. At one time, the calibration of Hunger's photographic plates had been questioned, with the suggestion that some equivalent widths, and hence surface gravities were too small (Walborn 1983). Hunger (1986a,b) has discussed these problems in some detail, and has determined that this is not the case, and concludes that the small masses must be attributed to the distance of  $\sigma$  Ori E being underestimated.

Some of the interpretations of the observations of  $\sigma$  Ori E described in the introduction of this chapter have already been mentioned briefly in chapter 1, but a further

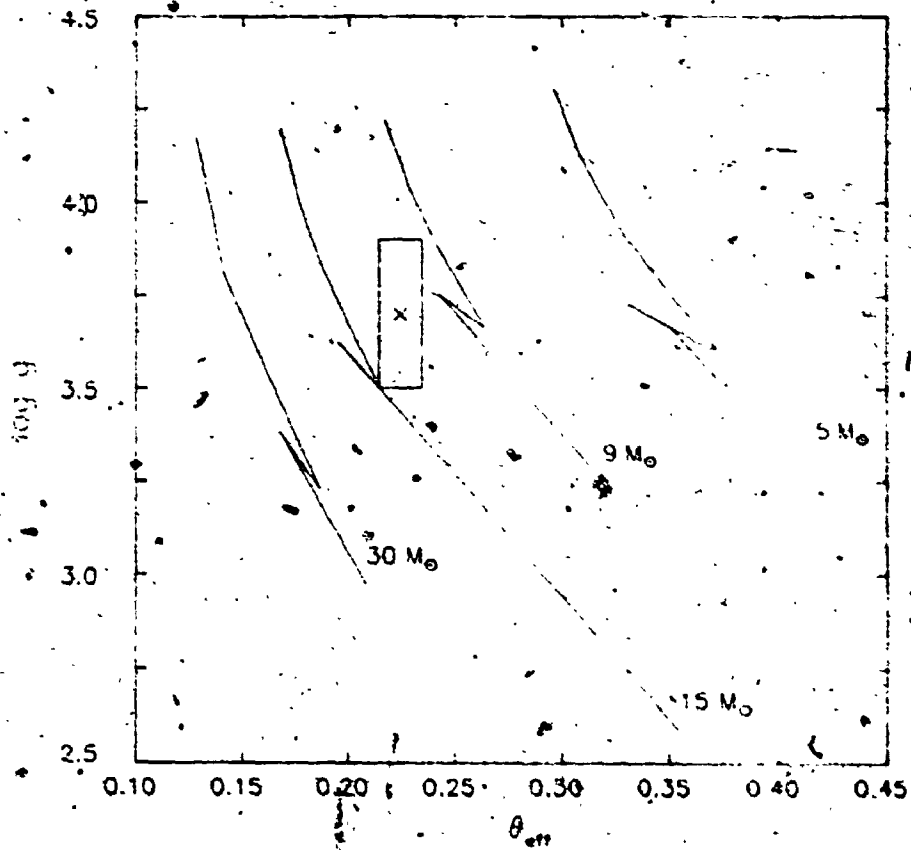


Figure 6.8 Location of  $\sigma$  Ori E in the  $\log g$  vs.  $\theta_{\text{eff}}$  plane. Symbols and evolutionary tracks are as in figure 4.8.

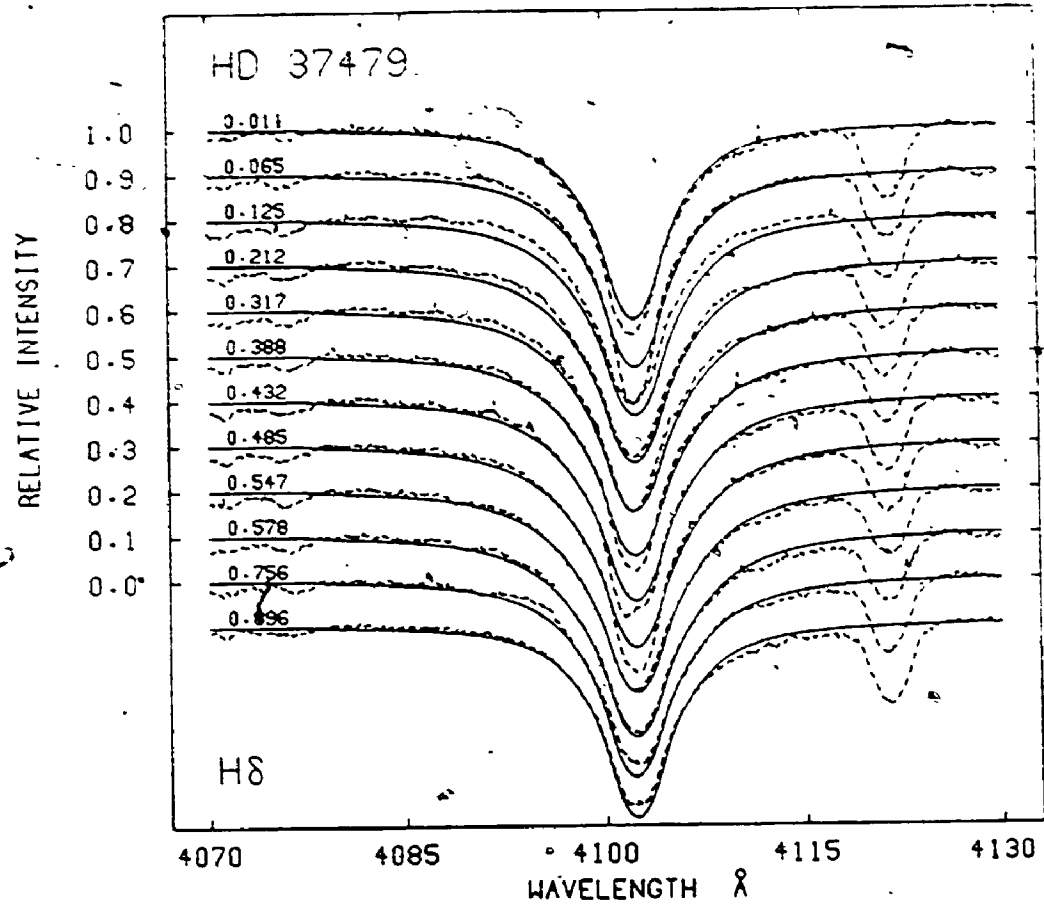


Figure 6.9 Observed (broken line) and modelled (solid line) H $\delta$  line profiles of  $\sigma$  Ori E. The hydrogen abundance geometry is described in the text.

Table 6.1.  $\sigma$  Ori E Abundance GeometriesHelium Spot Locations ( $\log \epsilon_{\text{He}} = -1.0$ )

<u>log <math>\epsilon_{\text{He}}</math></u>	<u>Colat.</u>	<u>Long.</u>	<u>Radius</u>
-0.222	120°	180°	30°
-0.155	70°	0°	60°

 $\log \epsilon_{\text{He}} = -0.82$  on Remainder of SurfaceSilicon Geometry ( $\log \epsilon_{\text{Si}} = -4.50$ )

Band:

\* Magnetic Colatitude: 100°-140° $\log \epsilon_{\text{Si}} = -3.80$ 

Spot:

<u>log <math>\epsilon_{\text{Si}}</math></u>	<u>Colat.</u>	<u>Long.</u>	<u>Radius</u>
-3.60	40°	180°	40°

 $\log \epsilon_{\text{Si}} = -4.8$  on Remainder of Surface

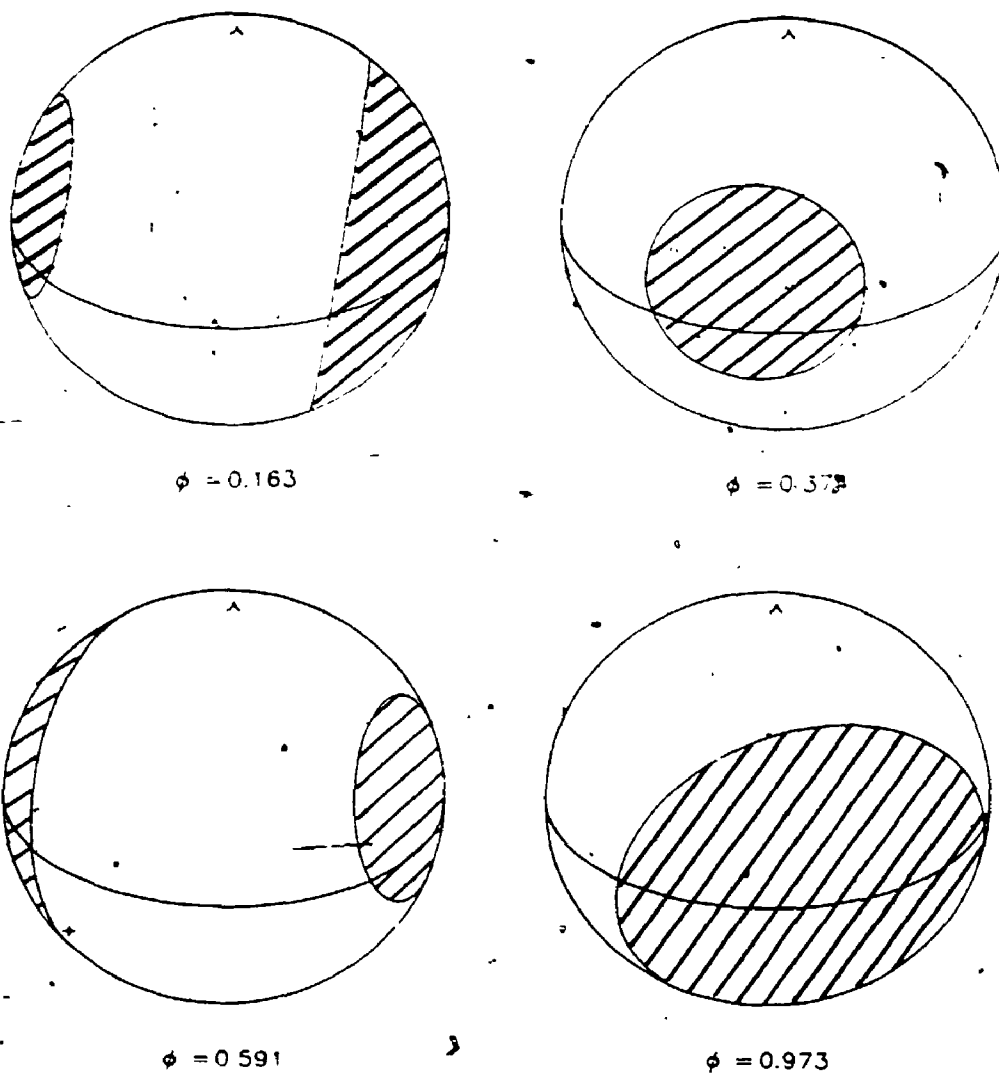


Figure 6.10 Illustration of the helium abundance geometry of  $\sigma$  Ori E. The hatched areas represent the locations of the helium-rich regions on the stellar surface. The locations and signs of the magnetic poles are indicated by the symbols - and +. Details of the model are outlined in the text. The rotational phases are given below each figure.

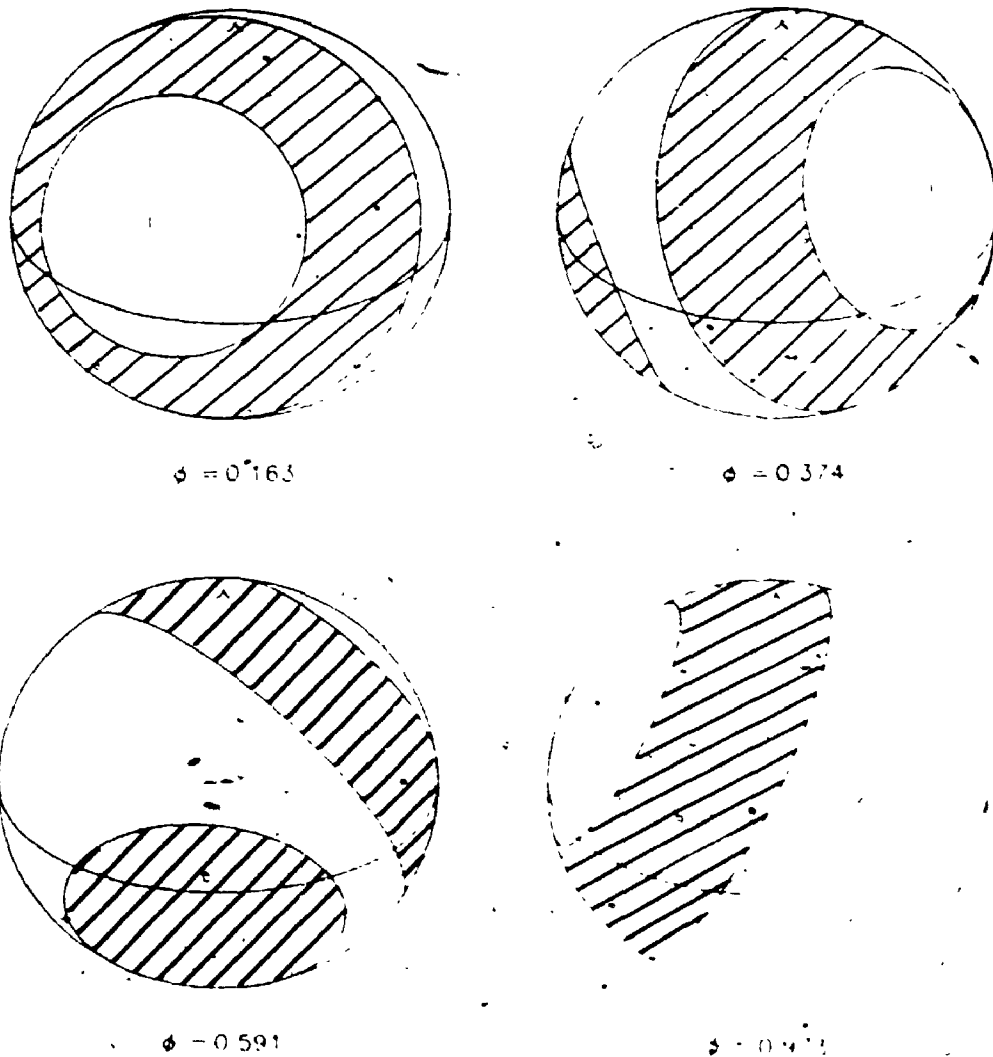


Figure 6.11 Illustration of the silicon abundance geometry of  $\sigma$  Ori E. The hatched areas represent the locations of the silicon-rich regions on the stellar surface. The locations and signs of the magnetic poles are indicated by the symbols - and +. Details of the model are outlined in the text. The rotational phases are given below each figure.

band centered about  $60^\circ$  from the negative magnetic pole and in a spot located near the line of sight at  $\theta = 0.591$ . With the above dipolar field strength, the relative strengths of the Si III  $\lambda\lambda 4567$  and  $4574$  lines are in good agreement. Models of these profiles without a magnetic field result in  $\lambda 4567$  profiles that are too weak in relation to  $\lambda 4574$ . Unfortunately, the inclination can not be constrained any further by this marginal differential magnetic intensification.

#### 6.4 Discussion

Until now, the large range of masses found for  $\sigma$  Ori E by various investigators (see section 6.1) has posed a serious problem in that a low mass suggests the uncomfortable idea of a global enrichment of helium in what must be a young star, while a large mass points to the peculiar helium abundance being confined to the atmosphere. At one time, the calibration of Hunger's photographic plates had been questioned, with the suggestion that some equivalent widths, and hence surface gravities were too small (Walborn 1983). Hunger (1986a,b) has discussed these problems in some detail, and has determined that this is not the case, and concludes that the small masses must be attributed to the distance of  $\sigma$  Ori E being underestimated.

Some of the interpretations of the observations of  $\sigma$  Ori E described in the introduction of this chapter have already been mentioned briefly in chapter 1, but a further

discussion is warranted here. Greenstein and Wallerstein (1958), and Klinglesmith et al. (1970) favoured a model in which  $\sigma$  Ori E was originally a very massive star and as a consequence, evolved very rapidly. During this rapid evolution, the star shed more than two-thirds of its initial mass, and exposed its helium-enriched interior. In contrast, Osmer and Peterson (1974) concluded from the surface gravities, temperatures, and abundances, that the helium-strong stars as a group are related to the Bp and Ap stars. However, Odell (1974) was the first to point out a possible mass problem for  $\sigma$  Ori E. Using a revised distance to the  $\sigma$  Ori AB system of 400 pc (Heintz 1974) and the data of Klinglesmith et al. (1970), he finds a mass of  $4.85 M_{\odot}$  and radius of  $3.44 R_{\odot}$ , which is inconsistent with a normal B2 star. This lower mass is consistent with stellar models with a helium mass fraction,  $Y$ , of approximately 0.6. With the age of the star constrained by the presence of the unevolved AB component, Odell was unable to provide a satisfactory explanation for the apparent evolved state of  $\sigma$  Ori E, although he considered scenarios of mixing due to rotational circulation, mass-loss, breakup of a single massive star, binary mass-transfer, and capture of an old star.

Hesser, Walborn, and Ugarte P. (1976) reconsidered the idea that  $\sigma$  Ori E could be a mass-transfer binary system, after discovering the interesting eclipse-like photometric behaviour of the star. In their picture, a B star has a

degenerate companion (with mass  $< 0.1 M_{\odot}$ ) surrounded by a synchronously rotating accretion disk with a hot-spot located where the mass stream from the B star makes contact. The primary photometric minimum occurs when the hot spot is occulted by the B star, and the secondary minimum occurs when the disk itself occults the hot spot. The phase separation of the eclipses and the general behaviour of the H $\alpha$  emission is also reasonably well explained by the model. Of course, the problem remains that the original primary component of the system must have been very massive. The authors also briefly discuss an alternate model with two ultraviolet bright spots located at the Lagrangian points of a binary system, with the leading spot somewhat brighter. The two minima in the light curve of the star are then the result of a single W-shaped eclipse. The linear polarization data of Kemp and Herman (1977) are also consistent with a mass-transfer binary model. The polarization is caused by reflection from, and emission by the accretion disk. A problem arises for the binary interpretation in that the observed radial velocities of the shell lines near the eclipses (Groote and Hunger 1977) require a retrograde rotation for the accretion disk or ring.

Partly because of these problems in the binary hypothesis, but mainly as a result of the discovery of the strong magnetic field of  $\sigma$  Ori E, Landstreet and Borra (1978) discussed the observed phenomena of the star in terms

of an oblique rotator model. They proposed that material is removed from the photosphere by radiation pressure and trapped in the magnetosphere a few stellar radii above the surface at the magnetic equator, where the flow velocity is reduced. The dense gas above the magnetic equator could produce the observed shell lines and eclipses, if the density of the material is high enough. Two shell phases and eclipses would occur for each rotation of the star, since the magnetic observations indicate that the magnetic equator passes through the line of sight twice per rotation. This gas might also be responsible for the linear polarization observed by Kemp and Herman (1977). Landstreet and Borra (1978) were also able to remove concern over the lack of observed helium line radial velocity variations predicted by the oblique rotator model (see the earlier discussion on this point). Unfortunately, the large velocities found in the H $\alpha$  emission can not be explained with this model.

The use of Groote and Hunger's  $T_{\text{eff}}$ , together with the value of  $\log g$  found from the present modelling leads to a mass of  $12.0 \pm 3.0 M_{\odot}$  and radius of  $8.1 \pm 3.0 R_{\odot}$  for  $\sigma$  Ori E. This mass is consistent with masses of normal B2 stars, so that the anomalous helium abundance must be confined to the atmosphere of the star, and arise from diffusion processes as described by Vauclair (1975) and Michaud et al. (1987). The distance to the star can be easily calculated from the angular diameter determination of Groote and Hunger (1982)

and is found to be 990 pc. This is in considerable disagreement with the  $M = 8.9 M_{\odot}$ ,  $R = 5.25 R_{\odot}$ , and  $d = 640$  pc recently determined by Hunger and Heber (1988, private communication) from a differential analysis of  $\sigma$  Ori E and the sharp-lined B2 star Gamma Peg. Both investigations, however, suggest that  $\sigma$  Ori E is not a member of the  $\sigma$  Ori system.

The helium abundance geometry derived above is reasonably consistent with the model of Shore (1987), which predicts a helium-rich equatorial zone for  $\sigma$  Ori E. The overall abundance of helium derived here is in reasonable agreement with previous determinations by Klinglesmith et al. (1970), Lester (1972), and Groote and Hunger (1982). The fact that helium seems to be concentrated in two spots near the intersections of the magnetic and rotational equators may indicate that rotation plays an important role in determining where diffusion processes are most pronounced. The adopted  $v \sin i$  and inclination of the model indicates an equatorial velocity of almost  $220 \text{ km s}^{-1}$ . Shore (1987) does not discuss the effects of rotation on the predicted locations of the helium overabundances, but a rotational velocity of this order may have an appreciable effect on the diffusion velocity of helium by reducing the effective surface gravity at the rotational equator of the star. Such effects are certainly important when considering the circumstellar material of the star (Nakajima 1981, 1985).

This star definitely merits additional work. The fits of the model H $\delta$  and He I  $\lambda$ 4471 profiles to the observations are not as satisfactory as similar fits for HD 64740, or for the slow rotators HD 58260 and  $\delta$  Ori C. The presence of emission in the H $\delta$  profiles is definitely part of the problem, but the large local abundances of helium needed to fit the observed variations of the He I  $\lambda$ 4437 line suggest that, for this star at least, the use of Kurucz's solar abundance model atmospheres is a poor approximation to the real atmosphere of the star.

## Chapter 7: HD 37776

### 7.1 Introduction

The helium-rich nature of HD 37776, another member of the Orion OB1 association, was first reported by Nissen (1976), who carried out narrow-band photometry of the He I  $\lambda 4026$  line, as well as  $uvby\beta$  photometry. The photometry also indicated that the helium line strengths are variable, which at the time made this the second known helium line variable among the helium-strong stars.

Pedersen and Thomsen's (1977) similar  $R$  index observations clearly show a double wave variation in the  $\lambda 4026$  line strength on a period of  $1.538 \pm 0.004$  days. (This is 4.05 times the 0.37968-day period found by Hill (1967), who claimed that the star is a  $\beta$  Cephei variable.) Pedersen and Thomsen's  $uvby\beta$  data also show  $y$  and  $c_1$  index variability in the sense that, when the  $R$  index values are small (corresponding to maximum helium line strength), the star is faint in  $y$  and the Balmer jump (as measured by  $c_1$ ) is small. The two helium line strength maxima have the same strength, but are less than 0.5  $P$  apart, which Pedersen and Thomsen (1977) claim is suggestive of an asymmetrical helium abundance geometry. Continued observations by Pedersen (1979) improved the period determination to  $1.5385 \pm 0.0003$  days. His average of several  $H\alpha$  scans also gave some evidence for  $H\alpha$  emission, but at a very low (2%) level. Adelman and Pyper (1985) have provided additional  $uvby\beta$

photometry, and find  $T_{\text{eff}} = 22500$  K by fitting their optical spectrophotometry with Kurucz's (1979)  $\log g = 4.0$  solar abundance model atmospheres.

Borra and Landstreet (1979) discovered a strong but peculiar magnetic field in HD 37776. Seven longitudinal field measurements, when plotted on Pedersen's (1979) period, showed an unusual double-wave variation in the magnetic field intensity, which seemed to be supported by the relative phasing of the helium line strength variations. The limited set of field measurements could be made to fit the more usual sinusoidal field variation for many periods between 0.5 and 1.0 days, but none of these periods satisfied the data of Pedersen and Thomsen (1977) and Pedersen (1979).

Groote and Kaufmann (1981) performed an analysis for HD 37776 similar to that carried out for  $\sigma$  Ori E by Groote and Hunger (1982, see chapter 6). From the observed ultraviolet, visible, and infrared continuum fluxes, theoretical fluxes from Kurucz's (1979) atmospheres and an  $E(B - V) = 0.06$ , they found  $T_{\text{eff}} = 22000 \pm 1000$  K and an angular diameter of 0.069 milliarcsec for HD 37776. They also present phase resolved results for the helium abundance (averaged over the visible hemisphere of the star at each phase), surface gravity, equivalent widths of hydrogen and helium lines, and radial velocity data. The number fraction of helium,  $x_{\text{He}}$ , varies from 0.15 to 0.60 with a variation similar to the  $R$  index observations. Helium and hydrogen

line equivalent widths vary in antiphase. In fact, the suspected hydrogen line variations are unique to the helium-strong stars. The surface gravity appears to vary from  $\log g = 3.7$  to  $\log g = 4.2$ , although the authors warn that part of this variation may be due to calibration errors in the reduction of the photographic plates. The hydrogen and helium lines have radial velocity variations of the order of  $20 \text{ km s}^{-1}$ , which again vary in antiphase.

In a paper appearing in the same conference proceedings as that of Groote and Kaufmann (1981), Shore and Adelman (1981) discuss IUE observations of HD 37776. The star shows ultraviolet variations similar to those seen in  $\sigma$  Ori E: helium line strengths vary in antiphase with lines of carbon, silicon, and aluminum. A temperature of  $20600 \pm 1000 \text{ K}$  is derived from the ionization equilibrium of lines of Si II, Si III, Si IV, and the non-LTE equivalent widths of silicon lines calculated by Kamp (1973, 1978). The star also shows evidence for a weak, and possibly variable, wind. Further IUE observations are given by Barker et al. (1982).

Walborn (1982) reported optical spectrum variations of silicon and possibly magnesium. He estimates a  $v \sin i$  of  $160 \text{ km s}^{-1}$  from the width of the He I  $\lambda 4121$  line.

Because of the peculiar nature of the magnetic field variation discovered by Borra and Landstreet (1979), Thompson and Landstreet (1985) performed a much more extensive series of longitudinal magnetic field measurements of the star. These observations confirmed the bizarre

nature of HD 37776's magnetic field curve. Thompson and Landstreet (1985) argue that the curve represents the real magnetic field variation of the star by ruling out an erroneous period determination, an intrinsic variation in the field of the star, a binary system consisting of two magnetic stars, or an eclipse of a single magnetic star as explanations of the peculiar field curve. The helium-strong star HD 37776 seems to be the first known star in which a quadrupole field geometry dominates the usual dipole field found in other peculiar magnetic stars.

Drake et al. (1987) failed to detect radio emission from HD 37776. They give a 3 $\sigma$  upper limit to the 6 cm radio luminosity of  $\log L_6 < 16.8$ . This may provide support for the quadrupole interpretation of the magnetic field of the star, because the field at a few stellar radii above the surface of HD 37776 would then be much weaker than for a dipolar field, since a quadrupolar field has an  $r^{-4}$  radial dependence compared to an  $r^{-3}$  dependence for a dipolar field.

Because of the peculiar magnetic field curve and the remarkable spectrum variability of the star reported below, HD 37776 is perhaps the most interesting member of the entire helium-strong class of stars. Some of the preliminary modelling that has been performed for this star is presented here.

## 7.2 Observations

Hand drawn fits to the  $y$  band photometry, helium  $R$  index observations, and longitudinal magnetic field measurements of HD 37776 are given in figure 7.1. Unlike HD 64740 and  $\sigma$  Ori E, the helium maxima and minima both occur at phases of magnetic nulls. The phases of the data in figure 7.1, and the CFHT spectra catalogued in table 2.1 were determined from the ephemeris of Thompson and Landstreet (1985):

$$JD (B_1+) = 2445724.669(\pm 0.02) + 1.53869(\pm 0.00007) E.$$

The spectrum variations of HD 37776 are extraordinary. For clarity, some samples of these are shown in figures 7.2 through 7.5; models of some of these line variations will be presented later. The  $H\alpha$  profiles shown in figure 7.2 show little evidence for the suspected emission (Pedersen 1979). Profiles of  $H\delta$  and He I  $\lambda 4121$  are shown in figure 7.3. The  $H\delta$  profiles are variable in strength, especially at  $\phi = 0.155$  and  $\phi = 0.495$ . This may provide support for the report of Groote and Kaufmann (1981) that the surface gravity of the star is variable, but the line variations might also be caused by a nonuniform abundance of helium: the  $\lambda 4121$  line strengths are obviously variable. The variations of the neutral helium lines are even more noticeable in figure 7.4, which presents excellent phase coverage of the  $\lambda\lambda 4437$  and  $4471$  lines. The helium line profiles would seem to support the idea of a band of enhanced helium which crosses the line of sight at  $\phi = 0.000$

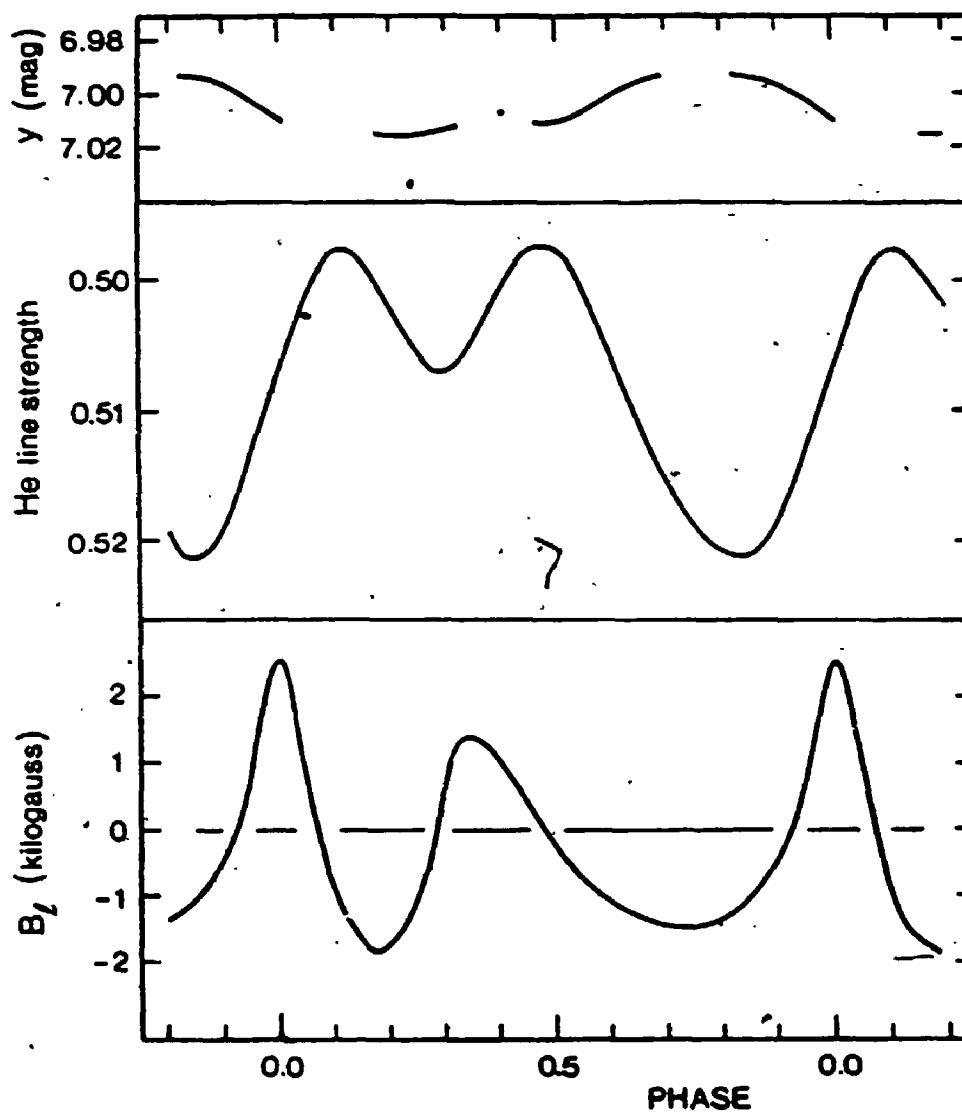


Figure 7.1 Strömgren  $y$ -band light variations, helium line strength index,  $R$ , and magnetic field curves of HD 37776. Each curve is a hand-drawn fits to the data. (From Thompson and Landstreet 1985.)

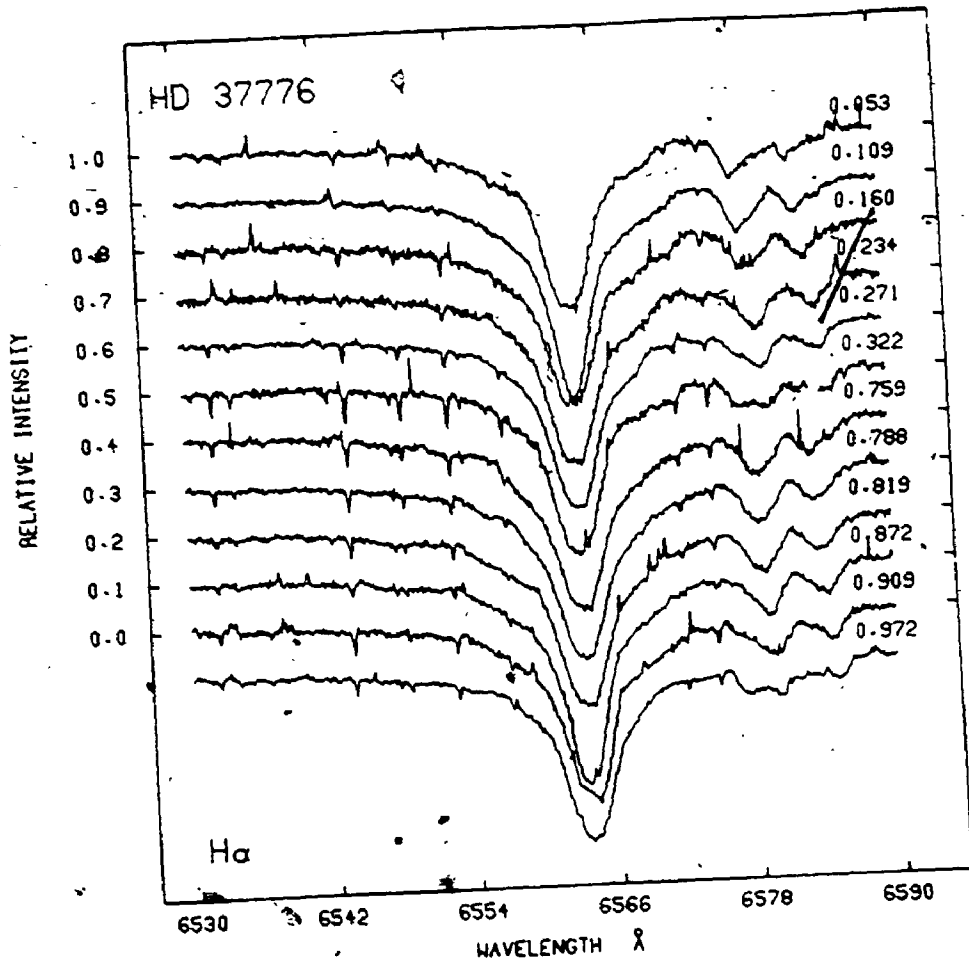


Figure 7.2 Observed H $\alpha$  line profiles of HD 37776. Rotational phases are given above each line profile and are calculated from the ephemeris given in the text.

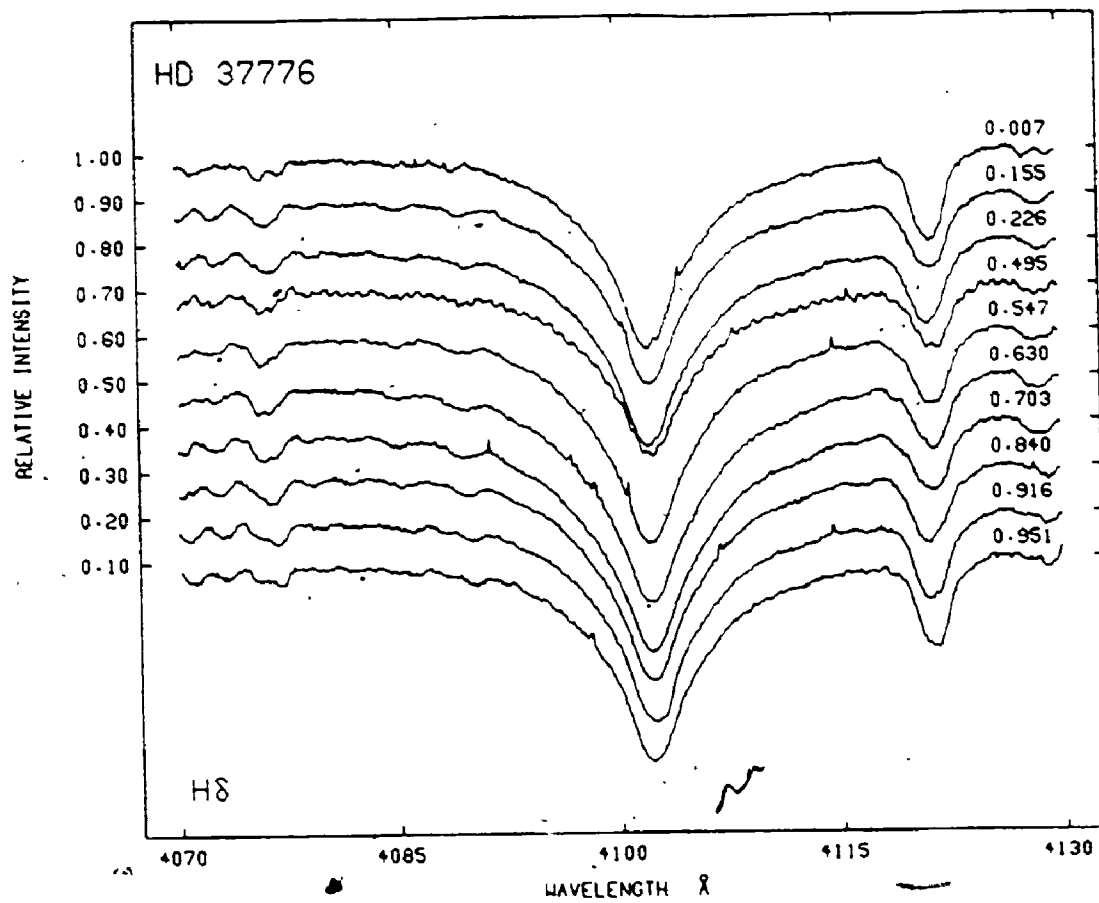


Figure 7.3 Observed H $\delta$  line profiles of HD 37776.

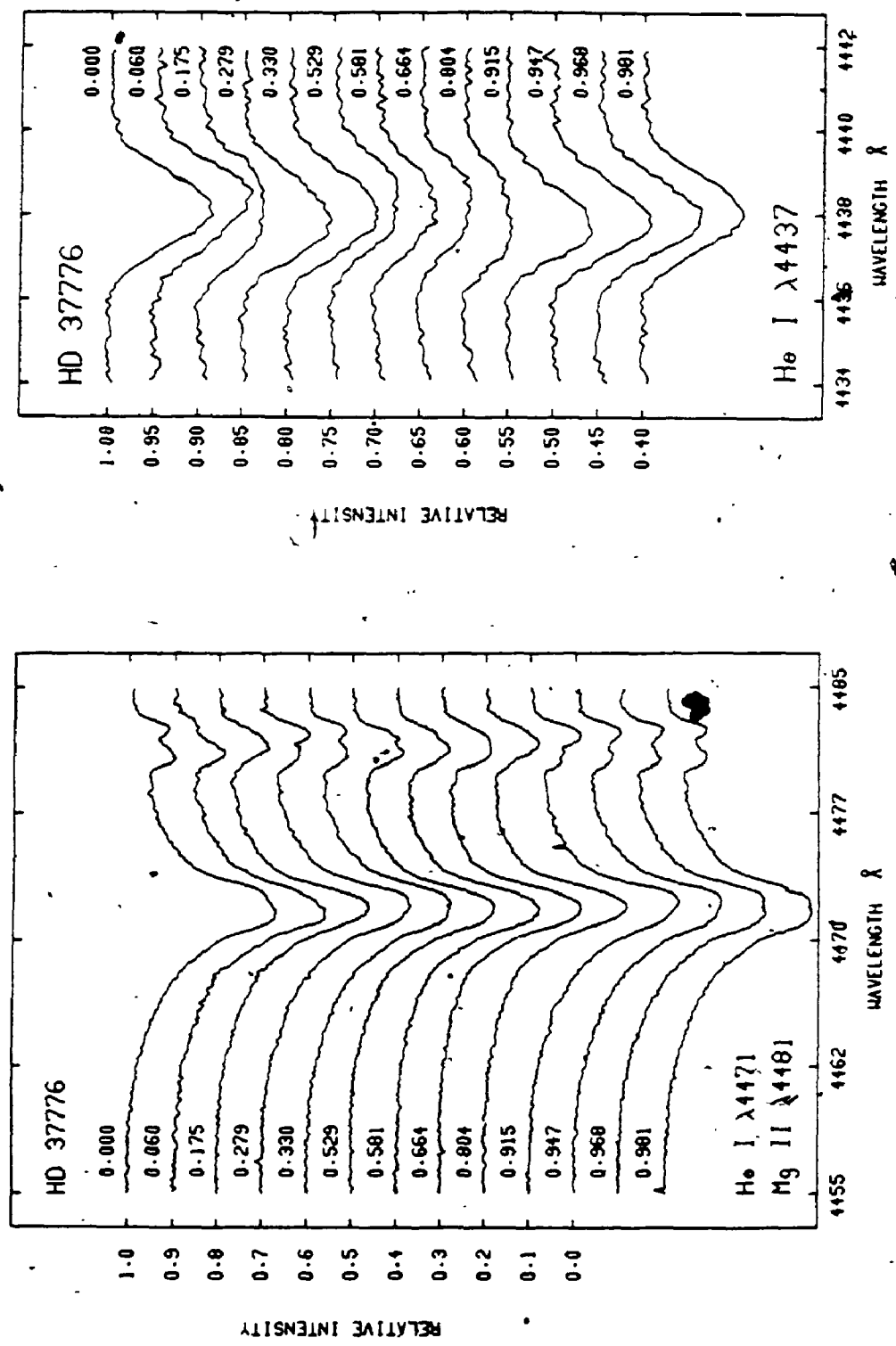


Figure 7.4 Observed He I  $\lambda 4437$  and  $4471$  line profiles of HD 37776. Note the oppositely directed radial velocity variations of the two lines near  $\phi = 0.060$  and  $\phi = 0.915$ .

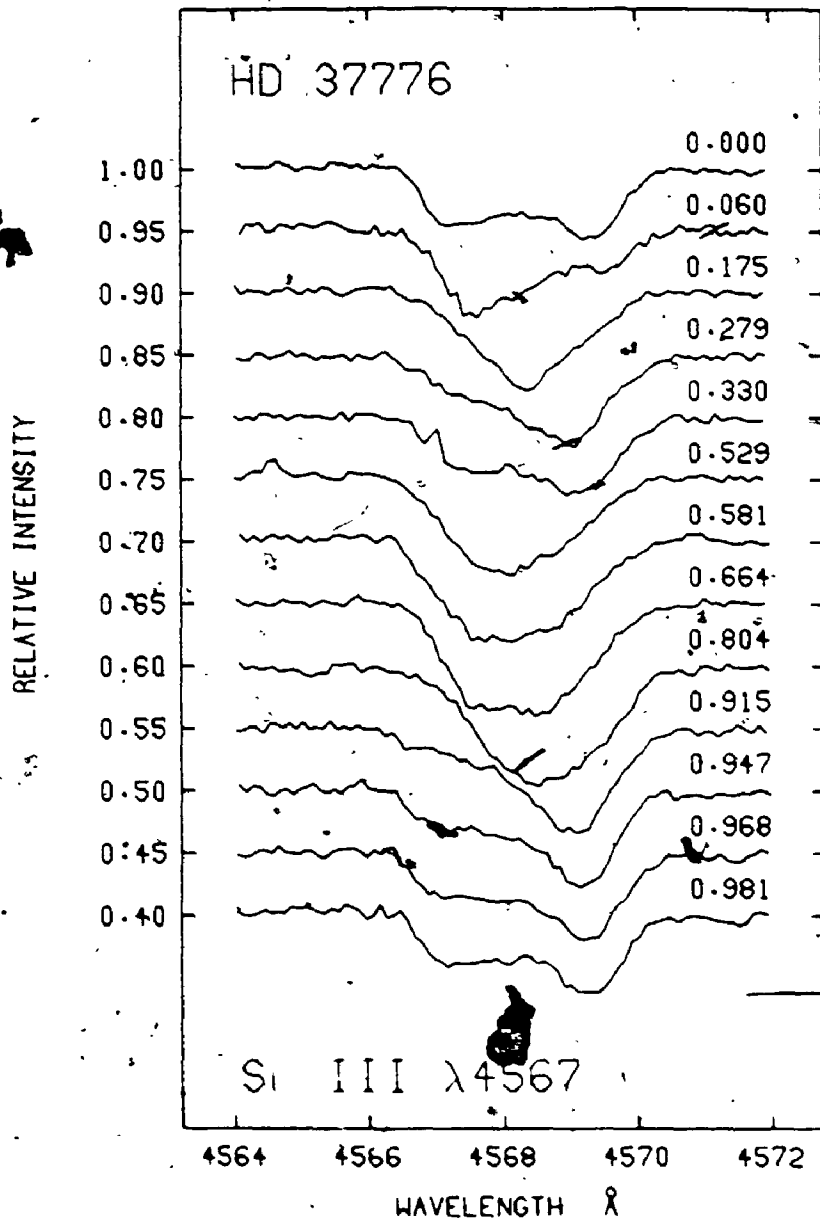


Figure 7.5 Observed Si III  $\lambda$ 4567 line profiles of HD 37776.

and  $\phi = 0.330$ , near the two positive extrema of the magnetic field. The tight phase coverage and rapid changes in the  $\lambda 4437$  line near these phases suggest that this band is quite narrow, and out of the field of view between  $\phi = 0.529$  and  $\phi = 0.804$ . The equivalent width variations of the  $\lambda 4437$  line follow the  $R$  index variation of figure 7.1 very closely. As noted in the previous chapter, the helium lines of HD 37776 clearly show the peculiar radial velocity behaviour first noted by Groote and Hunger (1982): This is particularly evident at phases 0.060, 0.279, and 0.915, when the cores of the  $\lambda 4437$  line are displaced in the opposite direction to those of the stronger  $\lambda 4471$  profile.

Line profiles of silicon are shown in figure 7.5. The variations of the profiles of this element, as well as magnesium (figure 7.4), nitrogen, oxygen, carbon, and aluminum are all similar, and indicate the presence of at least two regions of local enrichment of each element. However, their phase behaviour is different from that of helium. For example, a high local abundance of helium is near the line of sight at  $\phi = 0.000$ , while one patch of silicon is approaching, and another receding, from the line of sight at the same time. Thus, silicon and these other elements seem to be concentrated at the negative extrema of the effective field of HD 37776. This difference in phase behaviour is quite similar to what has been seen in HD 64740 and  $\sigma$  Ori E earlier.

As has already been noted, the magnetic field curve of

HD 37776 shown in figure 7.1 suggests that the field geometry of this star is dominated by a quadrupolar component. This then implies a large surface field, since to produce a given observable longitudinal field the polar field strength of a quadrupole must be substantially higher than that of a dipole. For example, if the line of sight is along the field axis, the polar field of a quadrupole must be approximately 7.7 times stronger than the corresponding dipolar field strength to produce the same effective field (Schwarzschild 1950). For an inclination of the field axis to the line of sight of  $45^\circ$ , the quadrupole must have a polar field more than 20 times larger than the dipole. A polar field strength of at least 50 kG is then needed to produce the observed maximum longitudinal magnetic field of about 2 kG for HD 37776. A surface magnetic field of this magnitude will certainly have a large effect on the relative strengths of the Si III multiplet 2 lines, as discussed in chapter 3. If such an effect is not seen, then the observed magnetic variation of the star must be the result of a different, and probably more complex field structure.

A model for the magnetic field geometry of HD 37776 will be developed in the next section. Models of the line profiles of the star, both with and without this field geometry, will be presented in section 7.4.

### 7.3 Magnetic Model

Forty years have passed since Babcock reported the first detection of a magnetic field in a star other than the sun (Babcock 1947). Since then, fields have been measured in approximately two hundred stars (see the catalogue of Didelon [1983]). These have included late type dwarfs, peculiar A and B stars, and white dwarfs. Of these, perhaps fifty have been studied in any detail, the majority being Ap and Bp stars.

Early photographic measurements indicated that most of the observed stars had magnetic field variations that were periodic, but not harmonic. Modern photoelectric observations of these same stars have demonstrated that most of these anharmonic magnetic field curves apparently originated in the reduction of the photographic plates. Borra (1974) suggested that the observer tends to over-emphasize the cores of the lines, giving unrealistically high fields at certain phases. Extensive surveys and modelling now suggest that almost all magnetic stars have well behaved fields and can be satisfactorily explained using the oblique rotator model of Stibbs (1950) with some modifications, such as the decentered dipole model of Landstreet (1970). Many other field geometries have been proposed and include dipole plus quadrupole models (Wolff and Wolff 1970), the general dipole model of Stift (1975), and the symmetric rotator model of Krauss and Oetken (1976). However, the behaviour of a few peculiar objects remains

poorly understood. These include HD 32633 (Borra and Landstreet 1980; Renson 1984), and, most notably, HD 37776.

Several theories have been put forward over the years to explain the variations of the magnetic Ap and Bp stars. Babcock (1960) suggested the magnetic oscillator as one possibility. This model was an extrapolation of the observed behaviour of the general solar field. In this picture, the effective field of a star, observed above one of its rotational poles (aligned with the magnetic axis), consisted of contributions from the polar field and from the toroidal component near the equator. Then the observed variations might be a manifestation of the migration of the toroidal field towards the pole and a reversal of the poloidal field, in analogy with the phenomena observed on the sun.

Ledoux and Renson (1966) interpreted the magnetic field variations in terms of a binary star model. In their picture all Ap stars are close binaries (the secondary must be a degenerate object, since no eclipses are seen) in which tidal effects produce a magnetic field through some sort of dynamo process. Mass transfer between the two stars is then postulated as the cause of the observed abundance peculiarities and radial velocity variations.

The above models are no longer generally accepted. Several observational results, most notably Deutsch's (1956) discovery that the width of spectral lines in magnetic stars decrease with increasing period, and the observation of the

transverse Zeeman effect (Borra and Vaughan 1976), now favour the oblique rotator model, a brief description of which was given in chapter 1. Such an interpretation will be assumed here for the peculiar magnetic field variation of HD 37776. To explain the field curve of the star, Thompson and Landstreet (1985) suggested that a quadrupolar component must be dominant. Centered or decentered dipole geometries, and dipole plus quadrupole models, with small contributions from the quadrupole are obviously not the answer. Since it is desirable to keep the number of free parameters in any model field geometry of HD 37776 to a minimum, an attempt has not been made to fit the observed field variations of HD 37776 with Stift's (1975) general dipole model or a variation of his model. It is expected that two strategically placed magnetic dipoles, with appropriate polar field strengths and orientations, will reproduce the observed magnetic variations. In fact this is just the model suggested by figure 3 of Thompson and Landstreet's paper (1985). Unfortunately such a model has a prohibitively large number of degrees of freedom and the question of uniqueness can probably never be answered satisfactorily. Other, simpler combinations of dipoles have not been attempted. For example, two dipoles situated at a common point in the star, but with differing polar field strengths and orientations will not reproduce the twice reversing field seen in figure 7.1.

Instead, a solution of the form employed by Wolff and

Wolff (1970) to model the magnetic field of  $\beta$  CrB, was first attempted for HD 37776. Here, it is assumed that the effective field curve can be represented by the Fourier series

$$B_e = A_0 + A_1 \cos \phi + B_1 \sin \phi + A_2 \cos 2\phi + B_2 \sin 2\phi. \quad (7.1)$$

The resulting least squares solution is not satisfactory. Adding higher order terms improves matters, somewhat, but only at the cost of additional free parameters.

Next, an attempt was made to expand the effective field variations of HD 37776 in the form of a Legendre series as suggested by Goossens (1979). He gives an expression for the effective magnetic field of an oblique rotator with an irrotational, axisymmetric field, and shows that centered dipole and quadrupole, decentered dipole, and models of Wolff and Wolff (1970), and Krauss and Oetken (1976) are all special cases of this general field distribution.

The most general axisymmetric, irrotational field is given (in the coordinate system defined by the magnetic axis) by

$$B_r = \sum_{n=1}^{\infty} (n+1) \frac{A_n}{r^{n+2}} P_n(\mu') \quad (7.2)$$

$$B_\theta = \sum_{n=1}^{\infty} \frac{A_n}{r^{n+2}} (1-\mu'^2)^{1/2} \frac{dP_n(\mu')}{d\mu'}$$

Adopting Goossens's notation,  $\mu' = \cos \theta'$  where  $\theta'$  is the

magnetic colatitude, the  $A_n$  are constants and  $P_n$  is the Legendre polynomial of order  $n$ . A limb darkening law of the form

$$I(\theta) = I_0(1 - u + u \cos \theta) \quad (7.3)$$

is assumed for the remainder of this discussion. The effective field  $B_e$  is defined by (Borra, Landstreet, and Mestel 1982)

$$B_e = \frac{\int B \cos \gamma I \, dA}{\int I \, dA} \quad (7.4)$$

where  $B \cos \gamma$  is the component of the field along the line of sight,  $I$  is the local surface intensity given by equation (7.3),  $dA$  is a surface area element, and the integration is performed over the visible hemisphere of the star. With considerable algebra equations (7.2) to (7.4) lead to the result (Goossens 1979)

$$B_e = W_1 \frac{A_1}{R^3} \cos \alpha + \frac{W_2}{4} \frac{A_2}{R^2} P_2(\cos \alpha) + W_3 \sum_{k=2}^{\infty} C_k \frac{A_{2k}}{R^{2k+2}} P_{2k}(\cos \alpha) + \sum_{k=1}^{\infty} W_4 D_k \frac{A_{2k+1}}{R^{2k+3}} P_{2k+1}(\cos \alpha) \quad (7.5)$$

with the constants  $W_k$ ,  $C_k$  and  $D_k$  given by

$$W_1 = (15 + u)/(30 - 10u) \quad (7.6)$$

$$W_2 = W_3 = 3u/(3 - u) \quad (7.7)$$

$$W_4 = 3(1 - u)/(3 - u) \quad (7.8)$$

and

$$C_k = (-1)^{k+1} \frac{(2k+1)(2k-3)!!}{2^k (k+2)!} \quad (7.9)$$

$$D_k = (-1)^k \frac{(k+1)(2k-1)!!}{2^k (k+2)!} \quad (7.10)$$

In equation (7.5)  $\alpha$  is the angle between the magnetic axis and the line of sight. Since  $B_e$  is observed as a function of the rotational phase  $\phi$  of a star, it is necessary to write  $\alpha$  as a function of the phase  $\phi = (2\pi/P)t + \phi_0$ , where  $t$  is the time and  $P$  the period. If  $i$  is the inclination of the rotation axis to the line of sight and  $\beta$  is the obliquity of the magnetic axis to the rotation axis then

$$\cos \alpha = \cos i \cos \beta + \sin i \sin \beta \cos \phi \quad (7.11)$$

In a more recent paper Goossens, Martens, and Gadeyne (1981) remove the restriction to irrotational fields.

A solution for the field geometry of HD 37776 was then found by making a least squares fit of the magnetic data to equation (7.5) and minimizing the test statistic

$$\chi^2 = \sum_i^N \left[ (\Delta B_i) / \sigma_i \right]^2 / (N-n-1) \quad (7.12)$$

where  $N$  is the number of magnetic observations,  $n$  is the highest order Legendre polynomial used in the expansion, the  $\Delta B_i$  are the differences between the observed and calculated field, and the  $\sigma_i$  are the errors associated with the magnetic field measurements. It was anticipated that a

large value of  $n$  would be required to give a satisfactory result. Instead, an excellent fit was found for  $n = 3$ . A model consisting of an aligned dipole, quadrupole, and octupole results in a  $\chi^2$  of 1.31. This best fit is represented by the solid line superposed on the magnetic field measurements in figure 7.6. It was assumed that  $i$  and  $\beta$  are  $90^\circ$ , and a limb darkening coefficient  $u = 0.3$  has been used. This choice of  $i$  and  $\beta$  will provide a lower limit to the polar field strengths. Clearly, the observed field variation is reproduced very well, except for the very sharp positive extremum near  $\phi = 0.000$ . Table 7.1 gives a summary of the various fits that were attempted. The first column gives the highest order in the expansion, followed by the multipolar field strengths indicated by the least squares fit, and the reduced chi-squared of the model. In all cases  $\phi_0 = 0.184$ . The signs of the polar field strengths give the polarity of the pole that crosses the line of sight at  $\phi = \phi_0$ . Results are presented for three values of the limb darkening coefficient to give some feeling for the sensitivity of the results to adjustments in this parameter. It is evident from the table that a third order fit is the minimum required, but interestingly, higher order fits do not improve the results markedly. Inspection of table 7.1 suggests that the surface magnetic field of HD 37776 must be substantial. In figure 7.6 the calculated surface magnetic field has also been plotted as a function of phase. The surface field is determined using the equation (Borra,

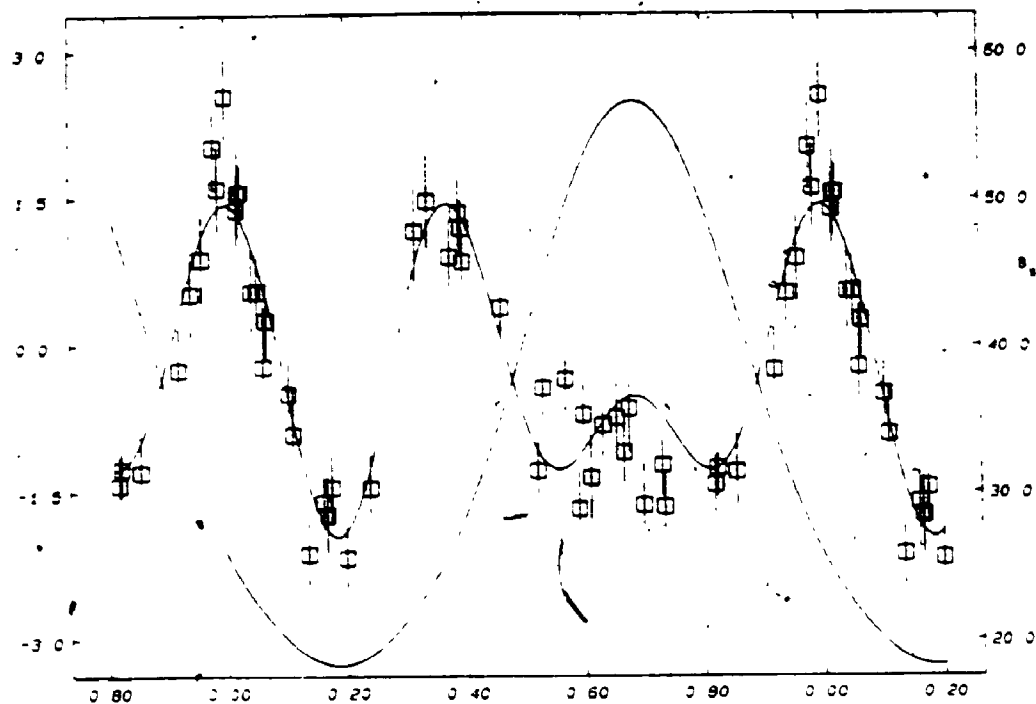


Figure 7.6 Longitudinal magnetic field measurements and model magnetic field curves for HD 37776. The field measurements are from Thompson and Landstreet (1985). The curve passing through the data is the longitudinal field variation derived from the model discussed in the text, with the scale given on the left of the figure. The approximately sinusoidal curve is the resultant surface magnetic field variation, with the scale given on the right of the figure.

Table 7.1 HD 37776 Magnetic Field Fitting Parameters

Order	$B_1$	$B_2$	$B_3$	$u$	$\chi^2$
2	1280	-41280	...	0.40	5.14
3	3350	-53800	45460	0.30	1.31
3	3200	-38730	51080	0.40	1.31
3	3060	-29880	58920	0.50	1.31
4	3240	-35940	51640...	0.40	1.30
5	3120	-35280	55640...	0.40	1.27
6	3100	-35910	55280...	0.40	1.29

\*adopted model

Landstreet, and Mestel 1982)

$$B_s = \frac{\int |B| I dA}{\int I dA} \quad (7.13)$$

where  $|B|$  is the local field strength and the other variables are as defined for equation (7.4).  $B_s$  was calculated numerically by dividing a model star into many small regions of equal area, adopting a model atmosphere with  $T = 22500$  K (see below), using the polar field strengths of table 7.1, and integrating over the surface of the star. The resulting surface magnetic field ranges from about 20 to 60 kG. The quadrupolar and octupolar contributions to the field have the same polarity at  $\phi = 0.684$ , which results in the very large surface field strength at this phase. At the minimum surface field strength ( $\phi = 0.184$ ) the polarities of these two components are opposite, leading to substantial cancellation in the field.

A variation of this general type of model was also examined. In this case, rather than assuming that the dipole, quadrupole, and octupole components are aligned, an extensive grid of effective field curves arising from field configurations with arbitrary phase shifts,  $\phi_0$ , for each field component were calculated. The obliquities of each multipole component were not adjusted, since this would have the sole effect of changing the polar field strength needed for the least squares fit, without changing the observed effective field. By varying the various  $\phi_0$ 's through a

sufficiently extensive range to cover the entire parameter space, it was found that the best fit to the field curve of HD 37776 does indeed occur when the dipole, quadrupole, and octupole field axes are all aligned. This model, with dipole, quadrupole, and octupole polar field strengths of 3350, 53000, and 45000 G respectively, will be used for some of the modelling discussed in the next section.

#### 7.4 Modelling

The effective temperature of 22500 K determined by the spectrophotometry of Adelman and Pyper (1985) has been adopted for this work on HD 37776. This is in good agreement with the value of 22000 K found by Groote and Kaufmann (1981) from a consideration of the ultraviolet to infrared fluxes, but since they do not illustrate the fit of their theoretical fluxes to the data, the slightly hotter temperature has been favoured. The *UBV*, Geneva, and *uvby $\beta$*  colour indices give  $T_{\text{eff}}$  of 25120 K, 2420 K, and 22360 K respectively.

The proposed magnetic field geometry receives some support when the line profile variations of helium (figure 7.4) and silicon (figure 7.5) are examined. The profiles of the helium  $\lambda 4437$  line suggest an axis of symmetry near  $\phi = 0.175$ , with the line strongest at times approximately 0.175 *P* earlier and later than this phase. The magnetic model locates the common magnetic axis of each field component at the line of sight at  $\phi = 0.184$ , very close to the axis of

symmetry for the line profiles. The opposite side of the star ( $\phi = 0.684$ ) must have an approximately uniform abundance of helium, since near this phase little in the way of profile variations is observed. This axis of symmetry is also apparent for the silicon line profiles, except in this instance, the profiles are suggestive of a spot of large silicon abundance near each pole. The spot, or band centered near  $\phi = 0.684$  must be quite large, since it first comes into view at  $\phi = 0.279$  and remains in sight until  $\phi = 0.060$ . Of course, the magnetic model predicts a very large field at  $\phi = 0.684$ , so that the shape of the line near this phase may be dominated by the surface field.

Because of the uncertainty in the magnetic field geometry of HD 37776, a first approximation to the surface abundance geometries of the star has been made by totally ignoring the contribution of the field to the line profiles. The resulting helium abundance geometry is then used to determine the surface gravity of the star in the usual manner, by fitting the wings of the gravity sensitive H $\delta$  and He I  $\lambda 4471$  profiles. An inclination and magnetic obliquity of  $90^\circ$  is assumed for simplicity.

The nature of the He I  $\lambda 4437$  line variations discussed above are suggestive of a helium abundance geometry consisting of a high latitude band of enhanced helium abundance, symmetric about the proposed magnetic axis of the star. This band must be located close to the magnetic pole located at  $\phi = 0.184$  in order to explain the lack of large

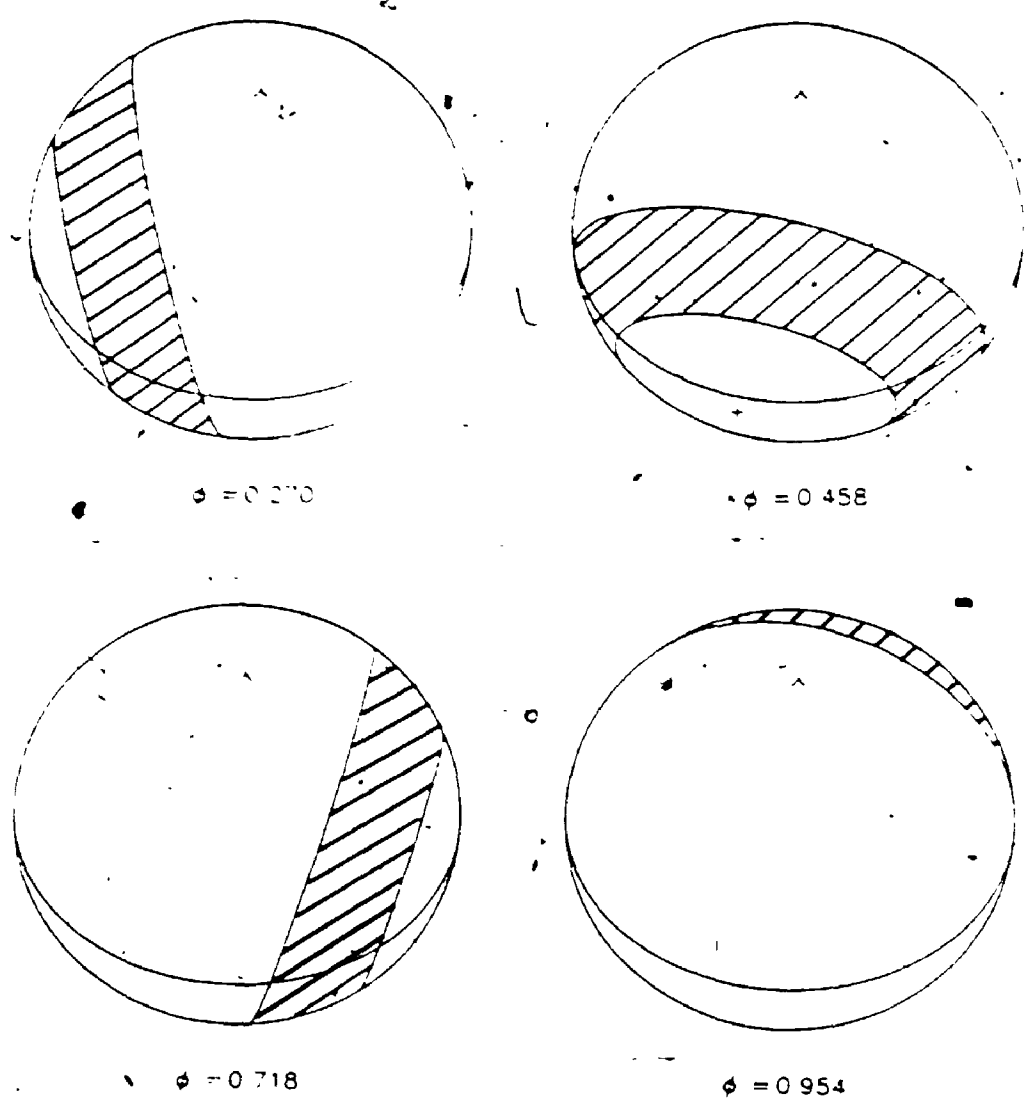
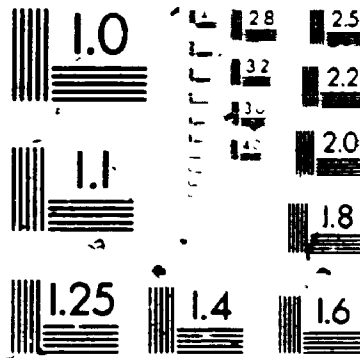


Figure 4.10 Illustration of the silicon abundance geometry of HD 64740. The hatched areas represent the locations of the silicon-rich regions on the stellar surface. The locations and signs of the magnetic poles are indicated by the symbols - and +. Details of the model are outlined in the text. The rotational phases are given below each figure.

# 3 of/de 3



**MICRO**

variations in the line profile half a rotation cycle later. The best fit that has been found for such a geometry is shown in figure 7.7 by the solid profiles. The details of the abundance are given in table 7.2. Helium is concentrated in a  $50^\circ$  band with  $c_{He} = 0.50$ . The helium abundance is  $c_{He} = 0.07$  elsewhere. The fit is poorest near  $\phi = 0.684$ , where the effects of the surface field are expected to be most important (assuming that the magnetic field model is correct). The  $v \sin i$  as determined from these profiles is  $100 \text{ km s}^{-1}$ .

This helium abundance geometry has then been used to estimate the surface gravity of HD 37776. Figures 7.8 and 7.9 illustrate the resulting H $\delta$  and He I  $\lambda 4471$  profiles for a constant  $\log g$  of 4.0. The wings of both sets of profiles are reproduced very well, except those of H $\delta$  at  $\phi = 0.155$  and  $\phi = 0.495$ . However, this discrepancy occurs when the line-of-sight helium abundance is large, so that the poor fits of H $\delta$  might be attributed to the inconsistency in the model atmosphere used for the line synthesis. Allowing again for this inconsistency, a  $\log g$  of  $3.9 \pm 0.15$  will be assumed for HD 37776.

The location of HD 37776 in the  $\theta_{eff}$  vs.  $\log g$  plane is shown in figure 7.10. A mass of  $10.0 \pm 2 M_\odot$  and radius of  $5.9 \pm 2 R_\odot$  are derived by interpolating from the evolutionary tracks in the figure. The angular diameter estimate of 0.069 milliarcsec (Groote and Kaufmann 1981) then gives a distance of  $400 \pm 140 \text{ pc}$ . HD 37776 would appear to be a true

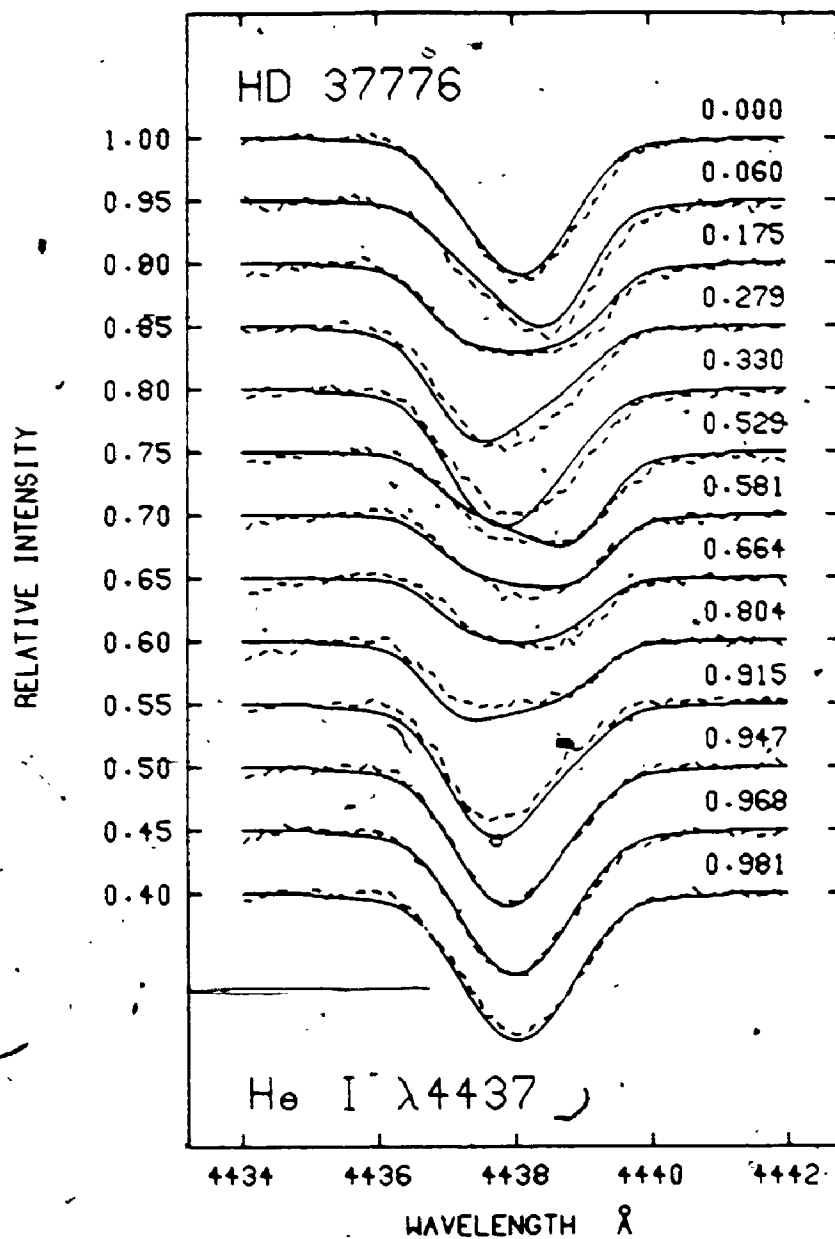


Figure 7.7 Observed (broken line) and modelled (solid line) He I  $\lambda 4437$  line profiles of HD 37776 for the non-magnetic model of the star. The helium abundance geometry is given in the text.

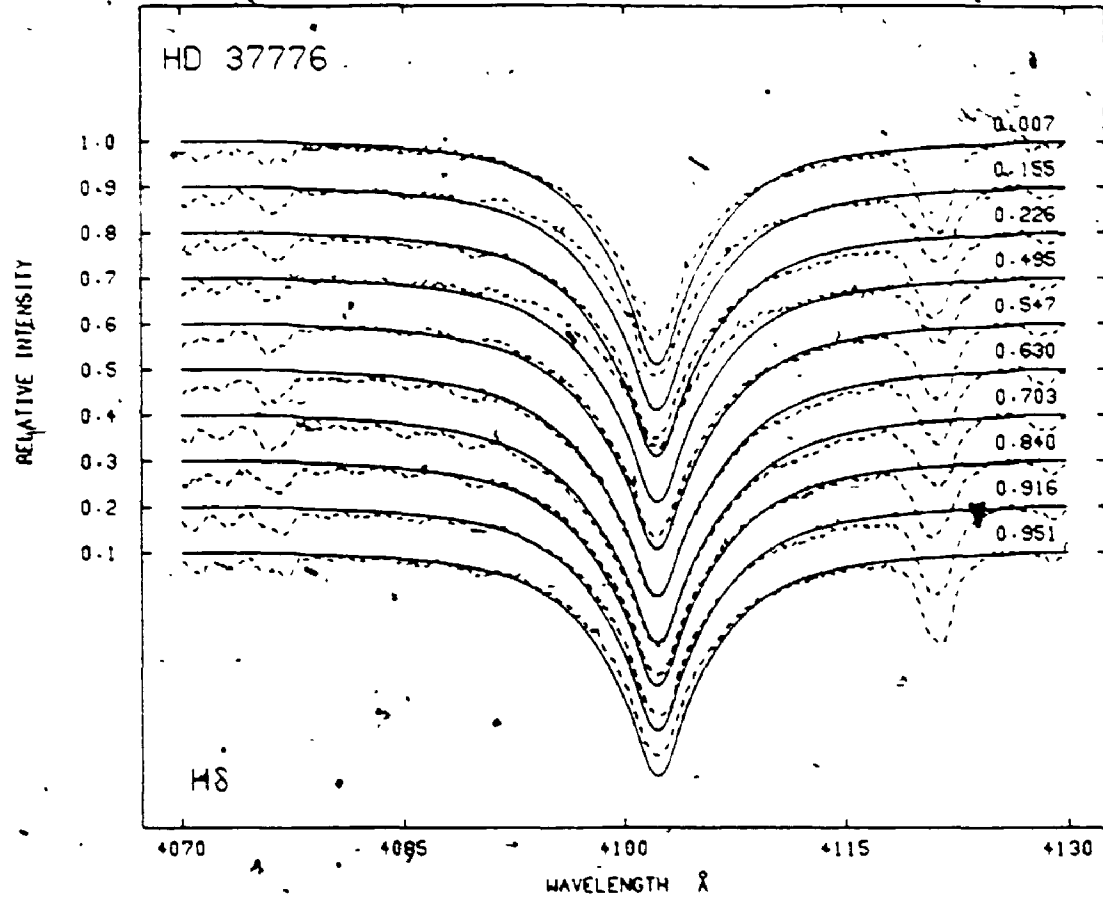


Figure 7.8. Observed (broken line) and modelled (solid line) H $\delta$  line profiles of HD 37776. The hydrogen abundance geometry is given in the text.

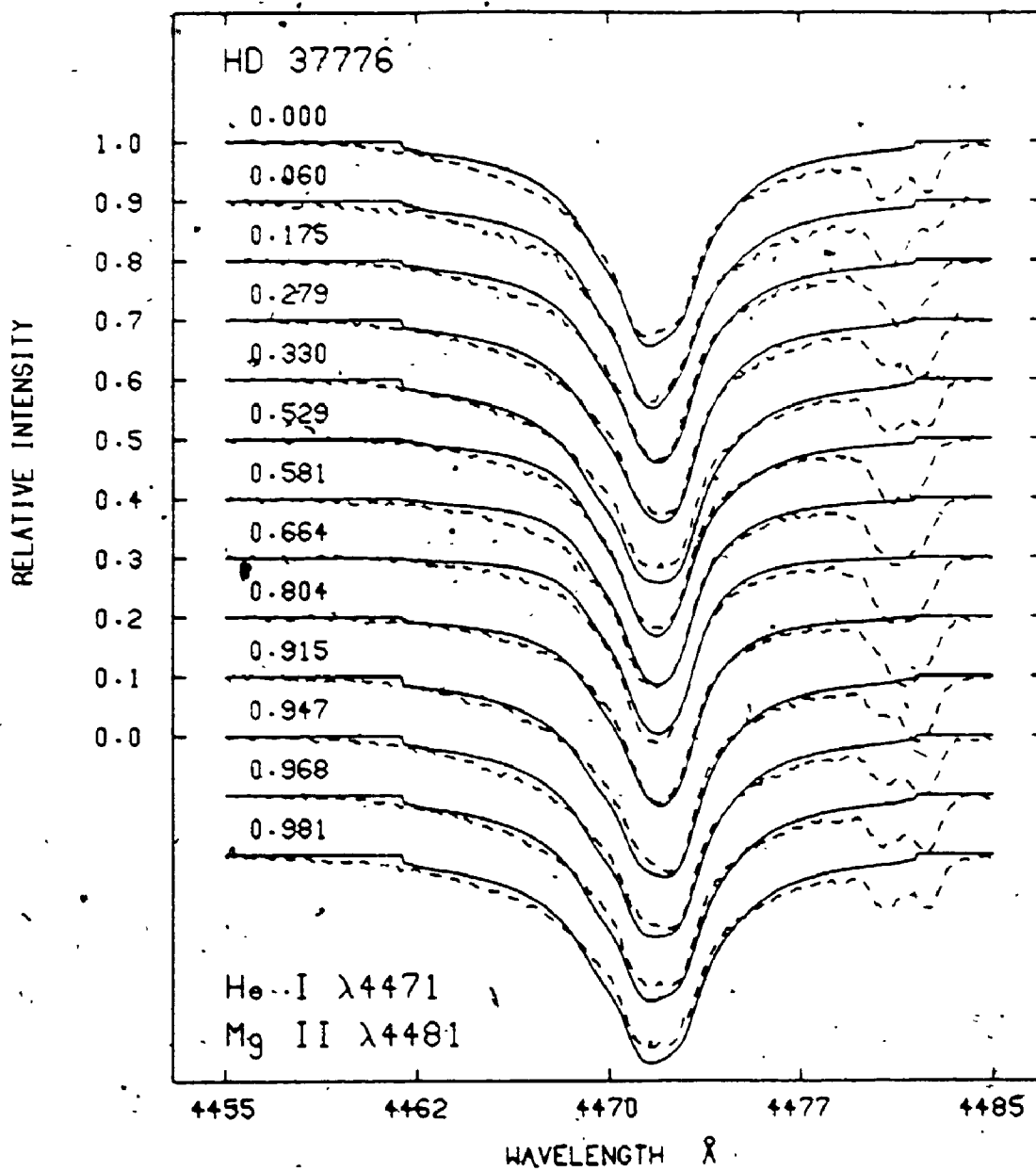


Figure 7.9 Observed (broken line) and modelled (solid line) He I  $\lambda 4471$  line profiles of HD 37776. The helium abundance geometry is given in the text.

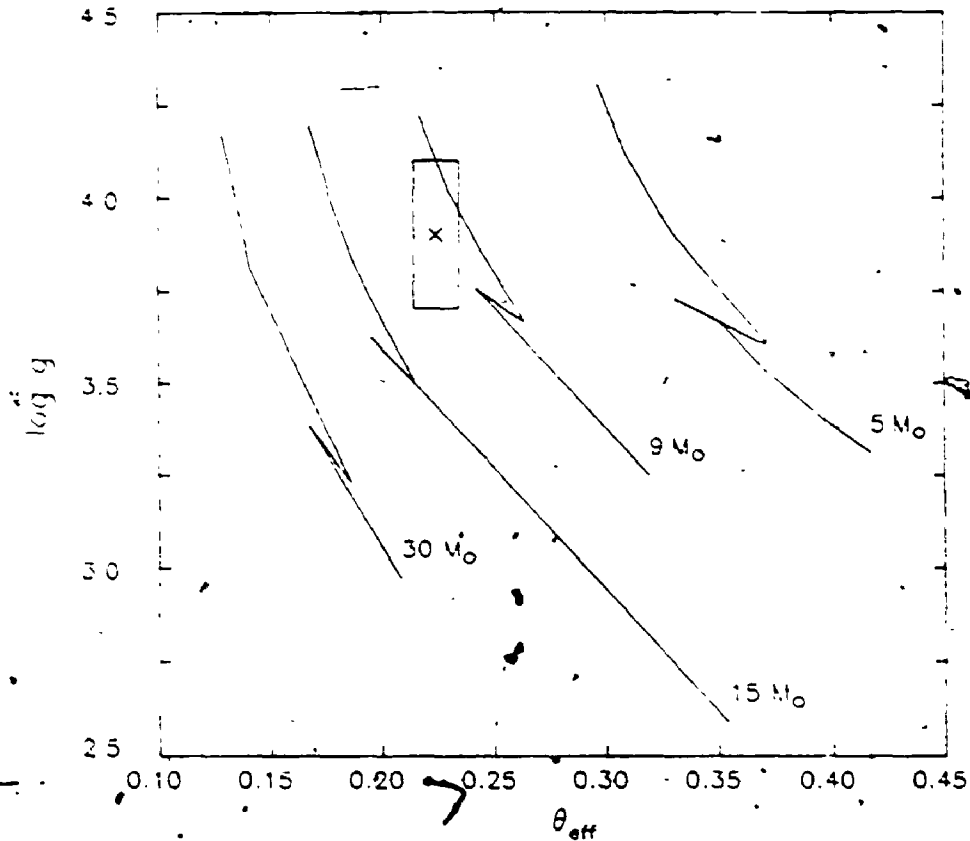


Figure 7.10 Location of HD 37776 in the  $\log g$  vs.  $\theta_{\text{eff}}$  plane. Symbols and evolutionary tracks are as in figure 4.8.

member of the Orion OB1 association.

A preliminary silicon abundance geometry was found by fitting the Si III  $\lambda 4567$  profiles of the star. Figure 7.11 displays the results of the adopted geometry for  $v \sin i = 100 \text{ km s}^{-1}$ . Silicon appears to be most abundant (approximately 100 times the normal abundance in this non-magnetic, LTE treatment) in a  $30^\circ$  radius spot located near the pole at  $\phi = 0.184$ , and in a  $50^\circ$  band situated close to the magnetic equator. The details of the silicon geometry are given in table 7.2. The same abundance geometry was then used to model the  $\lambda 4574$  profile as a function of phase. Again, the results are presented in figure 7.11. The fit to the  $\lambda 4567$  profiles is generally good, although the model profiles are a little weak. The model  $\lambda 4574$  profiles, on the other hand, are stronger than the observations, especially near  $\phi = 0.664$ . This can be considered further evidence for the presence of a very strong surface field on HD 37776, since according to the discussion in chapter 3, the Si III  $\lambda 4567$  profile will undergo a greater magnetic intensification than the  $\lambda 4574$  line because of its more complex Zeeman structure. This differential intensification appears to be greatest precisely where the postulated magnetic field geometry predicts the largest surface field strength.

The variations in the helium and silicon abundances over the visible hemisphere of HD 37776 are illustrated at several phases in figures 7.12 and 7.13 respectively. The

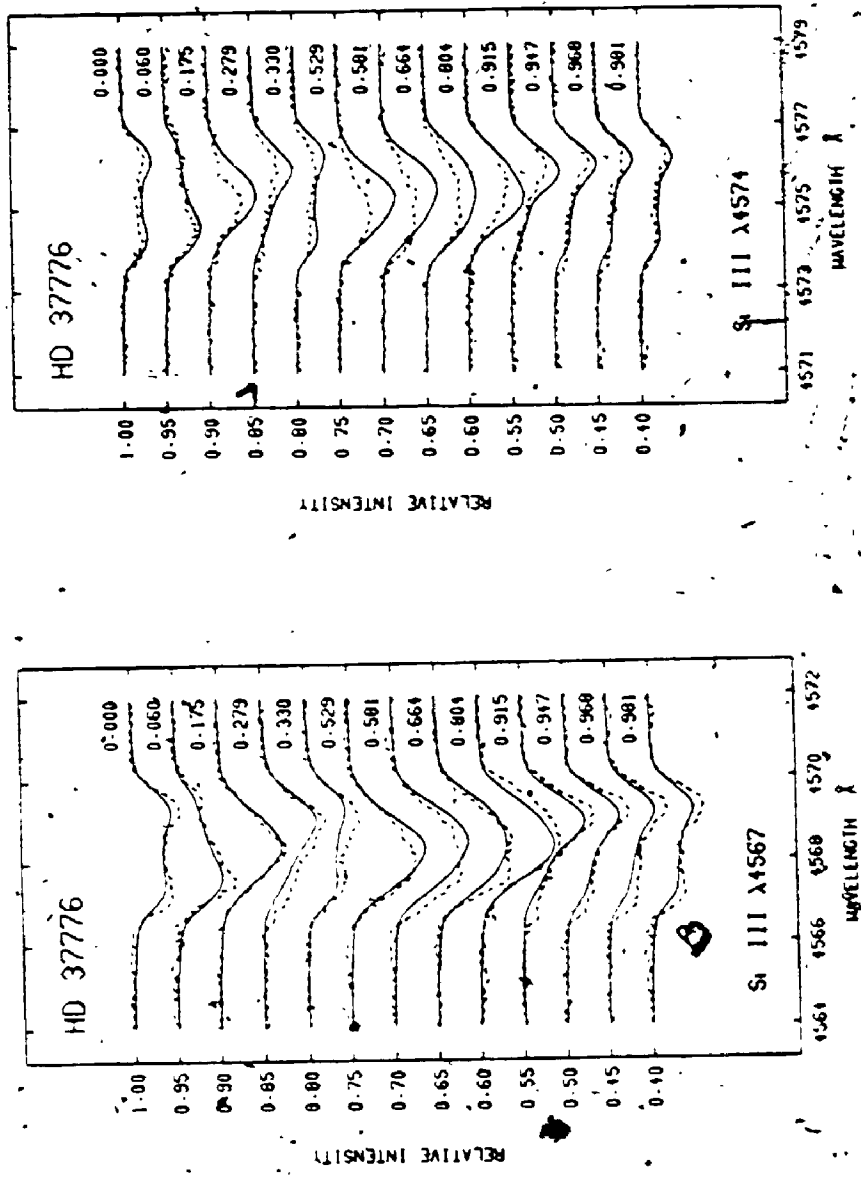


Figure 7.11 Observed (broken line) and modelled (solid line) Si III  $\lambda\lambda 4567$  and  $4574$  line profiles of HD 37776 for the non-magnetic model of the star. Note that the modelled  $\lambda 4567$  profiles are generally weaker than the observations, while the opposite is true of the  $\lambda 4574$  profiles. This illustrates the importance of magnetic intensification effects for HD 37776. The silicon abundance geometry is given in the text.

Table 7.2. HD 37776 Non-Magnetic Model  
Abundance Distribution

<u>log <math>\epsilon_{\text{He}}</math> (HD 37776)</u>			
Magnetic Colatitudes			
<u>log <math>\epsilon_0</math></u>	<u>0°-50°</u>	<u>50°-100°</u>	<u>100°-180°</u>
-1.0	-1.155	-0.301	+1.155

<u>log <math>\epsilon_{\text{Si}}</math> (HD 37776)</u>				
Magnetic Colatitudes				
<u>log <math>\epsilon_0</math></u>	<u>0°-30°</u>	<u>30°-100°</u>	<u>100°-150°</u>	<u>150°-180°</u>
-4.5	-2.40	-3.20	-2.70	-3.20

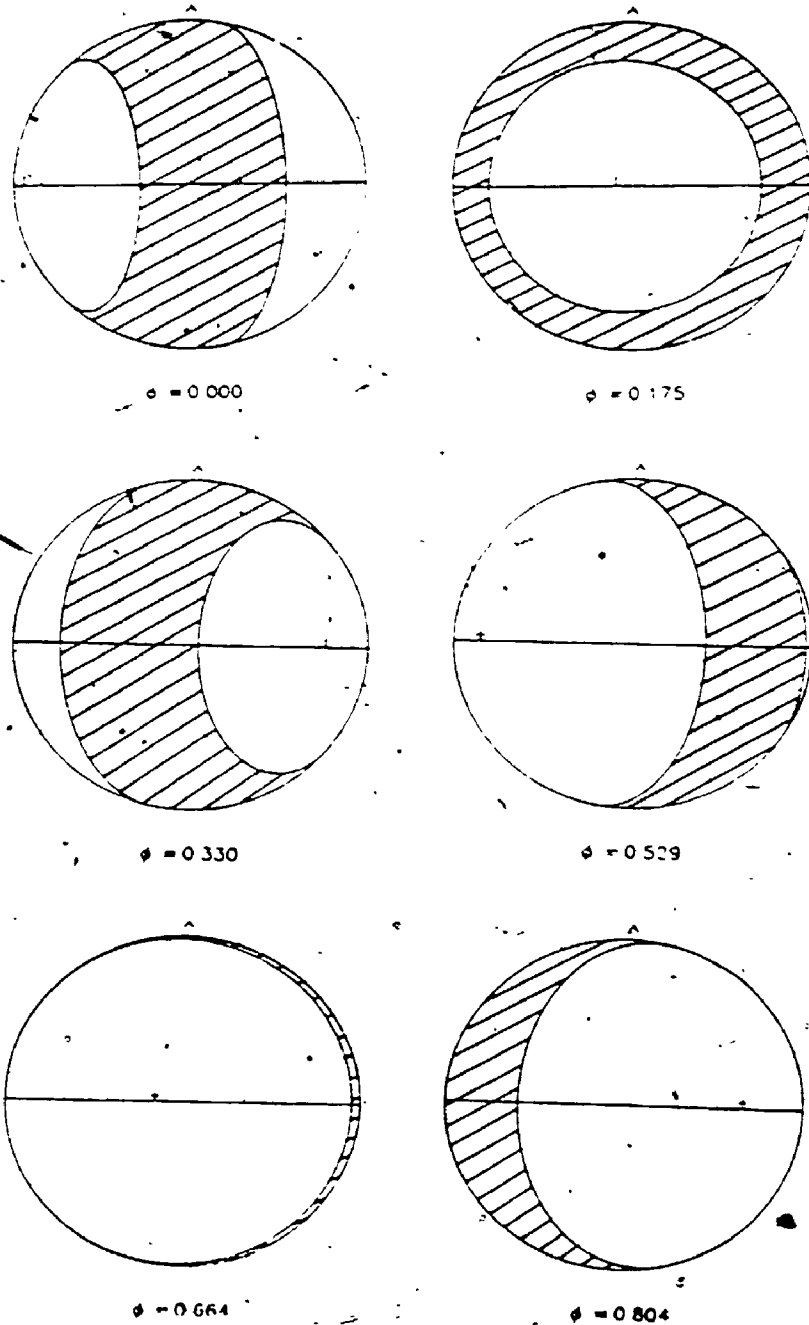


Figure 7.12 Illustration of the helium abundance geometry of HD 37776. The hatched areas represent the locations of the helium-rich regions on the stellar surface. The locations of the magnetic poles are indicated by the symbols - and +. Details of the model are outlined in the text. The rotational phases are given below each figure.

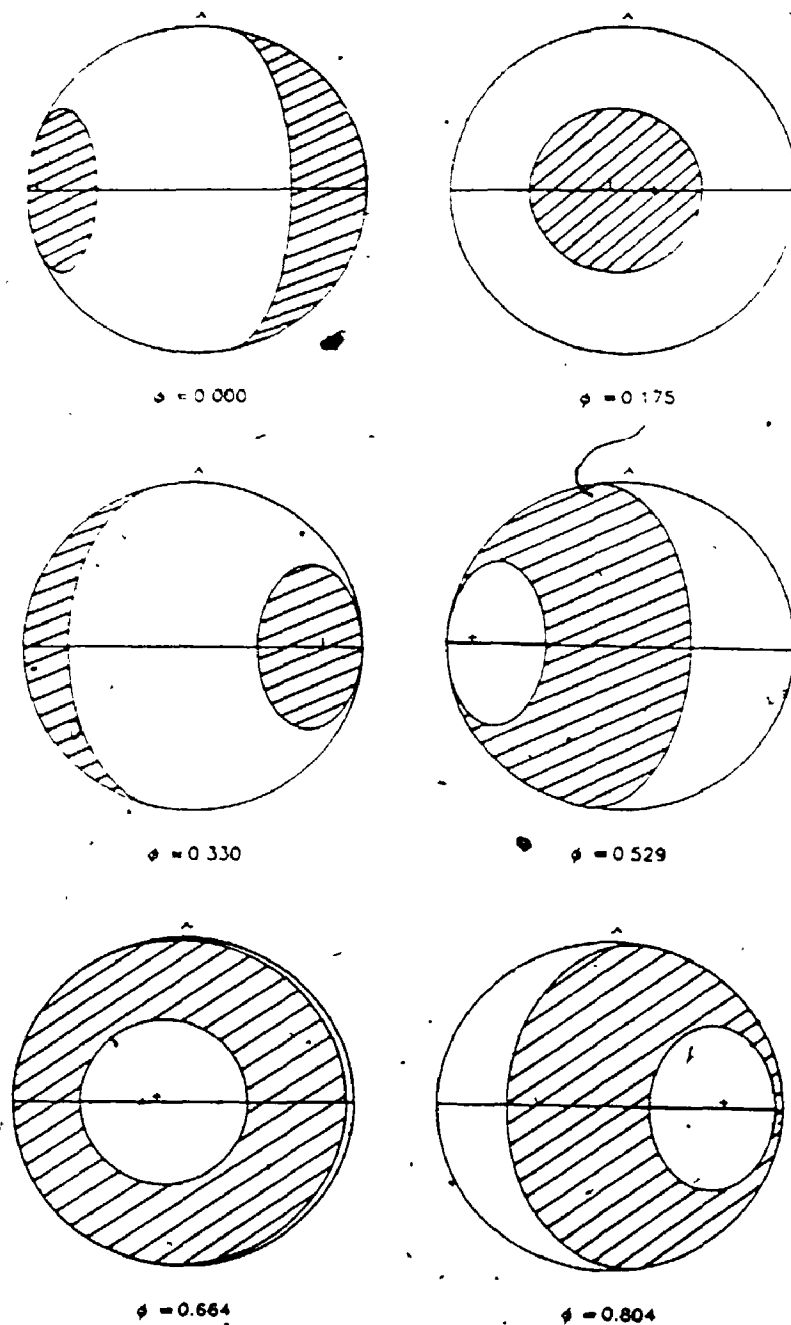


Figure 7.13 Illustration of the silicon abundance geometry of HD 37776. The hatched areas represent the locations of the silicon-rich regions on the stellar surface. The locations of the magnetic poles are indicated by the symbols - and +. Details of the model are outlined in the text. The rotational phases are given below each figure.

helium line strength is greatest when the helium-rich band crosses the line of sight, near phases 0.000 and 0.330. The silicon line profile variations result from the rotation of the silicon-rich spot and band into and out of the line of sight to the observer.

Since both the helium and silicon abundance geometries found above are axisymmetric about the adopted magnetic axis, it was decided to use the program ZEEABUN in an attempt to fit the observed profiles with the above magnetic model of the star. The resulting He I  $\lambda 4437$  and Si III  $\lambda \lambda 4567$  and  $4574$  profiles are given in figures 7.14 and 7.15 respectively. Note in these figures that phase zero refers to the passage of the weak magnetic pole through the sub-solar point; this corresponds to  $\phi = 0.184$  in the other figures. The fits were achieved after 20 to 30 iterations, and more than an hour of CPU time on the Cray Supercomputer. The abundances for each element in the 6 abundance rings assumed by ZEEABUN are given in table 7.3. The reduced chi-squared of the fits of the helium and silicon model profiles are 0.40 and 1.069 respectively, over all lines and phases. The plotted  $v \sin i$ 's are  $120 \text{ km s}^{-1}$ . An examination of tables 7.2 and 7.3 shows that the general topologies of the abundance geometries of helium and silicon are similar for both the non-magnetic and magnetic models, but the scale of the abundances is changed by a factor of approximately five to ten.

It is apparent from figures 7.14 and 7.15 that the

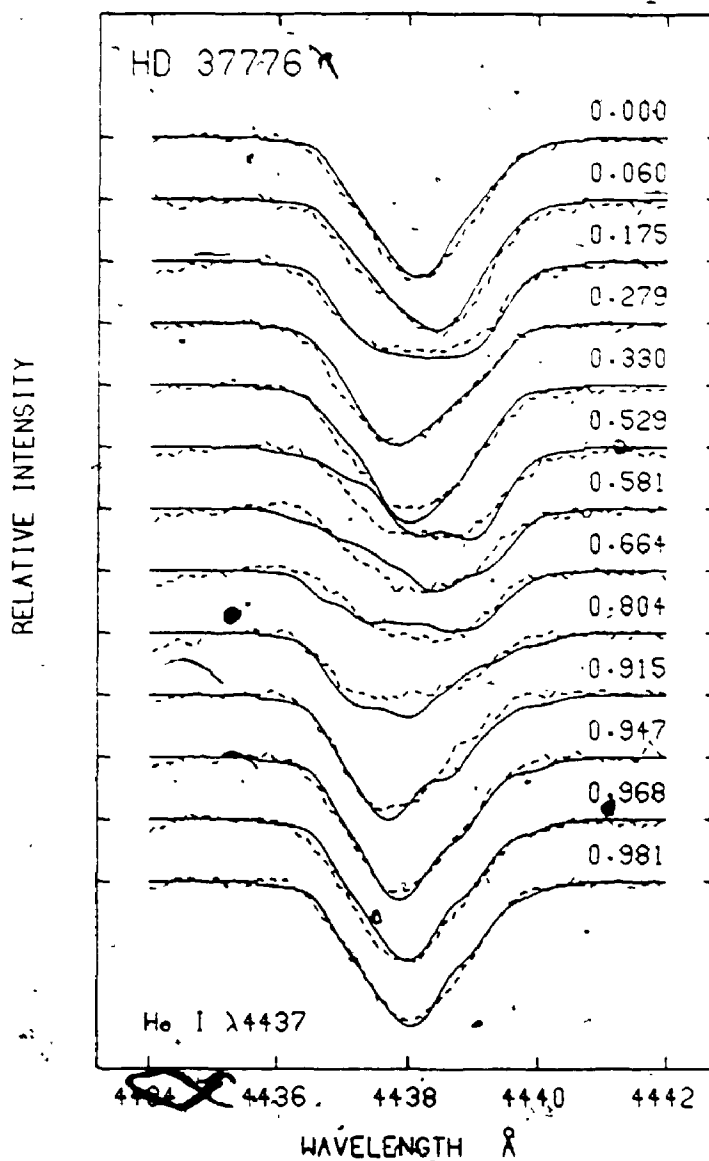


Figure 7.14 Observed (broken line) and modelled (solid line) He I  $\lambda 4437$  line profiles of HD 37776 for the magnetic model. The helium abundance geometry is given in the text.

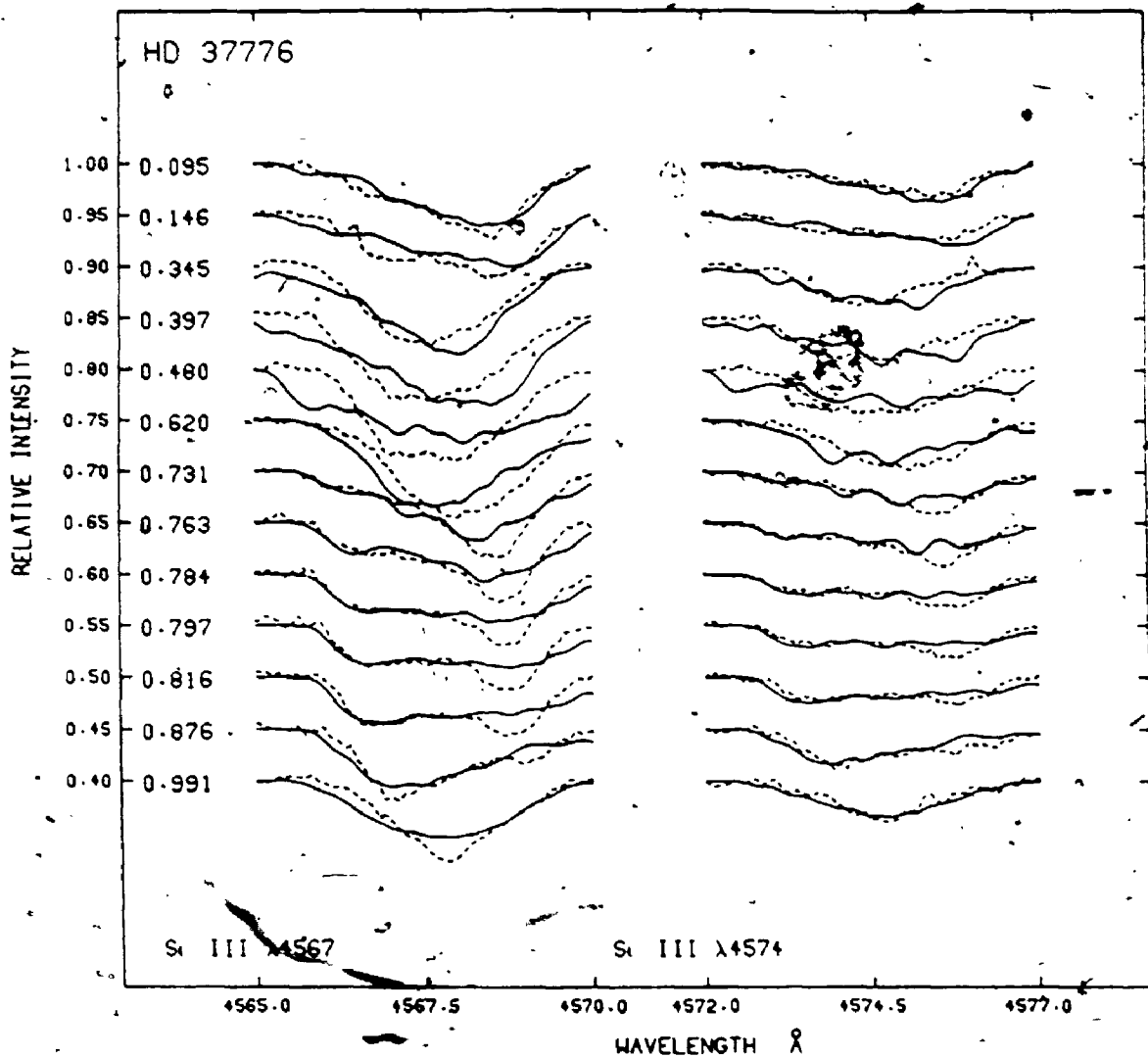


Figure 7.15 Observed (broken line) and modelled (solid line) Si III  $\lambda$ 4567 and 4574 line profiles of HD 37776 for the magnetic model of the star. Comparison with figure 7.11 suggests that the relative line strengths are matched much better by the magnetic model than in the non-magnetic case. The silicon abundance geometry is given in the text.

Table 7.3. HD 37776 Magnetic Model Abundance Distribution

Element	$\log \epsilon_0$	$\log \epsilon$ (HD 37776)					
		Magnetic Colatitudes					
		0°-30°	-60°	-90°	-120°	-150°	-180°
Helium	-1.0	-1.31	-0.73	-0.42	-1.12	-1.13	-1.36
Silicon	-4.5	-3.64	-4.34	-5.78	-4.16	-3.30	-4.51

model fits are poorest near  $\mu = 0.664$ , where the surface field is very large for the assumed magnetic geometry. The fit is also poorest at these phases for the non-magnetic models (figures 7.7 and 7.11). This suggests that the approximation for the magnetic field geometry may be poor at this point on the star's surface. As of yet, no attempt has been made to improve these model fits. Note, however, that the relative strengths of the silicon lines are reproduced much more accurately by the model incorporating the surface magnetic field geometry, than by the model which ignores the influence of the magnetic field. This is solid evidence in favour of the extremely large surface field of HD 37776.

#### 7.5 Discussion

Babcock's star, HD 215441, has the strongest surface magnetic field known for any peculiar star, ranging from 32 to 34.5 kG over its 9.5 day rotational period (Preston 1969). The strength of the field of this star is firmly established, because the  $\sigma$  and  $\pi$  Zeeman components of many of the spectral lines of the star are resolved. The effective field for this object ranges from 12 to 20 kG in phase with the surface field variations (Borra and Landstreet 1978). Borra and Landstreet (1978) and Stift (1980) have modelled these variations with decentered dipole and non-axisymmetric dipole models respectively. Landstreet (1988, private communication) is currently modelling the surface field geometry of the star using the same techniques

presented in this work.

If the magnetic geometry described above for HD 37776 is confirmed, this star will be unique in at least three respects: a) it will have the largest surface field of any non-degenerate star, b) it will possess the largest known variation in surface magnetic field over its surface, and c) it will be the first case of a star with a quadrupolar component dominating its field geometry. Three arguments in support of this large surface field have been presented here. First of all, the observed line profile variations of the star are consistent with an axisymmetric distribution of each element about the axis of the proposed magnetic field geometry. Secondly, the relative strengths of the Si III multiplet lines suggest a very large surface field. The intensities of the line profiles are produced much more accurately with a model incorporating a strong magnetic field, than for a model without a field. Finally, the quadrupolar magnetic field geometry of the star could explain the lack of radio emission detected for the star. Babcock's star, whose field geometry is predominantly dipolar, is a definite radio source (Drake et al. 1987).

The magnetic field geometry of HD 37776 could be important for a much more fundamental reason. Currently, there are two popular theories for the origin of the magnetic fields of early type stars. The fossil theory supposes that the observed field is the direct descendant of the interstellar field. Its structure may be influenced by

the various evolutionary sequences of a star, most notably the Hayashi phase of contraction to the main sequence, and also by the constraints of hydrostatic equilibrium and the effects of meridional circulation, but the overall field topology is expected to be preserved (e.g. Moss 1987a). In this case, it seems likely that the observed field would be uniform or dipolar. Dynamo theory (either a contemporary or a Hayashi phase dynamo) might lead to a dipolar or quadrupolar or mixed field geometry.

Moss (1985) has suggested that positive identification of a quadrupolar field component in a star would be strong evidence in favour of a dynamo origin for the field. Unfortunately the situation is probably not this simple. Moss (1987a) has cautioned that, if the fossil field was largely confined to one hemisphere of the star, the subsequent field structure could display a strong quadrupolar component, possibly consistent with the observed variation of HD 37776. However, calculations of the resulting effective and surface fields of such geometries do not reproduce the effective field variation of HD 37776 (Moss 1987b). Moss (1987b) is able to produce an effective magnetic field curve similar in shape to the observed curve of HD 37776 using a rather arbitrary four spot model in which all the surface magnetic field flux is confined to the interior of four circular spots. The spots were chosen in such a way that the net surface flux was zero. He suggests that this field distribution could be consistent with a

fossil origin of the field, if the primeval field has been distorted and concentrated into flux ropes during the Hayashi contraction phase of the star. If such a phase does not occur, then the flux rope structure might be acquired from the star formation process.

Scaling Möss's (1987b) effective and surface magnetic field curves for his spot model to values appropriate to the observed effective field of HD 37776, the maximum surface magnetic field strength produced would be of the order of 7.5 kG. This surface field is less than that estimated for HD 64740, for which it has already been shown that no significant magnetic intensification of the silicon lines occurs. In addition, this surface flux is concentrated in very localized regions of the star's surface, so that the overall effect on the line profiles is likely to be even smaller. This model, therefore, does not seem to be suitable for the field geometry of HD 37776.

At this point, all indications seem to suggest that the magnetic geometry of HD 37776 is dominated by a globally ordered quadrupolar component, and not by local regions of large surface magnetic fluxes. The star may then indeed represent evidence in favour of a dynamo interpretation for the origin of the fields in the upper main sequence stars.

Finally, it must be noted that the mass and radius of HD 37776 derived above, the observed  $v \sin i$  of 100 to 120 km s<sup>-1</sup>, and the 1.53869 day period yield an inclination of between 25° and 60° for the star using equation (4.3). With

such a small value of  $i$  the large spectrum variations of HD 37776 are very difficult to reproduce, and the surface magnetic field strength needed to produce the observed effective field variation is substantially larger. The only possible source of error in determining this inclination is the derived surface gravity of the star. More consistent model atmospheres could help remove this difficulty.

## Chapter 8 Conclusion

### 8.1 Summary

While the sample of stars is obviously statistically small, a few general observations can be made from the surface abundance and magnetic field geometries derived for the five helium-strong stars considered in this work.

With the exception of helium, the abundances derived for the program stars, for the limited number of elements with suitable lines, and averaged over their entire surfaces, appear to be approximately normal. This is quite different from the classical Bp and Ap stars in which overabundances of a few orders of magnitude are often seen for silicon, chromium, the rare earths, and other elements. In addition, while the surfaces of the helium-strong stars definitely have non-uniform abundances, the actual abundance contrast between distinct regions on the surface are not large, with the possible exception of the peculiar object HD 37776. Perhaps more important is the observation that for the three variable helium-strong stars studied here (HD 64740,  $\sigma$  Ori E, and HD 37776), the line profile variations of all the metals are consistent with similar locations of abundance patches for each element.

There does not appear to be any systematic behaviour in these stars, as far as the location of the helium-rich spots or bands are concerned, as might be expected according to Shore's (1987) model for the helium-peculiar stars. The

hottest star in the current investigation, HD 64740, has two helium patches located near the polar regions, in total disagreement with Shore's suggestion that the hottest helium-strong stars should have a helium-rich zone near the magnetic equator, if the magnetic field is dipolar.  $\sigma$  Ori E has a large concentration of helium in two patches situated near the intersection of the magnetic and rotation equators, and HD 37776 appears to have a middle (magnetic) latitude band with a large helium abundance. Of course, the latter object is not easy to interpret in terms of Shore's model because of the peculiar magnetic field geometry of the star. Note, however, that Michaud et al. (1987) claim that for helium enrichment to occur as a result of diffusive separation in the atmosphere of stars between  $T_{\text{eff}} = 20000$  K and  $T_{\text{eff}} = 25000$  K, the mass loss must decrease with increasing temperature. Shore assumes that the mass loss rate increases with temperature. This may be pertinent to the problem of HD 64740, but it will be difficult to determine the mass loss for the star to the accuracy required. Two other helium-strong stars, HD 37017 and HD 184927, show evidence for polar helium patches (Bohlender et al. 1987; Barker et al. 1982). It should be pointed out, however, that, except for HD 37776, the polarization and line profile data for the program stars do not rule out the possibility of moderate strength quadrupolar or higher order magnetic field components. In Shore's model, these higher order terms can lead to considerably different helium

abundance geometries than those discussed above, for the case of a dipolar field.

Unfortunately, little can be said about the significance of the location of the abundance patches for silicon, magnesium, and other elements on the surfaces of the helium-strong stars at this point in time. Theoretical work on the diffusion of silicon in magnetic stars has been confined to temperatures of about 14000 K (Vauclair, Hardorp, and Peterson 1979; Michaud, Mégessier, and Charland 1981; Alecian and Vauclair 1981), so that an extrapolation of these predictions to temperatures appropriate to the helium-strong stars is difficult. In these cooler stars, in the absence of a magnetic field (or when the field lines are vertical), silicon is only weakly supported by the radiation field. Si II and Si III both sink out of the atmosphere, while neutral silicon is elevated to the surface, so that only a weak overabundance is possible. If a horizontal magnetic field is present, the movement of the ions is impeded above  $\tau_{5000} = 0.1$ , so that much larger silicon accumulations are possible, up to a factor of 100 overabundance. Bands containing large abundances of the element should therefore be formed near the magnetic equator. Vauclair, Hardorp, and Peterson (1979) suggest that magnesium and iron will behave similarly. In fact, they claim that any element for which the radiative force on ionized atoms is of the same order of magnitude as gravity, but much larger for the neutral atoms, should follow the

same pattern as silicon. At higher temperatures, the radiative force should be larger, but the ionization equilibrium will be considerably different, with the result that very little silicon will be in the neutral state. It may then be much more difficult to produce a silicon overabundance. Since the average surface abundance seems to be approximately normal, perhaps horizontal diffusion processes are dominant on the surfaces of the helium-strong stars in the case of the metals. The variety in the location of the observed bands of silicon, and other elements, may then be explained by a migration of silicon from the magnetic equator to the poles as suggested by Michaud, Mégessier, and Charland (1984) and Mégessier (1984). A problem may arise in this interpretation, however, because of the timescale of  $10^6$  years estimated by Mégessier (1984) for this migration.

In this work, it has been assumed that the metal line variations are the result of non-uniform distributions of the various elements. Alternatively, the variations may be consistent with variations in the mean molecular weight and continuous opacity resulting from the inhomogeneous helium abundance on the surfaces of the helium-strong stars. Unfortunately, this possibility cannot be confirmed or ruled out without a more consistent and detailed treatment of the atmospheres of the program stars.

It is interesting to note that, if the magnetic field geometries derived above are accepted, the photometrically

variable helium-strong stars are brightest in the  $u$  band, when the strongest surface field is near the line-of-sight, and faintest at the opposite extremum in the surface field. (In figure 7.1 the photometric variation of HD 37776 in the  $y$  band is given, but the  $u$  band photometry is similar [Adelman and Pyper 1985]. In addition, the peculiar light-curve of  $\sigma$  Ori E makes this interpretation less certain in this star.) The field and photometric variations of the helium-strong stars HD 37017, shown in figure 8.1, and possibly HD 96446 (Matthews and Bohlender 1988), also provide support for this apparent trend.

Bolton (1983) has suggested that the photometric variations of the cooler helium-strong stars are caused by variations in the line blanketing due to elements other than helium. This blanketing is most pronounced in the ultraviolet and leads to a redistribution of flux into the visible region of the spectrum. For the hot members of the class, Bolton postulates that helium is an important contributor to the continuous opacity. He and Shore (unpublished, see Bolton 1983) calculated a grid of inhomogeneous model atmospheres with a local factor of four enhancement of helium in a region with variable upper and lower boundaries. Within the helium-rich region, they found that at a given mass column density, the temperature and gas and electron pressures are lower, and the opacities higher, than in an homogeneous atmosphere. Bolton (1983) then claims that these effects explain why the photometric minima

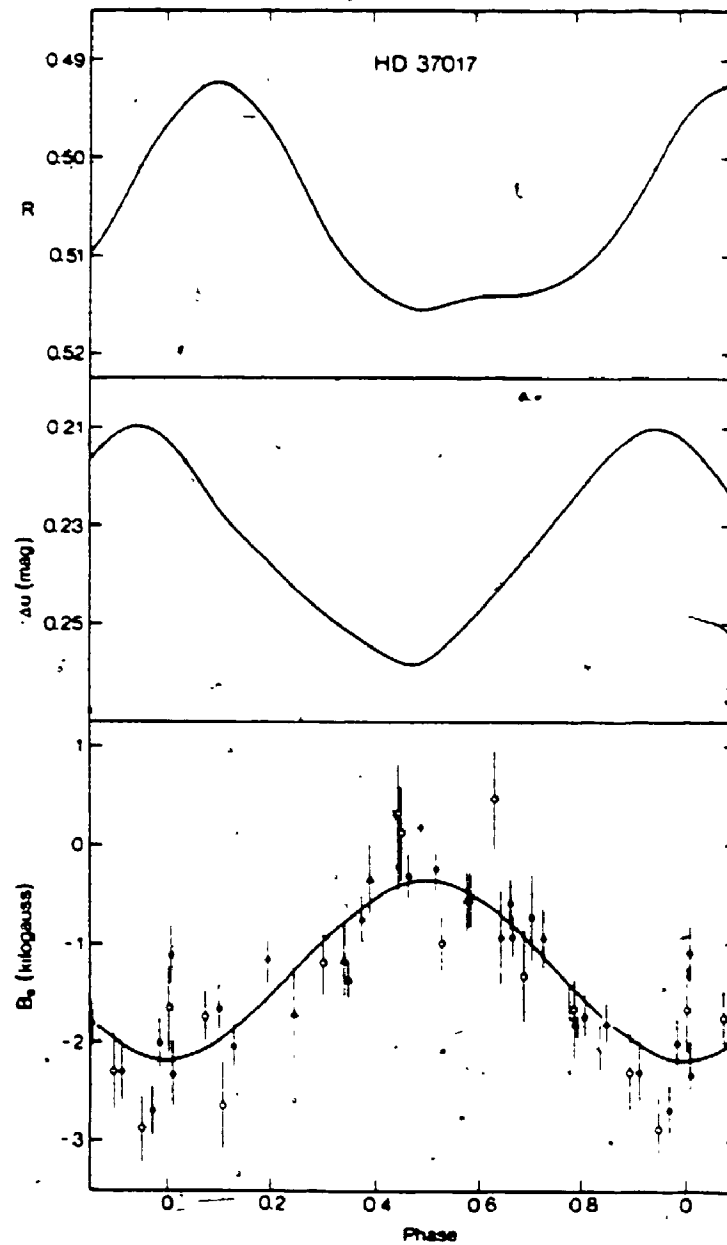


Figure 8.1 Helium line strength index,  $R$ , photometric and magnetic curves of HD 37017. The first two curves are hand-drawn fits to the data. Magnetic data symbols are as in figure 4.7. (From Bohlender et al. 1987.)

and helium line strength maxima of the hotter helium-strong stars coincide. This model seems to be supported by the helium line strength, and light variations of HD 37776 (figure 7.1) and possibly  $\sigma$  Ori E. HD 37017 seems to be an exception to the rule, as can be seen by inspection of figure 8.1. The lack of photometric variability of HD 64740 might be attributed to the relatively low helium abundance anomaly of the star.

### 8.2 *Suggestions for Future Work*

Not surprisingly, this investigation suggests several opportunities for improved modelling, extended observations, and badly needed theoretical work.

The surface gravities, and therefore masses, of the program stars have been fitted by modelling profiles of the pressure sensitive lines H $\delta$  and He I  $\lambda$ 4471, using the atmospheric structure given by Kurucz's (1979) grid of solar abundance atmospheric models. The serious inconsistency that this produces in the derived models has been mentioned several times. It would be very useful to repeat these gravity determinations using more appropriate model atmospheres. A previous investigation of the helium equivalent width variations in  $\sigma$  Ori E (Groote and Hugger 1982) assumed a uniform abundance of helium over the visible hemisphere of the star. A better approach might involve calculating a separate model atmosphere for each area element on the star's visible surface using a helium

abundance appropriate for the local surface abundance. This work would enable a definitive determination of the masses (and hence, radii and inclinations  $i$  and  $\beta$ ) of the helium-strong stars. Such a model could also be used to examine the photometric variations of the helium-strong stars by calculating the model fluxes as a function of rotational phase, and comparing these to the observed light curves of the stars. The question of the cause of the metal line variations might also be answered with this improved treatment. A problem with such a piece-wise approximation is that if the surface gravity is assumed to be constant, over the surface of the star, then considerable differences in atmospheric scale heights between regions of low and high helium abundance will lead to horizontal pressure gradients, and interesting 'weather' in the stellar atmosphere, unless an additional stabilizing force is introduced. Norris and Baschek (1972) have suggested that a vertically directed magnetic field could provide the required extra pressure. Mihalas (1973), on the other hand, feels that it is more physical to assume that there is horizontal pressure equilibrium, in which case a downward magnetic force is required in the regions with low helium abundance. He suggests that this could be supplied by a toroidal component to the magnetic field.

Up to this time, the full potential of the programs *ZEEMAN* and *ZEEABUN* have not been realized, since only the unpolarized intensity spectra of various stars have been

obtained. It would be very useful to obtain spectral observations of several interesting magnetic stars using an instrument such as the ESO CASPEC with the Zeeman analyser. Mathys (1988) has demonstrated the quality of polarized spectra obtainable with this instrument, but analyzes the data in a parametric manner. With ZEEAN and ZEEABUN, the capability exists to model the polarized profiles themselves with a careful consideration of the relevant physics involved. These data would be particularly useful for confirming the peculiar magnetic field geometry of HD 37776. There are also many more interesting magnetic Ap, Bp, and helium-weak stars for which continued CFHT observations would also be very productive.

The relatively sharp-lined helium-strong star  $\delta$  Ori C also presents some interesting possibilities which warrant consideration. With the data presently in hand, it is impossible to discriminate between the two models proposed for the star in chapter 5. Zeeman observations in a helium line (for example, the  $\lambda 5876$  line used by Bohlender et al. 1987) could possibly help in determining which of the models applies to the star. If the longitudinal magnetic field, as derived from a helium line, is significantly different from the roughly constant  $-3400$  G field found from  $H\beta$  observations, then the spot model might be preferred for the star, since in this case less than the entire visible disk of the star contributes to the longitudinal field. Unfortunately, models of the Stokes  $V$  profiles of the helium

$\lambda 4471$  line seem to indicate that the circular polarization in the wings of this line are similar for both the spot model of the star and the stratified model, so that such an effort might not be rewarded with a positive answer.

As discussed earlier,  $\delta$  Ori C appears to be a member of a small subset of helium-peculiar stars with peculiar helium line profiles. Other stars showing this peculiar helium line behaviour include 3 Sco (Norris and Strittmatter 1975),  $\alpha$  Cen (Norris and Baschek 1972) and HD 49333 (Hunger 1986a;b). Hunger (1988, private communication) has informed the author that at least three other candidates are known. It was also shown in chapter 5 that HD 58260 also showed marginal evidence of a peculiar helium  $\lambda 4471$  profile as well. The helium line profiles in these objects can be modelled with large vertical or horizontal variations in helium abundances over the surfaces of the stars. This group of stars all have effective temperatures between approximately 16000 and 20000 K, and all appear to have magnetic fields (Bohlender et al. 1987; Landstreet, Borra, and Fontaine 1977), although only a few low significance measurements are available to date for HD 49333 (Borra, Landstreet, and Thompson 1983).

In this temperature region there also exists a group of stars classified as *sn*, which have *sharp-lined* metallic spectra but *nebulous* or very diffuse helium lines (e.g. Mermilliod 1983). Mermilliod shows that essentially all slow rotators in this temperature region are *sn* stars, which

suggests a possible diffusion scenario for their origin, since slow rotation implies small meridional currents and therefore a stable outer envelope necessary for diffusion processes to occur. Vauclair (1975) has suggested that these peculiar profiles could be caused by a large abundance gradient in the line forming region (between  $r = 0.1$  and  $r = 1.0$ ).

Several helium-weak stars are also classified as *sn*, and interestingly, recent observations indicate that the only helium-weak stars that show evidence of stellar winds in their ultraviolet spectra are those with the *sn* designation (Shore, Brown, and Sonneborn 1987). These stars are not slow rotators but are magnetic, so that their atmospheres are presumably stable enough for diffusion processes to occur. The strong winds would then seem to be related to the presence of a strong, globally ordered magnetic field.

It would be useful to observe as many of these stars as possible spectroscopically. Observations of He I  $\lambda\lambda 4437$  and  $4471$ , for which a good broadening theory is available, and a Balmer line, would be needed to determine the helium abundances and surface gravities of these stars. Accurate effective temperatures should also be determined, either using ionization equilibrium of ions with suitable lines in the spectra, or using absolute ultraviolet and visible continuum fluxes, where available. These observations could provide important constraints for improved theories of

helium diffusion in hot stars, and give useful information on the roles of effective temperatures, magnetic fields and rotation on these diffusion processes. If the above conceptual picture is correct, then only rapidly rotating, non-magnetic stars in this temperature range will have 'normal' helium line profiles.

It has been suggested that the helium-strong stars may be closely related to the more common emission-line B (Be) stars (e.g. Barker et al. 1985). Bolton et al. (1986) have suggested that the helium-strong star  $\sigma$  Ori E is actually a magnetic Be star. In recent years, it has become apparent that many Be stars demonstrate photometric variability, that may be periodic, with time scales consistent with possible rotation rates for these stars (on the order of a day). Harmanec (1984), among others, has pointed out the similarity of these photometric variations with those seen in the helium-strong stars, and has suggested that many of these variables may have spotted surfaces, and measurable magnetic fields like  $\sigma$  Ori E. Also interesting is the fact that, among early B type main-sequence stars, only the Be and helium-strong stars have lines of very high ionization stages in their ultraviolet spectra (Marlborough 1982). The high ionization potentials of these lines imply a non-thermal, and possibly magnetic origin. It would be of considerable interest to monitor the Be stars, especially those with periodic photometric variations, for spectral and magnetic field variations on the same time scales as the

photometric variations. To date, no positive field detections have been reported for Be stars (Barker et al. 1981; 1985). The author has been involved in a program in collaboration with Harmanec to examine several of the photometrically variable Be stars, using the UWO polarimeter and the UWO 1.2 m telescope, in an attempt to measure possible longitudinal magnetic fields. Some of the data is suggestive of possible field detections, but at a low level of significance. This project would benefit from time on a larger telescope.

The helium-strong stars are the hottest known peculiar magnetic stars. The low temperature cutoff of the magnetic stars is thought to be well understood. In low mass stars diffusion occurs under the surface convection zone. These convection zones become very extensive in stars cooler than about F5 leading to very long diffusion time scales. As a result, abundance anomalies do not have enough time to develop. The surface magnetic field is believed to become much more complex and localized, as in the active regions on the sun, and hence, is undetectable by conventional polarimetry. The apparent high temperature limit of the magnetic stars is not as well explained. In fact, field strengths seem to increase with increasing effective temperature (Thompson, Brown, and Landstreet 1987). Stars hotter than 25000 K have strong stellar winds, which may prevent the formation of extreme spectral peculiarities, so there are probably few O-type analogues of Ap stars (Bolton

[1988, private communication] has pointed out possible exceptions, Zeta Ophiuchi and HD 93521, each of which has significant helium line variations). These winds, however, should not have a large effect on the magnetic field. There may therefore be a fraction of apparently normal stars hotter than 25000 K (earlier than B1 spectral type) with measurable magnetic fields, unless some other mechanism is acting to remove the field, change its topology, or prevent its formation in the first place.)

A recent compilation of stellar magnetic field measurements (Didelon 1983) shows that only a handful of stars hotter than 25000 K have been searched for magnetic fields. An additional observational project that should be carried out is a polarimetric survey of bright early B and O stars. If any fields are detected, a follow-up program will be necessary to determine the magnetic field variations of each object as a function of time. Again, some effort has been made along this line by the author: observations of early B and O stars in the Orion OB1 association have not indicated any new magnetic stars as yet. The possibility of detecting magnetic fields in O stars is quite exciting, and would be of considerable significance to studies of non-radiative processes in OB and Wolf-Rayet stars. The need for such a project has often been cited in the literature (e.g. Walborn 1984).

Little has been said about the modelling of the circumstellar material, and winds of the helium-strong

stars. Bolton is currently using much of the same CFHT data discussed here to tackle the problem of the H $\alpha$  emission source for  $\sigma$  Ori E. His early analysis has been discussed above. Very little quantitative work has been carried out yet with regards to the variable winds of these objects. Barker (1986) has discussed the observed behaviour and correlations of the wind features of the helium-strong stars, as related to other observations of the same stars. His main conclusion is that the strongest and most asymmetric C IV emission occurs in the stars that are viewed approximately pole-on or are the slowest rotators (e.g. HD 58260). H $\alpha$  emission is strongest in the rapid rotators. This is in agreement with the theoretical work of Nakajima (1981, 1985).

Much progress has been made theoretically in recent years, but much remains to be done. Nerney (1980), Barker (1982), Friend and MacGregor (1984), and Poe and Friend (1987) have demonstrated the importance of rotation and magnetic fields on the winds of hot stars. Extensions of this work should include the effects of arbitrary obliquities of the magnetic axis, although such work will be very difficult and require three-dimensional models. The works of Stepien (1978), Peterson and Theys (1981), Havnes and Goertz (1984), and Landstreet (1987) have given some indication of the importance of incorporating the effects of the magnetic field into the structure of the atmospheres of the peculiar stars, and work should continue along these

lines. Theoretical calculations of the diffusion of silicon and other elements in the presence of a magnetic field, and at temperatures appropriate to the helium-strong stars are badly needed.

It is hoped that the results of the present investigation will provide the initiative for some of these suggested investigations. The abundance and magnetic field geometries derived for this small sample of helium-strong stars provide an important observational constraint for future diffusion calculations, and also the required boundary condition for theoretical investigations regarding the winds of these remarkable stars.

## REFERENCES

- Abt, H. A., and Levato, H. 1977, *Pub. A. S. P.*, **89**, 797.
- Adelman, S. J. 1988, *Mon. Not. R. Astr. Soc.*, **230**, 671.
- Adelman, S. J., and Pyper, D. M. 1985, *Astr. Ap. Suppl.*, **62**, 279.
- Alcock, C., and Paczynski, B. 1981, *Ap. J.*, **223**, 244.
- Alecian, G., and Vauclair, S. 1981, *Astr. Ap.*, **101**, 16.
- Aller, L. H. 1963, *Astrophysics: the Atmospheres of the Sun and Stars* (New York: Ronald).
- Auer, L. H., and Mihalas, D. 1973, *Ap. J. Suppl.*, **25**, 439.
- Babcock, H. W. 1947, *Ap. J.*, **105**, 105.
- \_\_\_\_\_. 1949a, *Observatory*, **69**, 191.
- \_\_\_\_\_. 1949b, *Ap. J.*, **110**, 126.
- \_\_\_\_\_. 1960, in *Stars and Stellar Systems*, Vol. 6, *Stellar Atmospheres*, ed. J. L. Greenstein (Chicago: University of Chicago Press), p. 282.
- \_\_\_\_\_. 1962, in *Stars and Stellar Systems*, Vol. 2, *Astronomical Techniques*, ed. W. A. Hiltner (Chicago: University of Chicago Press), chap. 5.
- Barker, P. K. 1982, in *IAU Symposium 98, Be Stars*, ed. M. Jaschek and H.-G. Groth (Dordrecht: Reidel), p. 485.
- \_\_\_\_\_. 1986, in *IAU Colloquium 87, Hydrogen Deficient Stars and Related Objects*, ed. K. Hunger, D. Schönberner, and N. Kameswara Rao (Dordrecht: Reidel), p. 277.
- Barker, P. K., Landstreet, J. D., Marlborough, J. M., Thompson, I. B., and Maza, J. 1981, *Ap. J.*, **250**, 300.

Barker, P. K., Brown, D. N., Bolton, C. T., and Landstreet, J. D. 1982, in *Advances in Ultraviolet Astronomy: Four Years of IUE Research*, ed. Y. Kondo, J. M. Mead, and R. D. Chapman (NASA-CP-2238), p. 589.

Barker, P. K., Landstreet, J. D., Marlborough, J. M., and Thompson, I. B. 1985, *Ap. J.*, 288, 741.

Barnard, A. J., Cooper, J., and Smith, E. W. 1974, *J. Quant. Spectrosc. Radiat. Transfer*, 14, 1025.

Baschek, B., and Scholz, M. 1982, in *Landolt-Börnstein. Zahlenwerte und Funktionen aus Naturwissenschaften und Technik, Neue Ser., Group VI, Vol. 2b*, ed. K. Schaifers and H. H. Voigt (Berlin: Springer), p. 107.

Berger, J. 1956, *Contr. Inst. Ap. Paris*, No. 217.

Bohlender, D. A., Brown, D. N., Landstreet, J. D., and Thompson, I. B. 1987, *Ap. J.*, 323, 325.

Bolton, C. T. 1970, *Ap. J.*, 161, 1187.

----- 1971, *Astr. Ap.*, 14, 233.

----- 1974, *Ap. J.*, 192, L7.

----- 1983, *Hvar Obs. Bull.*, 7, 241.

Bolton, C. T., Fullerton, A. W., Bohlender, D. A., Landstreet, J. D., and Gies, D. R. 1986, in *IAU Colloquium 92, The Physics of Be Stars*, ed. A. Slettebak and T. P. Snow (Cambridge: Cambridge University Press), p. 82.

Bonsack, W. K., and Dyck, H. M. 1983, *Astr. Ap.*, 125, 29.

Borra, E. F. 1974, *Ap. J.*, 188, 287.

Borra, E. F., and Landstreet, J. D. 1977, *Ap. J.*, 212, 141.

- \_\_\_\_\_. 1978, *Ap. J.*, 222, 226.
- \_\_\_\_\_. 1979, *Ap. J.*, 228, 809.
- \_\_\_\_\_. 1980, *Ap. J. Suppl.* 42, 421.
- Borra, E. F., Landstreet, J. D., and Mestel, L. 1982, *Ann. Rev. Astron. Astrophys.*, 20, 191.
- Borra, E. F., Landstreet, J. D., and Thompson, I. B. 1983, *Ap. J. Suppl.*, 53, 151.
- Borra, E. F., and Vaughan, A. H. 1976, *Ap. J. (Letters)*, 210, L145.
- Bray, R. J., and Loughhead, R. E. 1964, *Sunspots* (New York: Dover), chap. 5.
- Brown, P. J. F., Dufton, P. L., and Lennor, D. J. 1988, *Mon. Not. R. Astr. Soc.*, 230, 443.
- Burden, R. L., Faires, J. D., and Reynolds, A. C. 1981, *Numerical Analysis*, (Boston: Prindle, Weber, and Schmidt), p. 107.
- Buser, R., and Kurucz, R. L. 1978, *Astr. Ap.*, 70, 555.
- Campbell, B., Walker, G. A. H., Johnson, R., Lester, T., Yang, S., and Auman, J. 1981, *Proc. SPIE*, 290, 215.
- Code, A. D., Davis, J., Bless, R. C., and Brown, H. R. 1976, *Ap. J.*, 203, 417.
- Cowley, C. 1971, *Observatory*, 91, 139.
- Cramer, N., and Maeder, A. 1979, *Astr. Ap.*, 78, 305.
- Cramer, N. 1984, *Astr. Ap.*, 132, 283.
- Deridder, G., and van Rensbergen, W. 1976, *Astr. Ap. Suppl.*, 23, 147.
- Deutsch, A. J. 1956, *Pub. A. S. P.*, 68, 92.

- 1958, in *IAU Symposium 6, Electromagnetic Phenomena in Cosmical Physics*, ed. B. Lehnert (Cambridge: Cambridge University Press), p. 209.
- Didelon, P. 1923, *Astr. Ap. Suppl.*, 53, 119.
- Drake, S. A., Abbott, D. C., Bieging, J. H., Churchwell, E., and Linsky, J. L. 1985, in *Radio Stars*, ed. R. M. Hjellming and D. M. Gibson (Dordrecht: Reidel), p. 247.
- Drake, S. A., Abbott, D. C., Bastian, T. S., Bieging, J. H., Churchwell, E., Dulk, G., and Linsky, J. L. 1987, *Ap. J.*, 322, 902.
- Drilling, J. S. 1981, *Ap. J.*, 250, 701.
- Drilling, J. S., and Hill, P. W. 1986, in *IAU Colloquium 87, Hydrogen Deficient Stars and Related Objects*, ed. K. Hunger, D. Schönberner, and N. Kameswara Rao (Dordrecht: Reidel), p. 499.
- Dufton, P. L., and Hibbert, A. 1981, *Astr. Ap.*, 95, 24.
- Egret, D., and Jaschek, M. 1981, in *Upper Main Sequence Chemically Peculiar Stars* (Liege: Institut d'Astrophysique), p. 435.
- Erhorn, G., Groote, D., and Kaufmann 1984, *Astr. Ap.*, 131, 390.
- Friend, D. B., and MacGregor, K. B. 1984, *Ap. J.*, 282, 591.
- Garrison, R. F., Hiltner, W. A., and Schild, R. E. 1977, *Ap. J. Suppl.*, 35, 111.
- Giannone, P., and Rossi, L. 1980, *Astr. Ap.*, 85, 252.
- Goossens, M. 1979, *Astr. Ap.*, 79, 210.

- Goossens, M., Martens, L., and Gadeyne, L. 1981, *Astr. Ap.*,  
95, 240.
- Greenstein, J. L., and Wallerstein, G. 1958, *Ap. J.*, 127,  
237.
- Griem, H. R., Baranger, M., Kolb, A. C., and Oertel, G.  
1962, *Phys. Rev.*, 125, 177.
- Groote, D., and Hunger, K. 1976, *Astr. Ap.*, 52, 303.  
----- 1977, *Astr. Ap.*, 56, 129.  
----- 1982, *Astr. Ap.*, 116, 64.
- Groote, D., Hunger, K., and Schultz, G. V. 1980, *Astr. Ap.*,  
83, L5.
- Groote, D., and Kaufmann, J. P. 1981a, in *Upper Main  
Sequence Chemically Peculiar Stars* (Liège: Institut  
d'Astrophysique), p. 435.  
----- 1981b, *Astr. Ap.*, 94, L23.  
----- 1984, *Astr. Ap.*, 130, 184.
- Groote, D., Kaufmann, J. P., and Hunger, K. 1978, *Astr. Ap.*,  
63, L9.
- Hardorp, J., and Scholz, M. 1970, *Ap. J. Suppl.*, 19, 193.
- Hardorp, J., Shore, S. N., and Wittmann, A. 1976, in *IAU  
Colloquium 32, Physics of Ap Stars*, ed. W. W. Weiss, H.  
Jenkner, and H. J. Wood (Vienna: Universitätssternwarte  
Wien), p. 419.
- Harmanec, P. 1984, *Bull. Astron. Inst. Czechosl.*, 35, 193.
- Hartoog, M. R., and Cowley, A. P. 1979, *Ap. J.*, 228, 229.
- Havnes, O., and Goertz, C. K. 1984, *Astr. Ap.*, 138, 421.
- Helsley, J. N., and Wolff, S. C. 1983, *Ap. J.*, 269, 634.

- Heintz, W. D. 1974, *Ap. J.*, 79, 397.
- Hessler, G. 1979, *Astr. Ap.*, 74, 284.
- Hesser, J. E., Moreno, H., and Ugarte P., P. 1977, *Ap. J.*  
(*Letters*), 216, L31.
- Hesser, J. E., Walborn, N. R., and Ugarte P., P. 1976,  
*Nature*, 262, 116.
- Higginbotham, N. A., and Lee, P. 1974, *Astr. Ap.*, 33, 277.
- Hill, G. 1967, *Ap. J. Suppl.*, 14, 263.
- Hiltner, W. A., Garrison, R. F., and Schild, R. E. 1969, *Ap. J.*, 157, 313.
- Hoffleit, D., and Jaschek, C. 1982, *The Bright Star Catalogue* (4th ed.; New Haven: Yale University Observatory).
- Hunger, K. 1974, *Astr. Ap.*, 32, 449.
- 1975, in *Problems in Stellar Atmospheres and Envelopes*, ed. B. Baschek, W. H. Kegel, and G. Traving (New York: Springer-Verlag), p. 57.
- 1986a, in *Upper Main Sequence Stars with Anomalous Abundances*, ed. C. R. Cowley, M. M. Dworetzky, and C. Megessier (Dordrecht: Reidel), p. 257.
- 1986b, in *IAU Colloquium 87, Hydrogen Deficient Stars and Related Objects*, ed. K. Hunger, D. Schönberner, and N. Kameswara Rao (Dordrecht: Reidel), p. 261.
- Hunger, K., and Kaufmann, J. P. 1973, *Astr. Ap.*, 25, 261.
- Jaschek, C., and Jaschek, M. 1987, *The Classification of Stars*, (Cambridge: Cambridge University Press), p.

195.

Kamp, L. W. 1973, *Ap. J.*, 180, 447.

\_\_\_\_\_. 1978, *Ap. J. Suppl.*, 36, 143.

Kaufmann, J. P., and Hunger K. 1975, *Astr. Ap.*, 38, 351.

Kaufmann, J. P., Schönberner, D., and Rahe, J. 1974, *Astr. Ap.*, 36, 201.

Kemp, J. C., and Herman, L. C. 1977, *Ap. J.*, 218, 770.

Klinglesmith, D. A. 1971, *Hydrogen Line Blanketed Model Stellar Atmospheres* (NASA SP-3065).

• Klinglesmith, D. A., Hunger, K., Bless, R. C., and Millis, R. L. 1970, *Ap. J.*, 159, 513.

Krauss, F., and Oetken, L. 1976, in *IAU Colloquium 32, Physics of Ap Stars*, ed. W. W. Weiss, H. Jenkner, and H. J. Wood (Vienna: Universitätssternwarte Wien), p. 29.

Kroll, R. 1987, *ESO Messenger*, 47, 15.

Kurucz, R. L. 1979, *Ap. J. Suppl.*, 40, 1.

Landstreet, J. D. 1970, *Ap. J.*, 159, 1001.

\_\_\_\_\_. 1980, *A. J.*, 85, 611.

\_\_\_\_\_. 1982, *Ap. J.*, 258, 639.

\_\_\_\_\_. 1987, *Mon. Not. R. Astr. Soc.*, 225, 437.

\_\_\_\_\_. 1988, *Ap. J.*, 326, 967.

Landstreet, J. D., and Borra, E. F. 1978, *Ap. J. (Letters)*, 224, L5.

Landstreet, J. D., Borra, E. F., and Fontaine, G. 1977, *Mon. Not. R. Astr. Soc.*, 188, 609.

Leckrone, D. S. 1971, *Astr. Ap.*, 11, 387.

- Ledoux, P. P. and Renson, P. 1966, *Ann. Rev. Astron. Astrophys.*, 20, 191.
- Lee, P., and O'Brien, A. 1977, *Astr. Ap.*, 60, 259.
- Lester, J. B. 1972, *Ap. J.*, 178, 743.
- 1976, *Ap. J.*, 210, 153.
- 1979, *Ap. J.*, 233, 644.
- Lester, J. B., Gray, R. O., and Kurucz, R. L. 1986, *Ap. J. Suppl.*, 61, 509.
- MacConnell, D. J., Frye, R. L., and Bidelman, W. P. 1970, *Pub. A. S. P.*, 83, 730.
- Maeder, A. 1981, *Astr. Ap.*, 102, 401.
- Maeder, A., and Mermilliod, J. C. 1981, *Astr. Ap.*, 93, 136.
- Marlborough, J. M., 1982, in *IAU Symposium 98, Be Stars*, ed. M. Jaschek and H.-G. Groth (Dordrecht: Reidel), p. 361.
- Martin, B., and Wickramasinghe, D. T. 1979, *Mon. Not. R. Astr. Soc.*, 189, 883.
- Mathys, G. 1988, *Astr. Ap.*, 189, 179.
- Matthews, J. M., and Bohfender, D. A. 1988, preprint.
- Megessier, C. 1975, *Astr. Ap.*, 39, 263.
- 1984, *Astr. Ap.*, 138, 267.
- Mermilliod, J.-C., 1983, *Astr. Ap.*, 128, 362.
- Mermilliod, M., and Hauck, B. 1979, *uvby HB Photoelectric Photometric Catalogue* (Geneva Observatory).
- Michaud, G. 1970, *Ap. J.*, 160, 641.
- Michaud, G., Montmerle, T., Cox, A. N., Magee, N. H., Hodson, S. W., and Martel, A. 1979, *Ap. J.*, 234, 206.

- Michaud, G., Megessier, C., and Charland, Y. 1981, *Astr. Ap.*,  
103, 244.
- Michaud, G., Dupuis, J., Fontaine, G., and Montmerle, T.  
1987, *Ap. J.*, 322, 302.
- Mihalas, D. 1973, *Ap. J.*, 184, 851.  
\_\_\_\_\_. 1978, *Stellar Atmospheres* (San Francisco: Freeman),  
p. 471.
- Mihalas, D., and Binney, J., 1981, *Galactic Astronomy* (San  
Francisco: Freeman), p. 187.
- Mihalas, D., Barnard, A. J., Cooper, J., and Smith, E. W.  
1974, *Ap. J.*, 190, 315.
- Moore, C. E. 1945, *NBS Tech. Note*, No. 36.  
\_\_\_\_\_. 1949, *NBS Circ.*, No. 467.
- Morgan, W. W., Abt, H. A., and Tapscott, J. W. 1978, *Revised  
MK Spectral Atlas for Stars Earlier than the Sun*,  
Yerkes Observatory and Kitt Peak National Observatory.
- Moss, D. 1985a, *Mon. Not. R. Astr. Soc.*, 213, 575.  
\_\_\_\_\_. 1987a, *Mon. Not. R. Astr. Soc.*, 226, 297.  
\_\_\_\_\_. 1987b, *Mon. Not. R. Astr. Soc.*, 228, 993.
- Nakajima, R. 1981, *Tohoku Univ. Sci. Rept.*, 2, 129.  
\_\_\_\_\_. 1985, *Ap. Space Sci.*, 116, 285.
- Nerney, S. 1980, *Ap. J.*, 242, 723.
- Nissen, P. E., 1974, *Astr. Ap.*, 36, 57.  
\_\_\_\_\_. 1976, *Astr. Ap.*, 50, 343.
- Norris, J. 1971; *Ap. J. Suppl.*, 23, 213.
- Norris, J., and Baschek, B. 1972, *Astr. Ap.*, 21, 385.
- Norris, J., and Strittmatter, P. A. 1975, *Ap. J.*, 196, 515.

- Odell, A. P. 1974, *Ap. J.*, 194, 645.
- Osmer, P. S., and Peterson, D. M. 1974, *Ap. J.*, 187, 117.
- Pedersen, H., 1979, *Astr. Ap. Suppl.*, 35, 313.
- Pedersen, H., and Thomsen, B. 1977, *Astr. Ap. Suppl.*, 30, 11.
- Peters, G. J. 1976, *Ap. J. Suppl.*, 30, 551.
- Peters, G. J., and Aller, L. H. 1970, *Ap. J.*, 159, 525.
- Peterson, D. M., and Theys, J. C. 1981, *Ap. J.*, 244, 947.
- Phillips, R. B., and Lestrade, J.-F. 1988, preprint.
- Poe, C. H., and Friend, D. B. 1987, preprint.
- Press, W. H., Flannery, B. P., Teukolsky, S. A., and Vetterling, W. T. 1987, *Numerical Recipes* (Cambridge: Cambridge University Press), p. 292.
- Preston, G. W. 1967, *Ap. J.*, 150, 547.
- 1969, *Ap. J.*, 156, 967.
- 1971, *Pub. A. S. P.*, 83, 571.
- 1970, *Ap. J.*, 160, 1059.
- Pyper, D. M. 1969, *Ap. J. Suppl.*, 18, 347.
- Renson, P. 1984, *Astr. Ap.*, 139, 731.
- Rufener, F. 1981, *Astr. Ap. Suppl.*, 45, 207.
- Schwarzschild, M. 1950, *Ap. J.*, 112, 222.
- Shore, S. N., 1978, Ph. D. thesis, University of Toronto.
- 1987, *A. J.*, 94, 731.
- Shore, S. N., and Adelman, S. J. 1981, in *Upper Main Sequence Chemically Peculiar Stars* (Liege: Institut d'Astrophysique), p. 629.
- Shore, S. N., Brown, D. N., and Sonneborn, G. 1987, *A. J.*,

94, 737.

Stepien, K. 1978, *Astr. Ap.*, 70, 509.

Stibbs, D. W. N. 1950, *Mon. Not. R. Astr. Soc.*, 110, 395.

Stift, M. J. 1975, *Mon. Not. R. Astr. Soc.*, 172, 133.

\_\_\_\_\_. 1980, *Astr. Ap.*, 82, 142.

Swings, J. P., Jamar, C., Vreux, J. M. 1973, *Astr. Ap.*, 29,  
207.

Thomsen, B. 1974, *Astr. Ap.*, 35, 479.

Thompson, I. B., and Landstreet, J. D. 1985, *Ap. J.*

(*Letters*), 289, L9.

Thompson, I. B., Brown, D. N., and Landstreet, J. D. 1987,

*Ap. J. Suppl.*, 64, 219.

Unno, W. 1956, *Pub. Astr. Soc. Japan*, 8, 108.

Van Rensbergen, W., Hensberge, H., and Adelman, S. J. 1984,

*Astr. Ap.*, 136, 31.

Vauclair, S. 1975, *Astr. Ap.*, 45, 233.

Vauclair, S., Hardorp, J., and Peterson, D. M. 1979, *Ap. J.*

227, 526.

Vidal, C. R., Cooper, J., and Smith, E. W. 1973, *Ap. J.*

*Suppl.*, 25, 37.

Vreux, J. M., Malaise, D., Swings, J. P. 1973, *Astr. Ap.*,

29, 211.

Walborn, N. R. 1974, *Ap. J. (Letters)*, 191, L95.

\_\_\_\_\_. 1982, *Pub. A. S. P.*, 94, 322.

\_\_\_\_\_. 1983, *Ap. J.*, 268, 195.

\_\_\_\_\_. 1984, in *The Origins of Nonradiative*

*Heating/Momentum in Hot Stars*, ed. A. B. Underhill, and

- A. G. Michalitsianos (NASA CP-2358), p. 21.
- Walborn, N. R., and Hesser, J. E. 1976, *Ap. J. (Letters)*,  
205, L87.
- Wallerstein, G. 1959, *Ap. J.*, 130, 338.
- Wiese, W. L., and Martin, G. A. 1980, *NSRDS-NBS, part 2*, US  
Government Printing Office, Washington, DC.
- Wiese, W. L., Smith, M. W., and Glennon, B. M. 1966, *NSRDS-  
NBS 4*, US Government Printing Office, Washington, DC.
- Wolf, R. E. A. 1973, *Astr. Ap.*, 26, 127.
- Wolff, S. C., Edwards, S., and Preston, G. W. 1982, *Ap. J.*,  
252, 322.
- Wolff, S. C., and Wolff, R. J. 1970, *Ap. J.*, 160, 1049.  
----- 1976, *Ap. J.*, 203, 171. /